NASA CONTRACTOR REPORT

NASA CR-2

NASA CR-2748

THE INVISCID PRESSURE FIELD ON THE TIP OF A SEMI-INFINITE WING AND ITS APPLICATION TO THE FORMATION OF A TIP VORTEX

G. F. Hall, S. J. Shamroth,
H. McDonald, and W. R. Briley

Prepared by
UNITED TECHNOLOGIES RESEARCH CENTER
East Hartford, Conn. 06108
for Langley Research Center

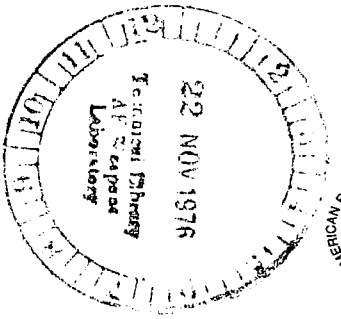

NATIONAL AERONAUTICS AND SPACE ADMINISTRATION • WASHINGTON, D. C. • OCTOBER 1976

1. Report No.	2. Government Accession No.	3. Recipient's Catalog No.
NASA CR-2748		

4. Title and Subtitle	5. Report Date
THE INVISCID PRESSURE FIELD ON THE TIP OF A SEMI-INFINITE WING AND ITS APPLICATION TO THE FORMATION OF A TIP VORTEX	October 1976
	6. Performing Organization Code: 36.300
7. Author(s): G. F. Hall, S. J. Shamroth, H. McDonald, and W. R. Briley	8. Performing Organization Report No.
9. Performing Organization Name and Address: United Technologies Research Center, East Hartford, CT 06108	10. Work Unit No.: 505-10-21-01
	11. Contract or Grant No.: NAS1-12794
12. Sponsoring Agency Name and Address: National Aeronautics and Space Administration, Washington, DC 20546	13. Type of Report and Period Covered: Contractor Report
	14. Sponsoring Agency Code

15. Supplementary Notes

Final Report

Langley technical monitor: W. H. Young, Jr.

16. Abstract

A method has been developed for determining the aerodynamic loads on the tip of an infinitely thin, swept, cambered semi-infinite wing at an angle of attack which is operating subsonically in an inviscid medium and is subjected to a sinusoidal gust. Under the assumption of linearized aerodynamics, the loads on the tip are obtained by superposition of the steady aerodynamic results for angle of attack and camber, and the unsteady results for the response to the sinusoidal gust. The near field disturbance pressures in the fluid surrounding the tip are obtained by assuming a dipole representation for the loading on the tip and calculating the pressures accordingly. The near field pressures are used to drive a reduced form of the Navier-Stokes equations which yield the tip vortex formation. The combined viscid-inviscid analysis has only been applied to determining the pressures and examining the vortex rollup in the vicinity of an unswept, uncambered wing moving steadily at a Mach number of 0.2 at an angle of attack of 0.1 rad.

The viscous tip flow calculation has shown features expected in the tip flow such as the qualitatively proper development of boundary layers on both the upper and lower airfoil surfaces. In addition, application of the viscous solution leads to the generation of a "circular" type flow pattern above the airfoil suction surface.

17. Key Words (Suggested by Author(s))	18. Distribution Statement
Tip vortex, wing tip, trailing vortex, Navier-Stokes, unsteady aerodynamics, blade-vortex aerodynamics	Unclassified - Unlimited Subject Category 34

19. Security Classif. (of this report)	20. Security Classif. (of this page)	21. No. of Pages	22. Price*
Unclassified	Unclassified	82	$4.75

*For sale by the National Technical Information Service, Springfield, Virginia 22161

THE INVISCID PRESSURE FIELD ON THE TIP OF A SEMI-INFINITE WING AND ITS APPLICATION TO THE FORMATION OF A TIP VORTEX

By G. F. Hall, S. J. Shamroth, H. McDonald and W. R. Briley
United Technologies Research Center

SUMMARY

A method has been developed for determining the aerodynamic loads on the tip of an infinitely thin, swept, cambered semi-infinite wing at an angle of attack which is operating subsonically in an inviscid medium and is subjected to a sinusoidal gust. Under the assumption of linearized aerodynamics, the loads on the tip are obtained by superposition of the steady aerodynamic results for angle of attack and camber, and the unsteady results for the response to the sinusoidal gust. The assumption that the major effects of the tip are confined to a relatively small finite spanwise length permits the loading over the inboard portions of the wing to be approximated by known results for the infinite wing. The tip region is treated by a numerical doublet-lattice method. The leading edge singularity in the loading is removed by applying a correction factor due to Lighthill. The near field disturbance pressures in the fluid surrounding the tip are obtained by assuming a dipole representation for the loading on the tip and calculating the pressures accordingly. In addition to providing insight into the inviscid flow behavior in the vicinity of the tip, the near field pressures are also used to drive a reduced form of the Navier-Stokes equations which yield the tip vortex formation.

Although the derivation is valid for the general conditions described above and several inviscid cases have been calculated, the combined viscid-inviscid analysis has only been applied to determining the pressures and examining the vortex rollup in the vicinity of an unswept, uncambered wing moving steadily at a Mach number of 0.2 at an angle of attack of 0.1 rad. Generally, the pressure behavior is as expected. As the wing surface is approached in the normal direction, the pressure magnitude increases, culminating at one-half the dipole magnitude at the surface. External to the region containing either the wing or the wake, the pressures go continuously and monotonically to zero as the wing plane is approached. In the wake, the magnitude increases as the wake is approached until, near the wake, an abrupt reversal in trend occurs and the magnitude goes to zero. Finally, in the

vicinity of the trailing edge, the pressure magnitude increases until, near the wing surface, a reversal in trend is noted with the magnitude decreasing and terminating at one-half the dipole strength. This behavior reflects the change in boundary condition at the trailing edge.

The viscous tip flow calculation has shown features expected in the tip flow such as the qualitatively proper development of boundary layers on both the upper and lower airfoil surfaces. In addition, application of the viscous solution leads to the generation of a 'circular' type flow pattern above the airfoil suction surface.

INTRODUCTION

In recent years, there has been a growing interest in the vortex formed due to the pressure equalization condition at the tips of lifting surfaces. This tip vortex, whose presence can often be neglected in isolated airfoil aerodynamics, requires a precise definition of its physical characteristics in problems involving interference aerodynamics. A primary example of this type of problem is the intersection of a helicopter rotor blade tip vortex with the next following blade. This intersection represents a potentially serious acoustic problem, (Ref. 1) and has been shown to have some effect on rotor performance (Ref. 2). In addition to the direct relevance to current helicopter problems, a more complete knowledge of tip vortex dynamics is needed to assist in the design of novel helicopter blade tips for optimum performance, and to provide basic information on the behavior of trailing tip vortices behind large aircraft, to name only two of many applications.

In the past, the tip vortex roll-up rate and position have been determined either by direct experimentation or by analytical techniques utilizing Trefftz plane calculations (e.g., Ref. 3). Experimental procedures are reasonable for many steady flow problems, but they are not yet sufficien ly sophisticated to show all the details of the vortex formation. Trefftz plane analyses generally predict the position of the tip vortex adequately, but yield roll-up rates much too slow. Hall (Ref. 4) has modeled the vortex wake behind a fixed wing starting impulsively from rest which predicts both a rate and position of the tip vortex more compatible with those observed, but this technique requires large amounts of computer time and storage. Another approach to determining the tip vortex behind a lifting surface is a direct numerical assault on the Navier-Stokes equations, but this approach also requires large amounts of computer time and storage. It should be noted that classical lifting surface analyses are incapable of treating the roll-up problem; the linearization inherent in these methods is not valid in the tip region. The analysis of the tip vortex formation is a highly nonlinear real fluid problem. Figure 1 is a sketch depicting this formation.

The present analysis is an attempt to provide a simplified model of the tip vortex formation problem. A boundary layer approach is used in which the vorticity laden fluid contained in the tip vortex originates in the region near enough the wing surface to be affected by viscosity. The boundary layer condition that the pressure field is unaffected by viscous displacement effects is assumed so that this pressure field can be determined from inviscid potential theory in which shed vorticity is modeled by discrete vortex elements. It is further assumed that the phenomenon is sufficiently confined to the tip region that a semi-infinite wing can be used to determine the pressure field. Since

the presence of the vortex requires a loading to exist on the wing, angle of attack, camber and unsteadiness must be considered, but thickness can be neglected, at least as a first approximation. This models the wing as an infinitely thin, curved plate in a subsonic compressible flow containing a sinusoidal gust. Once the loading on the wing is determined, the pressure field in the fluid around the wing is determined from a pressure dipole solution. The viscous roll-up is then obtained from a reduced form of the Navier-Stokes equation. A sketch of the expected tip vortex formation on a flat plate tip is shown in Fig. 2. A comparison with Fig. 1 shows that the only basic difference in the hypothesized vortex formation process is that on the wing of finite thickness the vortex initiation point may lie aft of the leading edge whereas on the infinitely thin wing the initiation point is forced to occur at the tip leading edge.

The approach to be used in this analysis is broadly based on the infinite wing analysis of Adamczyk (Refs. 5,6) and the doublet-lattice method of Giesing, et al (Ref. 7). In brief, Adamczyk examined the problem of an arbitrary gust encounter of an infinite swept wing in a subsonic flow. The solution, which basically treated the sinusoidal gust response, is used in a Fourier superposition method for any arbitrary disturbance, and this technique is employed herein for the unsteady vortex formation. Although Adamczyk's method is posed for an infinite wing, it is known that with appropriate modifications in the vicinity of a finite tip, such a two-dimensional method will still be valid at some distance inboard of the tip. Hence, the Giesing method is applied over the actual tip region and is matched to the Adamczyk solution inboard of the tip. The match point location was determined by numerical experimentation and was chosen to yield a smooth transition between inboard and outboard solutions. This procedure is described in the text below.

LIST OF SYMBOLS

a_o	Speed of sound, m/sec
A	Influence coefficient
b	Semichord, normal to span, m
c	Chord, parallel to free stream, m
C_p	Pressure coefficient $(p-p_o)\ 2/\rho_o U^2$
ΔC_p	Pressure coefficient change across lifting surface, $(p^{(x_2-)}-p^{(x_2+)})2/\rho_o U^2$
ΔC_{p_∞}	ΔC_p due to an infinite wing in a given flow
D	Sublayer damping factor
ΔC_{p_c}	Defined by Eq. 11
E(X)	Complex Fresnel integral
F,f	Equation of the lifting surface
J_o, J_1	Zeroth and first order Bessel functions, respectively
h	Wing thickness, m
h_1, h_2, h_3	metric coefficients
$H_o^{(1)}$, $H_1^{(1)}$	Zeroth and first order Hankel functions of the first kind
k	Gust wave number, m^{-1}
k_x	Gust wave number, x-component, m^{-1}
k_y	Gust wave number, y-component, m^{-1}
k_1	Gust wave number in streamwise direction (Ref. 7), m^{-1}

LIST OF SYMBOLS (Cont'd)

$\bar{k}$	k/b
L	Spanwise length outboard from which the tip effects are assumed concentrated, m
ℓ	Mixing length, m
p	Pressure, n/m^2
p_I	Inviscid pressure, n/m^2
p_o	Free stream static pressure, n/m^2
R	Radius, m or gas constant
t	Time, sec
T	Temperature, °K
T_L	Lift transfer function
u,v,w	Velocity components in viscous analysis, m/sec
U	Freestream velocity, m/sec
$\vec{U}$	Velocity vector, m/sec
u_2	Complex gust amplitude (Ref. 5), m/sec
w	Complex gust amplitude, m/sec
w_g	Gust velocity, m/sec
x,y	System coordinates, m; x streamwise; y normal to x and directed inboard. Origin at tip leading edge.
x,y,z	Cartesian coordinates in viscous analysis, m
x_1, x_2	System coordinate, m; x normal to span. x_3 parallel to span, directed inboard. Origin at midchord of tip.
x_2	Coordinate normal to plane of wing, m

LIST OF SYMBOLS (Cont'd)

α	Gust inclination angle, degree, or difference operator
β	Frequency parameter, defined by Eq. (22a)
γ	Cutoff parameter, defined by Eq. (22b)
ϵ	Included angle between a point at which induced velocity is calculated and the part at which the inducing load is located, deg
η	Transformed transverse variable
θ	Wing sweep angle, deg
μ	Viscosity, kg/m-sec
ρ	Density, kg/m^3
ρ_o	Freestream density, kg/m^3
ρ_2	Wing leading edge, radius, m
φ	Complex velocity potential, m^2/sec
ϕ	Complex amplitude of velocity potential, m^2/sec, or arbitrary dependent variable
$(\bar{\ })$	Complex amplitude
$(\_)$	Vector
-	Mean value
'	Fluctuating value

Subscripts

k, l	Identifies points at which boundary condition is satisfied
i,j,n,m	Identifies points at which inducing loads are located

THEORETICAL FORMULATION

It is assumed for the purpose of analysis that the semi-infinite wing is at rest in a subsonic compressible stream having an imbedded sinusoidal gust which is swept past the wing at the stream speed, U. The pertinent geometry of the semi-infinite wing is given in Fig. 3. Of particular interest is the spanwise distance, L. This length represents the distance within which the tip effect is assumed to be dominant; inboard of this distance the flow and the loading is essentially two-dimensional. Both the tip and the normal to the gust wave fronts are parallel to the freestream due to restraints imposed by the particular version of the doublet-lattice method selected. The wing is assumed infinitely thin so that thickness can be neglected, but the effects of camber and angle of attack are included in the analysis. It is further assumed that all disturbances are small enough that linearization is permitted. The disturbance velocity potential is thus defined by the standard linearized acoustic equation for subsonic compressible flow.

$$\nabla^2\phi - M^2\frac{\partial^2\phi}{\partial x^2} - 2\frac{M}{a_0}\frac{\partial^2\phi}{\partial x\partial t} - \frac{1}{a_0^2}\frac{\partial^2\phi}{\partial t^2} = 0 \tag{1}$$

A unique solution to the equation is obtained by applying the necessary boundary conditions (Ref. 5). The linearized pressure field is then obtained from

$$\frac{P}{\rho_o} = -\left[\frac{\partial\phi}{\partial t} + U\frac{\partial\phi}{\partial x}\right] \tag{2}$$

The necessary boundary conditions can be stated as follows:

$$P = 0 \qquad x < -y\tan\theta, \quad x > c - y\tan\theta, \quad \text{all } y, \quad x_2 = 0 \tag{3a}$$

$$P = 0 \qquad x = c - y\tan\theta, \quad y > 0, \quad x_2 = 0 \quad \text{(Kutta Condition)} \tag{3b}$$

$$\frac{DF}{Dt} = 0 \qquad x \geq -y\tan\theta, \quad x \leq c - y\tan\theta, \quad x_2 = 0, \quad y > 0 \quad \text{(Flow Tangency)} \tag{3c}$$

$$\phi \sim R^{-1/2} \qquad R \to \infty \quad \text{(Radiation Condition)} \tag{3d}$$

Note that the boundary condition 3a really expresses pressure continuity in the wake as well as no disturbance ahead of the wing in the wing plane so that

$$\frac{\partial \phi}{\partial t} + U\frac{\partial \phi}{\partial x} = 0 \qquad x > c - y\tan\theta \tag{3e}$$

and

$$\phi = 0 \qquad x < -y\tan\theta \tag{3f}$$

Inspection of both the flow tangency condition and the linearity properties of the velocity potential permits further simplification of the problem. Let the equation of the surface be given by

$$F(x_1, x_3, t) = x_3 - f(x_1, t) = 0 \tag{4}$$

Then

$$\frac{DF}{Dt} = \frac{\partial f}{\partial t} - U\frac{\partial f}{\partial x_1} + \frac{\partial \phi}{\partial x_2} - w_g = 0 \tag{5}$$

where $\partial\varphi/\partial X_2$ is the X_2-velocity induced by the wing and w_g is an imposed normal gust velocity. If the wing performs no unsteady motions, then the disturbance velocity potential must satisfy

$$\frac{\partial \phi}{\partial x_2} = U\frac{\partial f}{\partial x_1} + w_g(x_1, x_3, t) \tag{6}$$

Since the velocity potential is a linear function, superposition applies and a steady and unsteady component can be defined.

$$\phi = \phi_s + \phi_{us} \tag{7}$$

Thus the boundary condition can also be separated into steady and unsteady relationships.

$$\frac{\partial \phi_s}{\partial x_2} = U\frac{\partial f}{\partial x_1} \tag{8a}$$

$$\frac{\partial \phi_{us}}{\partial x_2} = w_g(x_1, x_3, t) \tag{8b}$$

This allows treatment of camber and angle of attack as separate solutions to the steady flow problem, while the response of the wing to an unsteady gust is obtained as simply the response of a flat plate to the gust.

Since the unsteadiness is represented by a gust harmonic in time, both the disturbance velocity potential and airload should be harmonic in time

$$\phi(\underline{x},t) = \phi(\underline{x})\, e^{i\omega t} \tag{9a}$$

$$P(\underline{x},t) = \bar{P}(\underline{x}) e^{i\omega t} \tag{9b}$$

$$\Delta C_P(\underline{x},t) = \overline{\Delta C}_P(\underline{x}) e^{i\omega t} \tag{9c}$$

This boundary value problem can be converted to a singular integral equation which relates the local flow angle at the surface to the loading of the surface in a manner that expresses the flow tangency condition explicitly with the remaining conditions implied

$$\frac{w}{U} e^{-i(k_x x + k_y y)} = \frac{1}{8\pi} \int_0^{\infty}\int_0^{C} K(x-\xi, y-\eta)\, \overline{\Delta C}_P(\xi,\eta)\, d\xi\, d\eta \tag{10}$$

where

$$\overline{\Delta C}_P = \frac{\bar{P}(x_2 = 0^+) - \bar{P}(x_2 = 0^-)}{\frac{1}{2}\rho_o U^2}$$

and $\lim_{\eta \to \infty} \overline{\Delta C}_p \to \overline{\Delta C}_{p\infty}$ which is the result for an infinite wing in the sinusoidal gust field. A pressure coefficient increment due to the presence of a finite tip can be defined by

$$\overline{\Delta C}_{P_C} = \overline{\Delta C}_{P_\infty} - \overline{\Delta C}_P \tag{11}$$

which satisfies

$$\lim_{\eta \to \infty} \overline{\Delta C}_{P_C} \to 0 \tag{12}$$

and which permits Eq. (10) to be rewritten in the form

$$8\pi \frac{w}{U} e^{-i(k_x x + k_y y)} = \int_0^{\infty}\int_0^{C} K(x-\xi, y-\eta)\left[\overline{\Delta C}_{P_\infty}(\xi,\eta) - \overline{\Delta C}_{P_C}(\xi,\eta)\right] d\xi\, d\eta \tag{13}$$

Eq. (13) for points (x,y) on the wing can then be rewritten in the following form

$$8\pi \frac{w}{U} e^{-i(k_x x + k_y y)} = \int_{-\infty}^{\infty}\int_{0}^{C} K\, \overline{\Delta C}_{P_\infty}\, d\xi\, d\eta - \int_{-\infty}^{0}\int_{0}^{C} K \overline{\Delta C}_{P_\infty} d\xi\, d\eta - \int_{0}^{\infty}\int_{0}^{C} K\, \overline{\Delta C}_{P_C}\, d\xi\, d\eta \tag{14}$$

Now the upwasn induced by an infinite wing in the sinusoidal gust field is given by

$$\int_{-\infty}^{\infty}\int_{0}^{C} K\, \overline{\Delta C}_{P_\infty}\, d\xi\, d\eta = 8\pi \frac{w}{U} e^{-i(k_x x + k_y y)}$$

and the upwash induced on the semi-infinite wing by another semi-infinite wing extending from the tip to $\eta = -\infty$ is given by the term

$$\int_{-\infty}^{0}\int_{0}^{C} K \overline{\Delta C}_{P_\infty} d\xi d\eta$$

The two wings summed would make an infinite wing. Hence the integral equation can be expressed as

$$\int_{0}^{\infty}\int_{0}^{C} K(x-\xi, y-\eta)\, \overline{\Delta C}_{P_C}(\xi,\eta)\, d\xi\, d\eta = -\int_{-\infty}^{0}\int_{0}^{C} K(x-\xi, y-\eta)\, \overline{\Delta C}_{P_\infty}(\xi,\eta)\, d\xi d\eta \qquad y \geq 0 \tag{15}$$

This equation expresses the physical phenomenon that the presence of a finite tip induces an upwash increment over the wing surface to account for the removal of that one half of an infinite wing which extends to $-\infty$. The previous result is a general result, applying equally to steady or unsteady motions as well as flat plates and cambered plates, and was also noted by Chu and Widnall (Ref. 8).

Solution For The Pressure Field At The Tip Of The Semi-Infinite Wing

The solution to the problem of determining the loading on the semi-infinite wing makes use of the simplification afforded by the linearization of the problem. The angle of attack and camber contributions to the loading can by computed separately utilizing steady state aerodynamic and then superimposed onto the unsteady results of a flat plate responding to a sinusoidal gust.

Equation 15 represents the basic equation to be solved for the finite tip pressure coefficient increment $\overline{\Delta C_{p_C}}$. The kernel function, K, has been calculated in a form suitable for numerical computation in Ref. 7 while $\overline{\Delta C_{p_\infty}}$ represents the solution to the infinite wing responding to the sinusoidal gust field and can be obtained from other sources (e.g., Refs. 5 and 6).

One approach to a solution is a combination of analytic and numerical techniques in which the known $\overline{\Delta C_{p_\infty}}$ is used to compute the upwash on a selected set of control points on the wing numerically. This is the right hand side of Eq. 15. Then the unknown $\overline{\Delta C_{p_c}}$ is computed at load points on the wing by assuming a series representation made up of chordwise and spanwise loading functions which satisfy the edge behavior of the semi-infinite wing using

$$\overline{\Delta C}_P \to \sqrt{1/\delta} \qquad x \to -y\tan\theta \quad \text{(leading edge)}$$

$$\overline{\Delta C}_P \to \sqrt{\delta} \qquad x \to C - y\tan\theta \quad \text{(trailing edge)}$$

$$\overline{\Delta C}_P \to \sqrt{y} \qquad y \to 0$$

$$\overline{\Delta C}_P \to \overline{\Delta C}_{P_\infty} \qquad y \to \infty$$

(where δ is the distance to the edge of the wing), and a set of unknown weighting functions. The weighting functions are determined by satisfying Eq. 15 at the selected load points for which the right hand side was calculated. This is essentially the method proposed in Ref. 8 and is quite satisfactory for small values of kM. As kM values increase, however, the chordwise distribution of $\overline{\Delta C_{p_\infty}}$ which defines the chordwise loading function, does not maintain as simple a form.

The present solution begins by casting Eq. 15 into a numerical form

$$\sum_{j=-\infty}^{0} \sum_{i=1}^{I} \overline{\Delta C}_{P_{\infty_{ij}}} K(x-\xi_i, y-\eta_j)\Delta\xi_i\Delta\eta_j = \sum_{m=0}^{\infty} \sum_{n=1}^{N} \overline{\Delta C}_{P_{Cnm}} K(x-\xi_n, y-\eta_m)\Delta\xi_n\Delta\eta_m \quad (16)$$

Thus, an infinite set of simultaneous equations, having a infinite number of unknowns can, in principle, be solved by standard matrix techniques for $\overline{\Delta C_{p_c}}$. However, this equation can be rewritten as

$$\sum_{j=-\infty}^{0} \sum_{i=1}^{I} A_{kl_{ij}} \overline{\Delta C}_{P_{\infty_{ij}}} = \sum_{m=0}^{M} \sum_{n=1}^{N} (\overline{\Delta C}_{P_{nm}} - \overline{\Delta C}_{P_{\infty_{nm}}}) A_{klnm} + \sum_{m=M}^{\infty} \sum_{n=1}^{N} (\overline{\Delta C}_{P_{nm}} - \overline{\Delta C}_{P_{\infty_{nm}}}) A_{klnm} \quad (17)$$

where M represents a practical limit on the spanwise position at which two-dimensional flow is attained, although ideally this is not satisfied except in the limit

$$\lim_{M\to\infty} \overline{\Delta C}_{P_{Cnm}} \to 0$$

Thus, for $x_3 \geq L \rightarrow m \geq M$, $\overline{\Delta C_{p_{nm}}} \cong \Delta C_{p_{\infty nm}}$ and Eq. 15 can be written

$$\sum_{j=-\infty}^{0} \sum_{i=1}^{I} A_{klij} \overline{\Delta C}_{P_{\infty ij}} + \sum_{m=0}^{M} \sum_{n=1}^{N} A_{klnm} \overline{\Delta C}_{P_{\infty nm}} + \sum_{M}^{\infty} \sum_{n=1}^{N} A_{klnm} \overline{\Delta C}_{P_{\infty nm}} \cong \sum_{m=0}^{M} \sum_{n=1}^{N} A_{klnm} \overline{\Delta C}_{P_{nm}} + \sum_{M}^{\infty} \sum_{n=1}^{N} A_{klnm} \overline{\Delta C}_{P_{\infty nm}} \tag{18}$$

where now the whole left hand side represents the upwash supplied externally and the second term on the right represents the effect of the two-dimensional inboard loading on the tip region. The entire region of the tip effect is bounded spanwise by m = o and m = M. Then Eq. (18) may be rewritten in the form

$$\text{L.H.S.} - \sum_{M}^{\infty} \sum_{n=1}^{N} A_{klnm} \overline{\Delta C}_{P_{\infty nm}} = \sum_{m=0}^{M} \sum_{n=1}^{N} A_{klnm} \overline{\Delta C}_{P_{nm}} \tag{19}$$

which gives a set of N by M simultaneous equations which can be solved directly for the tip loading by standard methods.

Now, the remaining term on the left hand side of Eq. (19) may be written as

$$\sum_{M}^{\infty} \sum_{n=1}^{N} A_{klnm} \overline{\Delta C}_{P_{\infty nm}} = \sum_{M}^{P} \sum_{n=1}^{N} A_{klnm} \overline{\Delta C}_{P_{\infty nm}} + \sum_{P}^{\infty} \sum_{n=1}^{N} A_{klnm} \overline{\Delta C}_{P_{\infty nm}} \tag{20}$$

The term A_{klnm} is the kernel function of subsonic aerodynamics (Ref. 7). Normally the complexity of this function precludes analytic treatment, but for load points that are far removed from the downwash points, the kernel function can be simplified so that some integration can be performed. Hence, in anticipation of these simplifications, the last term of Eq. (20) may be rewritten in integral form

$$\sum_{M}^{\infty} \sum_{n=1}^{N} A_{klnm} \overline{\Delta C}_{P_{\infty nm}} = \sum_{M}^{P} \sum_{n=1}^{N} A_{klnm} \overline{\Delta C}_{P_{\infty nm}} + \frac{1}{8\pi} \int_{yP}^{\infty} \int_{0}^{C} K(x_k - \xi, y_l - \eta) \overline{\Delta C}_{P_{\infty}} d\xi d\eta \tag{21}$$

and Eq. (20), rewritten in the form of Eq. (21), can be determined partly by numerical and partly by analytic means.

The formulation of the problem in this manner, with the external specification of the length, L, is a key development and permits a practical

generalization to the problem. Altering this length can alter the spanwise gradient in the tip region, although as this length increases, the effect on the tip loading will decrease. The choice of L for the present analysis is based on the results of Ref. 8, and was taken to be 4 chordlengths for the calculations performed herein.

The Pressure Loadings On An Infinite Wing Yawed To A Compressible Stream Containing An Imbedded Sinusoidal Gust

The solution to an infinite flat plate wing yawed to a compressible free stream containing an imbedded sinusoidal gust has been developed by Adamczyk (Refs. 5, 6). This solution represents an exact solution to the problem and was developed by casting the acoustic equation as a modified Mathieu equation and expressing the result, as determined by the boundary conditions, in an infinite series of Mathieu functions (Ref. 5). The analytic form of these functions is sufficiently complex that further analysis with then is difficult, but they are well suited to numerical computation. For ease in interpreting the equations of Ref. 6 the gust encounter geometry of Ref. 6 is given in Fig. 4.

The response of the infinite wing to a sinusoidal gust is characterized in Ref. 6 as a two-parameter solution.

$$\beta = \frac{\bar{k} b \cos\alpha}{1 - M^2 \cos^2\theta} \tag{22a}$$

$$\gamma = \frac{\bar{k} b \sin\alpha}{1 - M^2\cos^2\theta} \sqrt{M^{*2} - 1} = \frac{\bar{k} b \sin\alpha}{1 - M^2\cos^2\theta} \left[\left(\frac{M\cos\theta}{\sin\alpha} \right)^2 - 1 \right]^{1/2}$$
$$= \frac{\bar{k} b}{1 - M^2\cos^2\theta} \left[M^2 \cos^2\theta - \sin^2\alpha \right]^{1/2} \tag{22b}$$

The quantity, β, is simply the chordwise reduced frequency component and has its direct counterpart in unswept infinite wing theory. The parameter, γ, determines the behavior of solutions at large distances from the airfoil and is defined as the cutoff parameter in Ref. 6. It enters the problem formulation through a scaling procedure which reduces the acoustic equation to the following form (see Ref. 6).

$$\Phi_{x_1 x_1} + \Phi_{x_2 x_2} + \gamma^2 \Phi = 0 \tag{23}$$

The fundamental solution to this equation is a source with an asymptotic limit given by

$$\Phi \sim \frac{e^{i\gamma R}}{\sqrt{R}} \qquad R = \sqrt{x_1^2 + x_2^2} \tag{24}$$

Form its definition in Eq. (22b), γ^2 is either positive definite or negative definite, and hence γ will either be a pure real or a pure imaginary quantity. Now, if γ is imaginary the solution decays exponentially while if γ is real the solution approaches the asymptotic form of a cylindrical acoustical wave propagating outward from the origin. A key parameter here is M*, the phase Mach number of the disturbance along the span relative to the freestream flow (see Fig. 5a). Whether or not the cut-off parameter, γ, is real or imaginary depends on whether or not M* is greater or less than one.

The effect of the relative phase velocity, M*, is to introduce a spanwise velocity for which the flow appears stationary in an axis system also moving at the spanwise velocity. The nodal lines of the gust in this moving axis system are also stationary. The problem is thereby transformed from the non-stationary problem of a gust encounter at some angle relative to the wing, to a problem involving a stationary gust front parallel to M* and lying across a wing which moves spanwise at a velocity $M^* \cos\alpha$.

Adamczyk (Ref. 6) has successfully simplified the exact solutions for disturbance pressure for limiting cases of this compressibility cut-off parameter. From Ref. 6, the disturbance pressure can be written in several different forms for various values of the cut-off paramter, γ. When γ^2 is a small positive quantity,

$$P_S = -\frac{\rho_0 U \bar{u}_2 \cos\theta}{(1-M^2\cos^2\theta)^{1/2}} \sqrt{\frac{1-x_1}{1+x_1}} \left[\frac{J_0(\beta) - Z J_1(\beta)}{1+Z}\right] \cdot \tag{25}$$

$$\exp\left\{i\left[-\beta M^2 \cos^2\theta x_1 + \frac{\bar{k} b \sin\alpha}{(1-M^2\cos^2\theta)^{1/2}} x_3 - \bar{k} U \cos(\theta-\alpha) t\right]\right\}$$

with

$$Z = -\frac{iH_0(\beta) + i(\gamma/\beta)^2\left[H_0^{(1)}(\gamma/2) - H_0^{(1)}(\beta)\right]}{H_1^{(1)}(\beta)} \qquad 0 \le \gamma^2 \le 0.1$$

When γ^2 is negative,

$$P_S = -\frac{\rho_0 U \bar{u}_2 \cos\theta}{(1-M^2\cos^2\theta)^{1/2}} \sqrt{\frac{1-x_1}{1+x_1}} \frac{H(\gamma,\beta)}{I_0(\gamma) + I_1(\gamma)} \cdot$$

$$\exp\left[-(\gamma + i\beta M^2 \cos^2\theta) x_1 + \frac{i\bar{k} b \sin\alpha}{(1-M^2\cos^2\theta)^{1/2}} x_3 - i\bar{k} U \cos(\theta-\alpha) t\right] \tag{26}$$

where

$$H(\gamma,\beta)=\frac{\exp\left\{-i\sqrt{\gamma^2+\beta^2}\left[\cos\delta-\pi\left(\frac{\pi}{2}-\delta\right)\left(1+\frac{\sin\delta}{2}\right)\right]/\left(1+2\pi\sqrt{\gamma^2+\beta^2}\left(1+\frac{\sin\delta}{2}\right)\right)\right\}}{1+\pi\sqrt{\gamma^2+\beta^2}\left[1+\cos^2\delta+\pi\sqrt{\gamma^2+\beta^2}\,\sin\delta\right]}$$

$$\delta=\tan^{-1}(\gamma/\beta) \qquad 0>\gamma^2$$

For larger positive and negative values of γ^2,

$$P_S=-\frac{\rho_0 U\bar{u}_2\cos\theta}{(1-M^2\cos^2\theta)^{1/2}}\;\frac{1}{\sqrt{\pi(\beta+\gamma)}}\left\{\frac{1+i}{\sqrt{2x_1'}}-\frac{1+i}{2}+E^*\left(\sqrt{2\gamma(2-x_1')}\right)\right\}\cdot$$
$$\exp\left\{i\left[(\gamma-\beta M^2\cos^2\theta)x_1'+\bar{k}b\sin\alpha\,x_3-U\bar{k}\cos(\theta-\alpha)t\right]\right\} \qquad (27)$$

$$x_1'=x_1+1 \qquad |\gamma^2|>0.7$$

where

$$E(x)=C(x)-iS(x)$$

$$E^*(x)=\text{CONJUGATE } E(x)$$

The corresponding pressure loading on the yawed infinite flat plate wing responding to the sinusoidal gust can be obtained from

$$\overline{\Delta C}_{P_\infty}=\text{CONJ}\left[-\frac{2P_S}{\frac{1}{2}\rho_0 U^2}\;\exp i\,U\bar{k}\cos(\theta-\alpha)t\right] \qquad (28)$$

The complex conjugate is taken since Adamczyk solved the conjugate problem to the formulation described herein.

In the present analysis Eq. (25), (26), or (27) will be used, depending on the value of γ^2. If γ^2 does not fall within the prescribed ranges, the exact solution will be used (cf., Ref. 6).

The steady flow contribution from a flat plate at an angle of attack is obtained as a limiting case of the unsteady analysis at zero reduced frequency. The effect of the steady flow camber problem can be treated by obtaining a potential flow solution for an infinite wing and then accounting for compressibility by way of the Karman-Tsien relation (Ref. 9). A suitable potential flow result for an arbitrary mean line is given by the Munk integral (Ref. 3).

$$\Delta C_P(\psi)=-\frac{2\cos^2\theta}{\pi\sin\psi}\int_0^{2\pi}\frac{dx_2}{dx_1}(\tau)\left[\cot\left(\frac{\psi-\tau}{2}\right),\sin\tau+1+\cos\tau\right]d\tau \qquad (29)$$

where $\psi = \cos^{-1}\frac{2x_1}{c}$. Instead of using the Prandtl-Glauert correction factor to account for compressibility effects, the Karman-Tsien relationship, which is more accurate at high subsonic Mach numbers, is used. This relation is given by

$$\frac{C_{PM}}{C_{Pi}} = \frac{1}{\sqrt{1-M^2} + \frac{M^2}{1+\sqrt{1-M^2}}\frac{C_{Pi}}{2}} \tag{30}$$

where C_{p_M} is the pressure coefficient at the Mach number M, and C_{p_i} is the incompressible pressure coefficient at the same location in the flow.

At this point attention can be turned momentarily to the problem of determining the pressure in the flow field near the wing but off the surface. The leading edge pressure singularity, which is inherent in the theories of infinitely thin wings and which generally causes no problems in computing the aerodynamics of these wings, must now be treated. If the loading on the wing is represented by pressure dipoles, the disturbance pressures at any point in the flow may be directly determined by

$$\bar{p}(\underline{x}) = \frac{1}{4\pi}\frac{\partial}{\partial x_2}\int_{\text{WING AREA}} \frac{\Delta\bar{p}(\xi,\eta)}{R} e^{i\omega\left[\frac{-M(x-\xi)+\sqrt{(x-\xi)^2+(1-M^2)[x^2+(y-\eta)^2]}}{a_0(1-M)^2}\right]} d\xi\, d\eta \tag{31}$$

where $R = \sqrt{(x-\xi)^2 + x_2^2 + (y-\eta)^2}$

Unfortunately, the infinite strength dipole at the leading edge will then present infinite pressures throughout the fluid, an obvious physical unreality. Hence, the loadings in the vicinity of the leading edge must be modified to eliminate this singularity.

Lighthill (Ref. 10) has successfully modified incompressible two-dimensional thin airflow theory to eliminate the leading edge singularity. It is required that the flow near a smooth leading edge be the flow over a parabola, while at points away from the leading edge the flow is adequately predicted by thin airfoil theory. This moves the singularity inside the airfoil contour and provides a smooth flow exterior to the thin wing. As a result the pressure loading on a thin wing can be given, to a first approximation, by the following equation,

$$\frac{\Delta C_P}{\Delta C_{P\,T.A.}} = \frac{x}{x+\rho_L/2} \tag{32}$$

where x is the distance from the leading edge, ΔC_p is the actual pressure loading across the wing, $\Delta C_{pT.A.}$ is the thin airfoil theory result at the corresponding chordwide position and ρ_L is the airfoil leading edge radius of curvature. Since $\Delta C_{pT.A.}$ varies as $(x)^{-1/2}$ near the leading edge it is easily

seen that ΔC_p approaches zero continuously as the leading edge is neared. As x approaches unity, ΔC_p approaches its thin airfoil value. Without direct proof, it is assumed the same results will hold for subsonic compressible flow; this is based on the fact that the behavior of the leading edge singularity is the same regardless of compressibility or unsteadiness. That is, for unsteady compressible flow ΔC_p varies as $[x]^{-1/2}$ near the leading edge.

The solution to the problem of predicting the pressure field in the vicinity of a swept, semi-infinite wing consists of a numerical solution to Eq. (19), utilizing the proper value of $\overline{\Delta C_{p\infty}}$. The necessary doublet-lattice influence coefficients were developed by Giesing, et al (Ref. 7) and the underlying assumptions in their derivation restrict the solution to the case of tip chord parallel to the flow. Once the thin wing results for the loading are determined, the leading edge singularity is removed by Eq. (32) and the pressures in the near field are determined from the dipole distribution, Eq. (31).

An Asymptotic Solution For The Upwash Induced At The Tip By Portions of The Wing Far Removed From The Tip

Equation (21) which is repeated below for convenience, describes the upwash on the tip due to that portion of the wing which experiences two-dimensional flow.

$$\sum_{M}^{\infty}\sum_{n=1}^{N} A_{klmn}\,\overline{\Delta C}_{P_{mn}} = \sum_{M}^{P}\sum_{n=1}^{N} A_{klmn}\,\overline{\Delta C}_{P\infty_{mn}} + \frac{1}{8\pi}\int_{\lambda}^{\infty}\int_{-b}^{b} K(x_{l_m}-\xi_1, x_{3_n}-\xi_3)\,\overline{\Delta C}_{P\infty}\,d\xi_1\,d\xi_3 \qquad (21)$$

Here A_{klmn} represents a numerical form of the unsteady subsonic flow kernel function, $K(x_1-\xi_1, x_3-\xi_3)$, both of which are given in Ref. 7. The continuous form, K, of the kernel function is more amenable to analytic treatment. The following relations, from Ref. 7, are required to perform the integration in Eq. (21).

$$K(x_0,r)=e^{-i\omega x_0}\,K_1/r^2 \qquad K_1=I_1+\frac{Mr}{R}\left\{\frac{e^{-ik_1u_1}}{(1+u_1^2)^{1/2}}\right\} \qquad r=y_0$$

$$R=(x_0^2+\beta^2 y_0^2)^{1/2} \qquad x_0=x-\xi \qquad \beta=\left[1-M^2\right]^{1/2} \qquad y_0=y-\eta \qquad (33)$$

The integral I_1 is given exactly by

$$I_1 = \int_{u_1}^{\infty} \frac{e^{-ik_1 u} du}{(1+u^2)^{3/2}} \tag{34}$$

and approximately by

$$I_1 = e^{-ik_1 u_1}\left[1 - \frac{u_1}{(1+u_1^2)^{1/2}} - ik_1 I_0(u_1, k_1)\right] \tag{35}$$

where

$$I_0(u_1, k_1) \cong \sum_{n=1}^{11} \frac{a_n e^{-ncu_1}(nc - ik_1)}{n^2 c^2 + k_1^2} \tag{36}$$

was developed by Laschka (Ref. 11) and is reproduced in Ref. 7. The Laschka coefficients necessary for this approximation are a_n, n, and c.

In general the spanwise variation in $\overline{\Delta C_{p_\infty}}$ is oscillatory due to the spanwise component of the gust. From the form of Eqs. (25), (26), or (27) it can be seen that

$$\overline{\Delta C}_{P_\infty} = \overline{\Delta C}_{P_1}(\xi_1)\ e^{-i\beta M^2 \cos^2\theta \xi_1 + i\bar{k}\sin\alpha \xi_3} \tag{37}$$

Thus the term in integral form on the right hand side of Eq. (21) can be written as

$$\int_{-b}^{b} \overline{\Delta C}_{P_1} e^{-i\beta M^2 \cos^2\theta \xi_1} \int_{\lambda}^{\infty} e^{i\bar{k}\sin\alpha \xi_2}\ e^{-\frac{i\omega}{U}[(x_1-\xi_1)\cos\theta + (x_3-\xi_3)\sin\theta]} \frac{K_1}{r^2}\ d\xi_3 d\xi_1$$

Defining $\eta_r = x_3 - \xi_3$ this can be restated as

$$-\int_{-b}^{b} \overline{\Delta C}_{P_1} e^{-i\beta M^2 \cos^2\theta \xi_1}\ e^{i\bar{k}\sin\alpha x_3}\ e^{-\frac{i\omega}{U}(x_1-\xi_1)\cos\theta} \int_{x_3-\lambda}^{-\infty} e^{-i[\bar{k}\sin\alpha + \frac{\omega}{U}\sin\theta]\eta_r} \frac{K_1}{r^2}\ d\eta_1 d\xi_1$$

Define the distance along the span between the point at which the upwash is desired and the load is applied to be η_r. If this quantity is large certain approximations in the kernel function, K_1/r^2 can be made. In particular,

$$r^2 = y_o^2 \cong \eta_r^2 \cos^2\theta$$

$$rR \cong \eta_r^2 \cos^2\theta (\tan^2(-\theta+\epsilon) + \beta^2)^{1/2}$$

$$u_1 \cong \frac{M(\tan^2(-\theta+\epsilon)+\beta^2)^{1/2} - \tan(-\theta+\epsilon)}{\beta^2}$$

$$k_1 u_1 \cong \frac{\frac{\omega}{U}\eta_r \cos\theta\left[M(\tan^2(-\theta+\epsilon)+\beta^2)^{1/2} - \tan(-\theta+\epsilon)\right]}{\beta^2}$$

Combining these approximate forms, the kernal function has the following approximate form

$$\frac{K_1}{r^2} \cong \left[\frac{C_3}{C_4} + \frac{M}{C_1}\right] \frac{e^{-iC_2\eta_r}}{\eta_r^2} + \frac{1}{C_4} \sum_{n=1}^{N} \frac{b_n e^{-iC_2\eta_r}}{g_n^2 + \eta_r^2} - \frac{i}{C_4} \sum_{n=1}^{II} \frac{d_n e^{-ic_2\eta_r}}{\eta_r \left[g_n^2 + \eta_r^2\right]} \qquad (38)$$

with $C_1 = \cos^2\theta$ $\qquad C_2 = \frac{\omega}{U}\cos\theta \, \frac{\left[M(\tan^2(-\theta+\epsilon)+\beta^2)^{1/2} - \tan(-\theta+\epsilon)\right]}{\beta^2}$

$$C_3 = 1 - \frac{u_1}{\sqrt{1+u_1^2}} \qquad C_4 = C_1 \qquad b_n = a_n e^{-ncu_1} \qquad d_n = b_n * g_n \qquad g_n = \frac{nCU}{\omega\cos\theta}$$

$$u_1 \cong \left[M(\tan^2(-\theta+\epsilon)+\beta^2)^{1/2} - \tan(-\theta+\epsilon)\right]/\beta^2$$

The angle, ϵ, is the angle between the load point on the wing and the point at which flow tangency is satisfied, measured from a spanwise line through the load point (see Fig. 5b). Note that this angle is a function of chord, but for large spanwise distances between the loadpoint and the flow tangency point this variation can be neglected. The integral

$$\int_{x_3-\lambda}^{-\infty} e^{-i\left[\bar{k}\sin\alpha + \frac{\omega}{U}\sin\theta\right]\eta_r} \frac{K_1}{r^2} \, d\eta_r$$

can be evaluated by first defining a parameter

$$D = \bar{k}\sin\alpha + \frac{\omega\sin\theta}{U} + \frac{\omega\cos\theta}{U}\left[\frac{M(\tan^2(-\theta+\epsilon)+\beta^2)^{1/2} - \tan(-\theta+\epsilon)}{\beta^2}\right]$$

Use of this parameter then permits evaluation of the following integral forms:

$$\int_{x_3-\lambda}^{-\infty} \frac{e^{-iD\eta_r}}{\eta_r^2} \, d\eta_r ; \qquad \int_{x_3-\lambda}^{-\infty} \frac{e^{-iD\eta_r}}{g_n^2+\eta_r^2} \, d\eta_r ; \qquad \int_{x_3-\lambda}^{-\infty} \frac{e^{-iD\eta_r}}{\eta_r\left[g_n^2+\eta_r^2\right]} \, d\eta_r$$

The integrations are performed in the complex plane and the following simple form is obtained

$$\int_{x_3-\lambda}^{-\infty} e^{-iD\eta_r} \frac{K_1}{r^2} \, d\eta_r \cong \left[\frac{C_3}{C_4} + \frac{M}{C_1}\right] \frac{\pi D}{2} + \frac{SGN(D)}{C_4} \frac{\pi}{2} \sum_{n=1}^{II} \frac{a_n e^{-ncu_1}}{g_n} \left[1 - SGN(D)\, 2\, e^{-|G_n|}\right] \qquad (39)$$

where

$$G_n = Dg_n$$

This calculation represents a small, real component to the upwash due to portions of the wing far removed from the tip region.

NUMERICAL RESULTS FOR INVISCID PRESSURE FIELD

The computational procedure to determine the tip loading consists of representing the tip region ($0 < x_3 < L$) by the doublet-lattice model described in Ref. 7. Use of this model presently restricts the tip chord line to be parallel to the freestream. The length, L, at which the tip influence substantially disappears is adequately given by 4 chord lengths. The inboard reagion of the wing is described by a combination of analytical and numerical forms, utilizing the infinite wing results of Ref. 6, the numerical kernel function of Ref. 7, and Eq. (39). Camber effects due to an infinite wing in steady subsonic flow are treated by combining the incompressible solution of Eq. (29) with the Karman-Tsien equation (Eq. 30) to account for compressibility. Equation (19) is then solved numerically for the unknown pressure loads on the tip, ΔC_{pnm}. The final loads on the tip region are obtained by removing the leading edge singularity from the ΔC_{pnm} via Eq. (32).

Before applying the approximate pressure fields described by Eqs. (25), (26), and (27) to the solution for the semi-infinite wing, it is desirable to establish some limits of accuracy for these analytic forms. The quantity of primary interest is, of course, the pressure. However, the lift transfer function T_L (which is a normalized lift coefficient that includes the effects of compressibility and the wake) is also of interest and has been examined in the figures which follow. Adamczyk (Ref. 6) has developed these transfer functions for the following tentative values of the cut-off parameter.

$$T_L = e^{ibk\cos\alpha}\left[\frac{J_0(\beta)-iZJ_1(\beta)}{1+Z}\right]\left[J_0(M^2\beta\cos^2\theta)+iJ_1(M^2\beta\cos^2\theta)\right] \qquad 1>\gamma>0 \qquad (40)$$

$$T_L = \frac{I_0(\gamma+i\beta M^2\cos^2\theta)+I_1(\gamma+i\beta M^2\cos^2\theta)}{I_0(\gamma)+I_1(\gamma)}\,H(\gamma,\beta)\,e^{i\bar{k}b\cos\alpha}$$

$$H(\gamma,\beta) = \frac{e^{-i\sqrt{\gamma^2+\beta^2}}\left\{\cos\delta - \dfrac{\pi\left[\frac{\pi}{2}-\delta\right]\left[1+\frac{1}{2}\sin\delta\right]}{1+2\pi\sqrt{\gamma^2+\beta^2}\,[1+0.5\sin\delta]}\right\}}{1+\pi\sqrt{\gamma^2+\beta^2}\left[1+\cos^2\delta+\pi\sqrt{\gamma^2+\beta^2}\,\sin\delta\right]} \qquad \gamma^2<0 \qquad (41)$$

$$T_L = \frac{1}{\sqrt{\pi(\beta+\gamma)}}\left\{(1+i)\sqrt{\frac{\pi}{\gamma-\beta M^2\cos^2\theta}}\,E^*\left[\sqrt{2(\gamma-\beta M^2\cos^2\theta)}\right]\right.$$
$$+\left[1-e^{2i(\gamma-\beta M^2\cos^2\theta)}\right]\frac{1-i}{2(\gamma-\beta M^2\cos^2\theta)}+\frac{iE^*\left[\sqrt{4\gamma}\right]}{\gamma-\beta M^2\cos^2\theta}$$
$$\left.-\frac{i\sqrt{2\gamma}}{\gamma-\beta M^2\cos^2\theta}\,\frac{e^{2i(\gamma-\beta M^2\cos^2\theta)}}{\sqrt{\gamma+\beta M^2\cos\theta}}\,E\left[\sqrt{2(\gamma+\beta M^2\cos^2\theta)}\right]\right\} \qquad (42)$$
$$|\gamma^2|>>1$$

where Z and H (γ,β) are defined in Eqs. (25) and (26). Note these transfer functions are referred to the gust amplitude at the leading edge rather than mid-chord.

In Fig. 6 the "exact" solution for T_L is compared with the approximate forms for positive γ^2 in Eqs. (40) and (42). (The exact calculations were obtained by a direct numerical integration of Eq. 21 of Ref. 6.) The upper panel contains the comparison for M = 0.3 and the lower panel for M = 0.6, both over the range of reduced frequencies $0.05 \leq \bar{k}b \leq 6.0$. In both cases it is seen that Eq. (40) which is the low frequency approximation, compares favorably with the exact solution up to $\bar{k}b = 0.2$. Beyond this value Eq. (40) diverges from the exact solution, with a greater divergence at M = 0.6 than at M = 0.3. In contrast to this, Eq. (42), which is the high frequency approximation, is in poor agreement for $\bar{k}b < 0.5$, but improves in its ability to represent the exact solution as $\bar{k}b$ increases beyond this value. This is also illustrated in Fig. 7 in which the magnitude and phase angle of T_L are plotted versus the cut-off parameter γ. Based on the results of these two figures, it appears that Eq. (40) can be used for $\gamma \lesssim 0.3$ while Eq. (42) can be used for $\gamma \gtrsim 0.3$.

Figure 8 shows the chordwise pressure distribution on an infinite wing at a Mach number of 0.3 for a reduced frequency of 0.1 in part a (and shows the variation with reduced frequency at x/c = 0.2 in part b). Comparison of these results indicate that Eq. (25) yields acceptable pressure distributions for $\gamma \lesssim 0.2$ while Eq. (27) is more than adequate for $\gamma \gtrsim 0.2$. Figure 9 shows a similar set of comparisons for a Mach number of 0.6. For this set of conditions, Eq. (25) represents an adequate solution up to $\bar{k}b = 0.1$ and is possibly extendable to $\bar{k}b \cong 0.2$. Equation (27), however, appears to compare quite well with the exact results beyond $\bar{k}b \cong 0.2$. This implies that Eq. (27) still gives an adecritpion of the pressures for $\gamma \gtrsim 0.2$ while Eq. (25) is valid for $\gamma \lesssim 0.2$.

It should be noted that the foregoing comparisons relate to conditions for $\gamma^2 > 0$, in which acoustic propagation is present. The conditions for $\gamma^2 < 0$ have not been investigated herein and remain a field for further study.

Deviations begin to appear in both the lift transfer function and the pressure distributions at high values of reduced frequency at both Mach numbers considered with the deviations becoming more pronounced as Mach number increases. This is a result believed due to the truncation of the infinite series of Mathieu function which describes the exact solution. Equation (27) is a solution comprised of the first two terms of an infinite series in reduced frequency in which the disturbance due to the plate is modeled by acoustical waves emanating from the leading and trailing edges. This solution inherently

increases in accuracy as the reduced frequency increases (at a given Mach number $\neq 0$) and so it is expected the results of Eq. (27) are more accurate than the truncated representation of the exact solution at high values of $\bar{k}b$.

Pressure Loadings on The Semi-Infinite Wing

Figures 10 and 11 describe the spanwise variation in chordwise pressure distributions of the semi-infinite wing at various sweep angles. The wing is an uncambered flat plate at an angle of attack of 0.25 rad in incompressible flow. Generally, the chordwise distributions are of similar form, and the spanwise variation decreases smoothly to zero at the tips. The effect of sweep is to lower the overall magnitudes.

Figure 12 represents the steady response of a cambered (NACA 4415 profile) unswept semi-infinite wing at an angle of attack of 0.25 rad. A comparison of this figure with Fig. 10 shows that the effect of camber is to increase the chordwise load distribution. For completeness, the unsteady distribution for $\bar{k}b = 0.1$ is included in Fig. 13. As stated earlier in the text, the complete solution is the linear superposition of the steady and unsteady components of the response which are illustrated in Figs. 12 and 13.

Pressure Distribution In The Vicinity of Tip of Semi-Infinite Wing

Figure 14 shows the pressures in a region surrounding the tip of a semi-infinite unswept wing in steady subsonic flow at a Mach number of 0.2. The angle of attack is taken to be 0.1 rad and camber is zero. In each panel the pressure coefficient is plotted horizontally versus the normal distance to the plane of the wing. The left column of panels at $y/c = 2.0$ is the distribution two chordlengths inboard of the wing tip, and the right column of panels at $y/c = -2.0$ is the distribution two chordlengths outboard of the tip. The first horizontal row at $x/c = 0.15$ is the distribution at points that are 15 percent chord aft of the leading edge locus, the second row for $x/c = 0.95$ (consisting of a single panel) is at a point that is 95 percent chord aft of the leading edge locus, and the third row at $x/c = 1.45$ is for points that are 45 percent chord aft of the trailing edge locus. The right hand column can be dismissed immediately as representing typical variations of pressure in the vicinity of, but external to, a lifting surface and its wake. The top panel of the left hand column for a point near the wing leading edge contains the characteristic jump due to the dipole loading. Negative pressures ($C_p < 0$) are observed for $x_2 > 0$ while positive pressures are observed for $x_2 < 0$. The bottom panel of the left hand column for a point in the wing wake shows the far field dipole influence at points far removed from the wake $|x_2| \gg 0$.

However, as the wake is approached a reversal of this trend is observed and the boundary condition of zero pressure difference in the wake is satisfied. Finally, the center panel of the left hand column represents a point near the wing trailing edge. Here the pressure variation is transitional between the dipole jump on the wing and the continuous pressure in the wake. As the wing is approached the pressure magnitude initially increases. At a small but finite distance from the surface of the wing, the trend is reversed and the pressures tend toward zero, but terminate in a discontinuous dipole jump on the surface. This combination of form, near a point where the boundary conditions change abruptly, is characteristic of the elliptic equations which describe subsonic steady flow.

VISCOUS FLOW CONSIDERATIONS

General

Although an accurate solution of the potential flow equations can give a qualitative picture of the flow in the region of an airfoil tip, the flow field in this region is affected significantly by three-dimensional viscous phenomena arising from boundary layers on both the upper and lower wing surface as well as on the wing tip itself. Viscous effects could be modeled partially in a potential flow solution through use of isolated and discrete vortex filaments. The filaments would represent the vorticity originally generated in the viscous boundary layers which break away from the airfoil to form the wake. However, a complete potential flow solution which includes discrete vortices would require a calculation of the interaction of the vortices with each other as well as their combined effect upon the wing. However, even such a complete potential solution could not satisfy the surface no-slip boundary condition. Although failure to satisfy the no-slip boundary condition may not be serious in determining the pressure field, it may lead to inaccurate predictions of secondary flows in the vicinity of the wing even in regions which have little direct viscous effects. In addition, a vortex filament solution would require assumptions on the vortex core size and upon the position and angle at which the filaments leave the wing as both of these items are dependent upon viscous effects.

Since a complete interacting vortex filament-potential flow solution would not be able to model either the airfoil boundary layer or the viscous core correctly but would still present a formidable computational problem, it is appropriate to consider viscous solutions of the tip flow field. One possible viscous solution would attack the full three-dimensional Navier-Stokes equations. Solutions of the full Navier-Stokes equations can now be considered possible (e.g., see Briley and McDonald(Ref. 12)), however, their relatively long computer run times dictate that the full three-dimensional Navier-Stokes equations be solved only when no suitable alternative is available.

Although flow situations exist for which a three-dimensional Navier-Stokes solution is appropriate and necessary, the wing tip problem does contain simplifying features that may alleviate the need for a full three-dimensional Navier-Stokes solution. In particular, the tip flow region contains a primary flow direction which, for the zero camber case considered in the present effort, is in the plane of the oncoming flow and at only a small angle relative to the wing chord. Furthermore, the velocity component in the streamwise direction is considerably greater than velocity components normal to this

streamwise direction and derivatives in the streamwise direction are expected to be considerably less than derivatives normal to this streamwise direction. In this sense, the problem appears to be similar to the classical three-dimensional boundary layer problem. However, the classical three-dimensional boundary layer approach imposes two additional assumptions which are not valid in the airfoil tip region. Under the first of these additional assumptions the static pressure is assumed to be invariant in a plane normal to the streamwise direction; obviously, such an assumption upon the static pressure clearly makes classical three-dimensional boundary layer theory invalid for the airfoil tip problem. Secondly, three-dimensional boundary layer theory assumes that significant gradients exist in one direction only, i.e., that a thin relatively flat boundary sheet exists wherein viscous effects resulting from the mean flow gradients are significant only as a result of the velocity change across the sheet and not along the sheet. Obviously the assumption of a thin relatively flat boundary sheet is inappropriate in the region of a wing tip.

The need to develop a three-dimensional forward marching viscous calculation procedure which is more general than three-dimensional boundary layer theory has been motivated by a variety of fluid mechanics problems such as three-dimensional duct flow problems, three dimensional jet problems, and the airfoil tip problem. Therefore, considerable recent effort has been expended upon development of computational procedures for three-dimensional viscous flows with a dominant streamwise direction. These procedures would not be limited by the classical three-dimensional boundary layer assumption of constant static pressure in planes normal to the approximate flow direction but would still allow treatment of the flow field in question as an initial value problem. Such three-dimensional viscous forward marching solutions have been developed by Patankar and Spalding (Ref. 13), Caretto, Curr and Spalding (Ref. 14) and Briley (Ref. 15) all of whom developed numerical solutions for laminar incompressible flows in straight ducts with rectangular cross sections. The governing equations were solved by integrating in a primary flow coordinate direction while retaining viscous stresses in <u>both</u> transverse coordinate directions as opposed to only one direction for three-dimensional boundary layer theory. In addition, certain assumptions were made about the behavior of pressure gradient terms for incompressible flow to permit solution by forward marching integration. Subsequently, this general approach has been used to compute laminar incompressible flow in helical tubes by Patankar, Pratap and Spalding (Ref. 16).

Recently in companion studies, Briley and McDonald (Refs. 12, 17) have developed a stable and efficient noniterative implicit numerical technique for application to systems of coupled nonlinear multidimensional parabolic and/or hyperbolic equations. These general techniques were applied in

Ref. (17) to the computation by forward marching integration of laminar supersonic flow in rectangular jets. Finally, the technique was extended in Ref. (18) to the prediction of subsonic turbulent compressible flow in curved ducts. In the present effort this same basic viscous, three-dimensional forward marching technique is applied to the airfoil tip problem, and a preliminary assessment of its potential for calculating the tip flow field is made.

The Governing Equations

Central to the present analysis is the formulation of approximate governing equations which can be solved by forward marching integration in the direction of a "primary flow". The entire flow field then can be obtained by a sequence of essentially two-dimensional calculations, and this feature of the method results in a substantial saving of computer time and storage compared to that which would be required for solution of the full (elliptic) Navier-Stokes equations. Although the present effort utilizes a cartesian coordinate system to represent the airfoil tip flow field, the equations have been derived and coded in a more general orthogonal system. The reduction to a cartesian system is straightforward and is indicated during the discussion.

The equations are derived in a curvilinear orthogonal coordinate system which is aligned with the flow geometry such that one coordinate direction can be identified as the primary flow direction while the remaining two coordinate directions determine the secondary flow plane. The transverse plane is assumed to be perpendicular to the airfoil. Only the tip region of the airfoil within one-half chord of the edge is considered. The airfoil tip is assumed to lie in the plane $z = 0$ between $0 \leq x \leq c$ and $-h/2 \leq y \leq h/2$ where h is the airfoil thickness. The leading and trailing edges of the airfoil are assumed to lie in the planes $x = 0$ and $x = c$, respectively. A sketch of the airfoil tip coordinate system used in the viscous analysis is presented in Fig. 15.

In the general case x, y, and z represent the approximate streamwise (primary flow) and two transverse coordinates in an orthogonal coordinate system, respectively. Since the analysis consideres a general orthogonal system, metric coefficients h_1, h_2, and h_3 are defined such that an incremental distance $(\delta s)^2 = (h_1 \delta x)^2 + (h_2 \delta y)^2 + (h_3 \delta z)^2$; for a cartesian system $h_1 = h_2 = h_3 = 1$. The governing equations are derived from the Navier-Stokes equations describing the compressible flow of a viscous, heat conducting, perfect gas. In vector form, these equations are given by

$$\partial\rho/\partial t + \nabla \cdot (\rho\vec{U}) = 0 \tag{43a}$$

$$\rho\partial\vec{U}/\partial t + \rho(\vec{U}\cdot\nabla)\vec{U} + \nabla p = F \tag{43b}$$

where U is the velocity vector, ρ is density, t is time, p is pressure, F is a vector representing the viscous force acting on the surface of a fluid element and ∇ is the gradient operator. The total enthalpy E may be specified through an energy conservation equation (Ref. 18); however, in the present effort the assumption is made that the total temperature is constant throughout the flow field. The equation of state is $p = \rho RT$, where R is the gas constant. Expressions defining F in an orthogonal coordinate system are given by Pai (Ref. 19) and may be found in Ref. 18.

In the present analysis the reasoning followed to estimate the order of magnitude of viscous terms and turbulence quantities is the same as is often employed to derive three-dimensional boundary layer equations. The rationale is discussed in detail in Ref. 18, and for convenience this discussion is now repeated in a condensed form. As discussed in Ref. 18, it is assumed that, viscous effects are negligible except in thin layers near solid boundaries, and thus boundary layer concepts can be employed to examine the relative importance of viscous terms in the governing equations. Consequently, viscous terms which are considered important for boundary layer flow on solid surfaces aligned with either of the two coordinate planes which are parallel to the primary flow coordinate are retained throughout the entire region of the viscous flow calculation; other viscous terms are neglected. In the context of the present investigation the lower and upper surfaces of the wing represent solid surfaces aligned in the 'y'-direction and the tip represents a solid surface aligned in the 'z'-direction. Both of these solid surfaces are parallel to the primary flow direction, 'x'. If the flow is turbulent, the governing equations are time-averaged in the usual manner for turbulent flows (e.g., Hinze, Ref. 20). The dependent variables are represented as the sum of a time-averaged quantity denoted by an overbar ($\bar{}$) and an instantaneous fluctuating quantity denoted by a prime ('). This process of averaging produces turbulent correlations which are conventionally termed Reynolds stresses. The order of magnitude of viscous terms, including the turbulent Reynolds stresses, is examined under two sets of circumstances, namely, those appropriate for boundary layer flow near either of two types of wall, one for which y is constant (a y- wall) and one for which z is constant (a z- wall). Near a y-wall, (v/U_{REF}) and $\partial(\ )/\partial(y/L_{REF})$ are assumed to be of order δ and $1/\delta$ respectively; near a z-wall, (w/U_{REF}) and $\partial(\ )/\partial(z/L_{REF})$ are of order δ and $1/\delta$. Here, δ is the shear layer thickness. If the viscous terms are to be

of the same order of magnitude as the remaining terms, then the dimensionless molecular viscosity ($\mu/\rho_{REF}\nu_{REF}L_{REF}$) must be of the order δ^2. Similarly, it is assumed that dimensionless turbulent double correlations are of order δ (i.e., turbulent fluctuations are of order $\delta^{\frac{1}{2}}$) and that triple correlations are negligible. All other dependent variables and derivatives are assumed to be of order unity. Retaining only those terms which are of order unity in <u>either</u> of the two types of shear layers described above, the viscous terms are greatly simplified, and the time-averaged governing equations can be written in the following form:

$$\frac{\partial}{\partial x}\left(h_2 h_3 \bar{\rho}\,\bar{u}\right) + \frac{\partial}{\partial y}\left(h_1 h_3 \overline{\rho v}\right) + \frac{\partial}{\partial z}\left(h_1 h_2 \overline{\rho w}\right) = 0 \tag{44a}$$

$$\frac{\partial}{\partial x}\left(h_2 h_3 \bar{\rho}\bar{u}^2\right) + \left[\frac{\partial}{\partial y} + \frac{1}{h_1}\frac{\partial h_1}{\partial y}\right]\left(h_1 h_3 \overline{\rho v}\,\bar{u}\right) + \left[\frac{\partial}{\partial z} + \frac{1}{h_1}\frac{\partial h_1}{\partial z}\right]\left(h_1 h_2 \overline{\rho w}\,\bar{u}\right)$$

$$- h_3 \bar{\rho}\bar{v}^2 \frac{\partial h_2}{\partial x} - h_2 \bar{\rho}\bar{w}^2 \frac{\partial h_3}{\partial x} + h_2 h_3 \frac{\partial \bar{p}}{\partial x} \tag{44b}$$

$$= h_1 h_3 \frac{\partial}{\partial y}\left[\frac{\mu}{h_2}\frac{\partial \bar{u}}{\partial y} - \bar{\rho}\overline{v'u'}\right] + h_1 h_2 \frac{\partial}{\partial z}\left[\frac{\mu}{h_3}\frac{\partial \bar{u}}{\partial z} - \bar{\rho}\overline{w'u'}\right]$$

$$\left[\frac{\partial}{\partial x} + \frac{1}{h_2}\frac{\partial h_2}{\partial x}\right]\left(h_2 h_3 \bar{\rho}\,\bar{u}\bar{v}\right) + \frac{\partial}{\partial y}\left(h_1 h_3 \overline{\rho v}\;\bar{v}\right)$$

$$+ \left[\frac{\partial}{\partial z} + \frac{1}{h_2}\frac{\partial h_2}{\partial z}\right]\left(h_1 h_2 \overline{\rho w}\,\bar{v}\right) - h_3 \bar{\rho}\bar{u}^2 \frac{\partial h_1}{\partial y} - h_1 \bar{\rho}\bar{w}^2 \frac{\partial h_3}{\partial y}$$

$$+ h_1 h_3 \frac{\partial p}{\partial y} = h_1 h_2 \frac{\partial}{\partial z}\left[\frac{\mu}{h_3}\frac{\partial \bar{v}}{\partial z} - \bar{\rho}\overline{w'v'}\right] \tag{44c}$$

$$\left[\frac{\partial}{\partial x} + \frac{1}{h_3}\frac{\partial h_3}{\partial x}\right]\left(h_2 h_3 \bar{\rho}\,\bar{u}\bar{w}\right) + \frac{\partial}{\partial z}\left(h_1 h_2 \overline{\rho w}\;\bar{w}\right) + \left[\frac{\partial}{\partial y} + \frac{1}{h_3}\frac{\partial h_3}{\partial y}\right]\left(h_1 h_3 \overline{\rho v}\;\bar{w}\right)$$

$$- h_2 \bar{\rho}\bar{u}^2 \frac{\partial h_1}{\partial z} - h_1 \bar{\rho}\bar{v}^2 \frac{\partial h_2}{\partial z} + h_1 h_2 \frac{\partial p}{\partial z} = h_1 h_3 \frac{\partial}{\partial y}\left[\frac{\mu}{h_2}\frac{\partial \bar{w}}{\partial y} - \bar{\rho}\overline{v'w'}\right] \tag{44d}$$

For entirely supersonic flows, Eqs. (44a-d) together with boundary and initial conditions can be solved without further approximation by forward marching integration in the x direction as was demonstrated by McDonald and Briley (Ref. 17) for laminar flow in rectangular jets. For subsonic flow, however, the inviscid flow region is known to be governed by equations which are elliptic; that is, by equations which require downstream boundary conditions for solution. Therefore, in the subsonic case, if the pressure is required to emerge from the solution it is by no means clear that a stable numerical solution could be obtained from a forward marching calculation and even if a stable numerical solution could be obtained, solution by forward marching integration is not physically appropriate, at least not without some sort of iterative procedure to satisfy the downstream boundary conditions. Therefore, it appears that in the subsonic case some approximation must be made in regard to the pressure field. The present airfoil tip analysis follows the approach of Ref. 18 and assumes the pressure field appropriate for inviscid flow represents a given reasonable first approximation to the actual pressure field. Thus, the inviscid streamwise pressure gradient computed with appropriate downstream boundary conditions is "imposed" upon the flow, as a known source term in the streamwise momentum equation much as in conventional boundary layer theory, so as to permit solution by forward marching integration of the viscous flow equations for subsonic flows. This choice of the pressure approximation is not the only possible choice and the manner in which the necessary pressure approximation is made is still a subject of current investigation. In any case the imposition of inviscid pressure gradients incorporates a priori the elliptic effects associated with a subsonic pressure field without the necessity of solving elliptic equations other than for an inviscid flow. In the present application, the inviscid pressure distribution was obtained via the inviscid analysis described in the previous sections.

Method of Solution

The governing equations can be solved (after modeling the Reynolds stresses in the case of turbulent flow) following the general approach developed by McDonald and Briley (Ref. 17) for laminar supersonic flow in rectangular jets. A detailed discussion of the calculation procedure is not included here, as such a discussion would be lengthy, and discussions of the general approach are available elsewhere (Refs. 12, 17, 18). The method used is based on an implicit scheme which is potentially stable for large step sizes. Thus, as a practical matter, stability restrictions which limit the streamwise step size relative to the transverse mesh spacing and which become prohibitive for even locally refined meshes (e.g., in laminar sublayers) are not a factor in making the calculations. The general approach is to employ an implicit difference formulation and to linearize the implicit equations by

expansion about the solution at the most recent streamwise location. Terms in the difference equations are then grouped by coordinate direction and one of the available alternating-direction implicit (ADI) or splitting techniques is used to reduce the multidimensional difference equations to a sequence of one-dimensional equations. These linear one-dimensional difference equations can be written in block-tridiagonal or a closely related matrix form and solved efficiently and without iteration by standard block elimination techniques. The general solution procedure is quite flexible in matters of detail such as the type and order of accuracy of the difference approximations and the particular scheme for splitting multidimensional difference approximations. Based on previous experience, however, it is believed that the consistent use of a formal linearization procedure, which incidentally requires the solution of coupled difference equations in most instances, is a major factor in realizing the potential favorable stability properties generally attributed to implicit difference schemes.

As indicated above the details of the method of solution are quite lengthy and have been discussed in elsewhere. Rather than repeat the discussion in detail within the body of the present report, the specific numerical method is described in Ref. (18) and given briefly in Appendix A. The topics in this appendix include the difference operators, the linearization process, the difference equations and the matrix inversion procedure.

In brief, the numerical technique represents first and second derivatives by either first or second order difference formulas. However, a simple direct substitution of the difference representations into the differential equations would lead to a nonlinear set of algebraic difference equations. Therefore, a linearization procedure is required. The linearization procedure is based upon previous work by Briley and McDonald (Refs. 12 and 17) which assume the solution to the equations is Taylor expandable and, therefore, approximates the solution at streamwise station n + 1 through a Taylor expansion of the known solution at station n. The result is a set of linear difference equations representing the nonlinear differential equations at station n + 1. The finite difference solution itself is an ADI solution based upon the splitting technique of Yanenko (Ref. 21) which results in a two step procedure in advancing the solution from station n to station n + 1. Each step requires the inversion of a block diagonal matrix which is accomplished through a standard block elimination technique (e.g., Ref. 22). Further details of these procedures are found in Appendix A.

Grid Transformation, Difference Representation and Boundary Conditions

The minimization of the computational effort necessary to compute a solution requires that a nonuniform grid spacing be used to ensure that grid points are closely spaced in regions where the solution varies rapidly and widely spaced elsewhere. In the present calculations, steep gradients occur in the boundary layers on the airfoil surface and in the vicinity of the airfoil tip and it is in these regions that closely spaced grid points are required. In the present procedure grid point packing is obtained using a transformation originally devised by Roberts (Ref. 23). For the purpose of demonstrating the Robert's transformation suppose that N grid points are to be used in the range $y_1 \le y \le y_2$ and a boundary layer or sublayer of thickness $\epsilon(y_2-y_1)$ is present near y_1, then Roberts' transformation $\eta(y)$ is given by

$$\eta(y) = N + (N-1) \log \left(\frac{y+b-c}{y+b+c}\right) \Big/ \log \left(\frac{b+a}{b-a}\right) \tag{45}$$

where $a = y_2-y_1$, $b^2 = a^2/(1-\epsilon)$, and $c = y_2$. The use of equally spaced points in the transformed coordinate η ensures an adequate resolution of both the overall region between y_1 and y_2 and the boundary layer region between y_1 and $y_1 + \epsilon\,(y_2-y_1)$. Derivatives with respect to the physical coordinate y are obtained from the following formulae:

$$\frac{\partial}{\partial y} = \frac{d\eta}{dy}\,\frac{\partial}{\partial \eta}$$

$$\frac{\partial^2}{\partial y^2} = \left(\frac{d\eta}{dy}\right)^2 \frac{\partial^2}{\partial \eta} + \frac{d^2\eta}{dy^2}\,\frac{\partial}{\partial \eta} \tag{46}$$

The use of three-point difference operators for η derivatives in Eqs. (46) produces similar operators for y derivatives. These y-derivative operators can be computed at the start of the calculation and stored, along with the y locations of grid points.

In the present calculations the grid was resolved in the y-direction along both the upper and lower surfaces of the airfoil and in the z-direction in the vicinity of the airfoil tip. In the y-direction the limits of the computational region were taken between $-.5 \le y/c \le .5$ and transformations were performed both above and below $y = 0$ (the wing centerplane). For the transformation above the wing centerplane, y_2 was taken as 0.5c, y_1 was taken as 0.0 and ϵ was taken as .04; below the wing centerline y_2 was taken as -0.5c, y_1 was taken as 0.0 and ϵ was taken as .04. Similarly, in the z-direction transformations were performed both inboard and outboard of the wing tip plane. In these transformations y_1 was set to zero, ϵ to 0.04 and y_2 was set to +0.4

Results

Inviscid Calculation - Although the present section is concerned primarily with results of the viscous calculation procedure, the viscous procedure requires as input an inviscid approximation to the pressure field. Since this inviscid pressure field is used as an imposed source term in the streamwise momentum equation, the inviscid pressure distribution plays a significant role in determining the viscous results. Therefore, before examining the results of the viscous procedure, it is appropriate to review briefly the inviscid calculation procedure and to examine the inviscid predictions in the airfoil tip region.

Under the present effort, the inviscid flow field was determined by a doublet lattice method (see previous sections of the present report). For steady flows the doublet lattice method reduces to the modeling of the wing by a group of horseshoe vortices. The wing is divided into N rectangular sections and the bound filament of a horseshoe vortex is placed in each segment. In addition, one collocation point is placed in each rectangular segment. Generally, the bound filament is placed along the local quarter chord line of each rectangular element and the collocation point at the 3/4 chord point midway between the tips of the element. The strength of each bound vortex is chosen so that the total normal wash due to the oncoming free stream flow and to all horseshoe vortex elements is zero at all collocation points. Therefore, in the doublet lattice method the zero normal wash condition need be satisfied at only N discrete points on the wing; normal wash may be present at all other points on the wing.

The doublet lattice method does represent an efficient and versatile method of solving the inviscid flow about a wing of general planform and may be capable of giving accurate predictions of lift and moment coefficients. However, unless an extremely large number of rectangular sections and collocation points are used, the procedure suffers from obvious deficiencies in its ability to determine the flow field in the immediate vicinity of the wing. The deficiency results from the zero normal wash boundary condition being satisfied only at isolated points (one per section) and, therefore, at all other points the correct physical boundary condition is not being satisfied. In the present inviscid calculation which was used to obtain the inviscid pressure field required by the viscous procedure only a moderately dense grid was used and, consequently, the zero normalwash condition in the immediate vicinity of the wing tip was not well satisfied. A typical spanwise distribution of the normalwash velocity is presented in Table I. The distribution was calculated by summing the contributions from each horseshoe vortex and the oncoming free stream flow. The distribution is taken at $x/c = 0.325$ and $y/c = 0.02$; the velocity is normalized by the oncoming free stream velocity.

and -0.4c for the outboard and inboard transformations, respectively. It should be noted that the y-grid is symmetric about the wing centerplane and the z-grid is symmetric about the wing tip. The locations of the grid points versus point number are presented in Fig. 16.

In regard to the finite difference representation, in the present effort second derivatives are represented by three point central difference operators. First derivatives are represented by two different difference operators. In the spanwise direction a two point backwards difference operator is used. In the transverse y direction for points above the wing centerplane a two point backwards difference is used whereas for points below the wing centerplane a two point forwards difference is used. It should be noted that with this difference scheme, differencing is always done away from boundaries which in truth can only be set at infinity.

The final item to the specified before proceeding to a discussion of results is the application of boundary conditions. During the course of the present effort several combinations of boundary conditions were investigated. One possible choice along all outer boundaries of the computational region is the specification of the inviscid function values. However, this specification should require the flow in the outer portions of the computational region to be free from both direct and indirect (viscous displacement) viscous effects. In the present computations, the regions in the vicinity of the upper and lower (y= constant) boundaries are not expected to be free from inner layer viscous displacement effects and, therefore, along these boundaries second derivatives of u, w, and ρ were set to zero. The most satisfactory boundary condition for the fourth variable, v, was obtained by setting the first derivative, $\partial v/\partial y$, equal to the inviscid value. On the left hand z-boundary (which cuts through the wing) the second derivatives of u, v and ρ are set to zero and the spanwise velocity, w is set equal to its inviscid value modified by a boundary layer profile, $f(y/\delta)$, in the vicinity of the wind surface. Finally, on the right hand z=constant boundary, which should be reasonably free from all viscous effects, ρ, u and v are set to their inviscid values and $\partial^2 w/\partial^2 z$ is set equal to zero.

Once a calculation has begun to march downstream, the continuity equation and the three momentum equations are solved in finite difference form. However, a special procedure is required to start the calculations. In this special starting procedure during the y-implicit sweeps of the ADI procedure, the y-momentum equation is replaced by the condition that the pressure equal the inviscid pressure. Likewise during the z-implicit sweeps the z-momentum equation is replaced by the inviscid pressure condition. This special starting procedure only is required on the first step of the calculation and serves to generate a viscous flow field compatible with the inviscid pressure distribution.

Table I - Calculated Inviscid Normalwash Velocity

z/c	-.20	-.15	-.10	-.05	0
v/u	.002	.009	.02	.07	.21

Obviously, the zero normalwash condition is not being held in the immediate vicinity of the tip. Therefore, for the purpose of the viscous calculation, the tip was taken to be at z/c = -.1 and the z-location was then shifted by +0.1 so as to put the new assumed tip location back to z/c = 0.

In addition to the problem of nonsatisfaction of the zero normalwash condition (which in principle could be overcome through a dense calculation grid), the doublet lattice method assumes the trailing vortices to lie in a plane which in the present inviscid calculation coincides with the plane of the wing. This restriction further constrains the flow since the vortices are not free to interact one with the other. Although such a constraint may not represent a significant problem in lift and moment coefficient calculations, the constraint may lead to critical inaccuracies if the correct detailed flow field in the vicinity of the airfoil wing is the object of the investigation. Therefore, in summary the inviscid calculation procedure used has two drawbacks in so far as the wing tip flow field is concerned: (i) satisfaction of the zero normalwash condition only at specific points and (ii) constraint of the vortex trailing filaments to a specified plane.

Predictions of the inviscid flow field obtained with the doublet lattice method are presented in Fig. 17-22. Figures 17-19 show contour plots of the streamwise, normal and spanwise (u, v, and w) velocity components, respectively, at x/c = 0.175. As can be seen in these figures the streamwise velocity above the wing is greater than that below the wing and the normal and spanwise flow velocities show flow around the wing. Flow around the wing can be deduced from the prediction of positive v at the wing tip in conjunction with positive w below the wing and negative w above the wing. In addition it should be noted that a strong positive v-velocity occurs just beyond the wing tip location for the inviscid flow calculation (z/c = 0.1). This reaches a maximum value of approximately v = 0.2. Far from the wing the ratio of v/u approaches a value of approximately 0.1 which is consistent with a 0.1 radian incidence angle. It should be noted that the inviscid solution shows no evidence of a circular secondary flow pattern in the y-z plane. Above the wing the spanwise velocity w is consistently negative while below the wing it is consistently positive. The normal velocity is always positive. The lack of any circular inviscid flow pattern in the y-z plane is a result found at all stations examined and may be due to constraining the trailing vortices in a planar wake. Figures 20-22 show the three inviscid velocity components at the plane x/c = 0.375; the flow pattern is similar to that found in the upstream flow plane.

Viscous Solution - The inviscid flow field obtained from the doublet lattice procedure is used as input for the viscous calculation. The inviscid pressure field is imposed unchanged upon the streamwise momentum equation and the inviscid velocity field is used to obtain both upstream initial conditions and some boundary conditions. Although the tip flow field in general will be turbulent, the present calculations were run as laminar at a chord Reynolds number of approximately 2000. It is expected that the tip flow field region will be qualitatively similar in the laminar and turbulent cases and, therefore, a laminar prediction should serve to assess the three-dimensional viscous flow field generated by the code. Treatment of the turbulent problem would add the complication of hypothesizing a turbulence model and furthermore would require a simultaneous assessment of the turbulence model and the basic three dimensional calculation. The separation of these two items in one calculation is difficult at best and, therefore, it is proper in this first assessment to avoid the complications of a turbulent flow. Turbulent flow can be considered at a later date by adding an appropriate turbulence model to the calculation procedure.

The calculation was initiated at the station $x/c = 0.175$ by inputting the inviscid velocity field and adding a boundary layer correction in the vicinity of the wing. The computational grid used consisted of twenty-one points in the spanwise direction and forty-one points in the transverse direction. In the present calculation a boundary layer thickness, δ, was chosen to initiate the calculation and each velocity component, u_j, was scaled such that

$$u_j = u_{j\ \text{INVISCID}}\ f(y/\delta) \tag{47}$$

where y is the distance from the wing and $f(y/\delta)$ is the Pohlhausen velocity profile. For the purpose of this preliminary assessment of the procedure, a convenient boundary layer thickness was simply assumed. Inboard of the wing tip ($z < 0$) the boundary layer thickness was assumed to be $\delta_1 = .08$ c and outboard of the wing tip ($z > 0$) δ_2 was assumed to be .015 c. Although the initial plane flow field obtained by superimposing a Pohlhausen type profile upon an independently calculated inviscid flow does give a qualitatively reasonable set of initial plane conditions, the procedure may give profiles which change rapidly during the first few stations of the viscous flow calculation. This problem is likely to be particularly acute in the region of the airfoil tip. The generation of initial plane conditions which are in concert with both the inviscid pressure field and the viscous flow equations is a major problem which must be faced in the three-dimensional viscous flow analysis.

The results of the viscous calculation are shown in Figs. 23-30. For the y-z plane grid used, the calculation of one streamwise step required approximately 30 system seconds of UNIVAC 1110 CAU time. The velocity fields at the fifth streamwise station, x/c = 0.19, are presented in Figs. 23-25. The streamwise velocity, u, presented in Fig. 23 clearly shows the velocity boundary layers on both the upper and lower wing surfaces as well as at the wing tip. A detailed examination of the calculation shows the boundary layer thickness on the upper surface, δ_1/c, is approximately 0.08 and the boundary layer thickness at the tip is approximately 0.035. It should be noted that in order to define the boundary layer region, the scale in Fig. 23 is considerably less than that in Fig. 17. The major difference between the inviscid 'u' field of Fig. 17 and the viscous 'u' field of Fig. 23 is the viscous requirement of a no slip boundary condition. Outside of the boundary layer region the inviscid and viscous predictions of the 'u' component of velocity are very similar. The v and w components of velocity are shown in Figs. 24 and 25. Again the scale of Figs. 24 and 25 are less than those of Fig. 18 and 19. However, a comparison of the detailed calculations of Figs. 18 and 24 show that the 'v' distribution is modified significantly by viscous effects. Both above and below the wing, 'v' is modified by boundary layer displacement effects whereas in the vicinity of the wing tip, the rapid changes of 'v' with respect to z in the inviscid calculation are considerably softened by the viscous solution. Finally, the symmetry in the inviscid v-component field above and below the wing is not present in the viscous case. This destruction of symmetry results from the boundary layer above the wing being subjected to an adverse pressure gradient whereas that below the wing being subjected to a favorable pressure gradient. The major difference between viscous and inviscid solutions is found in the spanwise w-velocity calculations. In the inviscid calculation 'w' is negative at all points above the wing (Fig. 19), however, in the viscous calculation a thin layer of positive 'w' appears immediately above the wing (Fig. 25). At this stage since 'v' is positive above the wing, no circular flow pattern can be discerned.

Viscous calculations at x/c = .35 are presented in Figs. 26-30. The region in the immediate vicinity of the tip is shown in detail in Figs. 26-27. In particular, Fig. 26 shows the v-velocity component field and it should be noted that at this station negative values of 'v' have appeared above the wing. Figure 27 shows that the region above the wing also contains both positive and negative values of 'w'. Therefore, a 'circular' type flow pattern has appeared with a center at the location where v = w = 0; this center point has the approximate coordinates y/c = .025, z/c = -.04. This 'circular' flow pattern does not contain the nearly circular streamlines expected in a tip vortex since $w \gg v$; furthermore, the vortex is relatively weak. However,

considering that the inviscid flow field prediction shows no evidence of a vortex (Figs. 21 and 22) this emergence of a 'circular' flow pattern, due to viscous effects and pressure gradients generated by the viscous solution in the secondary flow plane, does indicate the potential capability of the three-dimensional viscous flow procedure in treating the airfoil tip problem.

The overall flow field encompassing more than the immediate tip region is shown in Figs. 28-30. When compared against the analagous calculations for $x/c = .175$ (Figs. 23-25), it is clear that the major difference is that at this latter station the boundary layers now encompass more of the flow field. In addition some spurious spanwise velocities have appeared at the outer calculation boundaries ($|y/c| > .3$) which are beyond the locations shown in the figures. These velocities are unrealistic and indicate more effort must be devoted to the treatment of boundary conditions, however, they are confined to the outer part of the flow calculation region and, therefore, do not influence the immediate tip region shown in Figs. 26 and 27. A table of calculated velocities in the vicinity of the wing tip at $x/c = .354$ is presented in Appendix B.

Summary and Conclusions for Viscous Procedure

A three dimensional forward marching, viscous, subsonic flow calculation procedure has been applied to the airfoil tip problem. The procedure integrates a reduced set of Navier-Stokes equations in which (i) streamwise diffusion is neglected and (ii) the pressure gradient in the streamwise momentum equation is obtained from an external source. In the present effort the doublet lattice method was used to generate the streamwise pressure gradients and with the inviscid calculation grid used this method did not properly define the flow in the vicinity of the tip. Furthermore, the doublet lattice method constrains the trailing vortices to lie in a plane.

These deficiencies in the inviscid pressure field make an assessment of the viscous procedure somewhat difficult. However, the viscous procedure has shown features expected in the flow such as the qualitatively proper development of the viscous boundary layers both on the upper and lower surfaces of the airfoil as well as on the airfoil tip surface. The viscous calculation also shows the generally expected flow pattern around the tip from the lower to the upper surface of the airfoil. Finally, the viscous procedure does predict a 'circular' type flow pattern to appear above the airfoil suction surface; this feature was completely lacking in the inviscid solution. Therefore, the procedure is promising in its application to the airfoil tip problem, however, the results presented must be regarded as preliminary. Further investigations which would include improvements of the viscous as well as the inviscid procedure used to generate the required streamwise pressure gradients must be made before the present approach can be fully assessed.

APPENDIX A

SOLUTION PROCEDURE

Numerical Techniques

As an outline of the particulars of the numerical method, the treatment of the continuity equation is considered, as this is the simplest equation, and yet this discussion will cover most aspects of the method. The flow region is discretized by grid points having equal spacings Δx, Δy, and Δz. Provisions for nonuniform grid spacing will be introduced subsequently. The subscripts i, j and superscript n are grid point indices associated with y, z, and x, respectively. Thus $\phi^n_{i,j}$ denotes $\phi\,(x^n, y_i, z_j)$ where ϕ can represent any of the dependent variables. The subscripts are frequently omitted if clarity is preserved, so that ϕ is equivalent of $\phi^n_{i,j}$. For convenience, the following shorthand difference operator notation is used for derivative difference formulas:

$$\delta_y \phi^n = \left[\alpha(\phi^n_{i,j} - \phi^n_{i-1,j}) + (1-\alpha)(\phi^n_{i+1,j} - \phi^n_{i,j})\right] / \Delta y \qquad (48)$$

$$\delta_y^2 \phi^n = \left[\phi^n_{i-1,j} - 2\phi^n_{i,j} + \phi^n_{i+1,j}\right] / (\Delta y)^2 \qquad (49)$$

with analogous definitions for δ_z, δ_z^2. Here a parameter α has been introduced ($0 \le \alpha \le 1$) so as to permit continuous variation from backward to forward differences. The standard central difference formula is recovered for $\alpha = 1/2$. Throughout the following discussion, it is assumed that the solution is known at x^n and is desired at x^{n+1}.

Consider the continuity equation

$$\partial(h_2 h_3 \rho u)/\partial x + \partial(h_1 h_3 \rho v)/\partial y + \partial(h_1 h_2 \rho w)/\partial z = 0 \qquad (50)$$

Equation (50) is differenced in the x or marching direction as follows:

$$\frac{(h_2 h_3 \rho u)^{n+1} - (h_2 h_3 \rho u)^n}{\Delta x} + \frac{1}{(1+\beta)}\left[\partial(h_1 h_3 \rho v)/\partial y + \partial(h_1 h_2 \rho w)/\partial z\right]^{n+1}$$

$$+ \frac{\beta}{(1+\beta)}\left[\partial(h_1 h_3 \rho v)/\partial y + \partial(h_1 h_2 \rho w)/\partial z\right]^{n} = 0 \qquad (50)$$

Here a parameter β has been introduced so as to permit a variable centering of the scheme in the x direction. Equation (51) produces a backward difference formulation for $\beta = 0$ and a Crank-Nicolson formulation for $\beta = 1$. The dependent variables in Eq. (51) are linearized by expansion about the solution at x^n (Refs. 12 and 17). Here a first-order accurate linearization is used for the x derivative, and the result is

$$h_2^n h_3^n \frac{(\rho^n u^{n+1} + \rho^{n+1} u^n - 2\rho^n u^n)}{\Delta x} + \rho^n u^n \frac{(h_2^{n+1} h_3^{n+1} - h_2^n h_3^n)}{\Delta x}$$

$$+ \frac{1}{(1+\beta)} \delta_y \left[h_1^{n+1} h_3^{n+1} (\rho^n v^{n+1} + \rho^{n+1} v^n - \rho^n v^n) \right] + \frac{\beta}{(1+\beta)} \delta_y (h_1^n h_3^n \rho^n v^n)$$

$$+ \frac{1}{(1+\beta)} \delta_z \left[h_1^{n+1} h_2^{n+1} (\rho^n w^{n+1} + \rho^{n+1} w^n - \rho^n w^n) \right] + \frac{\beta}{(1+\beta)} \delta_z (h_1^n h_2^n \rho^n w^n) = 0 \tag{52}$$

After eliminating the pressure gradients in Eqs. (44 b-d) via the equation of state, the procedure outlined above for the continuity equation can be employed to derive linear implicit different approximations analogous to Eq. (52) for the three momentum equations. The resulting difference approximations can be grouped by coordinate direction and written in the following compact linear matrix difference operator notation as

$$\frac{A}{\Delta x} (\Phi^{n+1} - \Phi^n) = D_y \Phi^{n+1} + D_z \Phi^{n+1} + S \tag{53}$$

where Φ is a column vector containing the dependent variables, ρ, u, v, w, and A is a square (4 x 4) matrix. D_y and D_z are 4 x 4 matrices containing elements which are themselves spatial difference operators for the y and z directions, respectively. S is a column vector reserved for any source terms which may be present. The matrices A, D_y, and D_z contain only quantities which are known from a computational viewpoint. Equation (53) is linear in Φ^{n+1}.

The advantage in grouping the dependent variables by the direction of differencing is that numerous ADI or splitting techniques are immediately available for reducing the multidimensional implicit equation (53) to a sequence of one-dimensional equations (e.g., Douglas & Gunn, Ref. 24; Yanenko, Ref. 21), and this permits efficient solution while retaining the favorable stability properties of the basic implicit scheme. In the present application, however, the technique of splitting (Yanenko, Ref. 21) is being employed. Using the technique of splitting, Eq. (53) can be written as the following two-step scheme.

$$\frac{A}{\Delta x}(\Phi^* - \Phi^n) = D_y\Phi^* + S_1 \qquad (54a)$$

$$\frac{A}{\Delta x}(\Phi^{n+1} - \Phi^*) = D_z\Phi^{n+1} + S_2 \qquad (54b)$$

where Φ^* is an intermediate result having computational significance but no particular physical significance, and where $S_1 + S_2 = S$.

As discussed in the main body of the report, for subsonic flow, an inviscid solution is used as a first approximation to the pressure field. This is accomplished by setting $p = p_I$ in the axial momentum equation, where p_I is the inviscid pressure. In the axial momentum equation, the pressure gradient is therefore replaced by

$$\frac{\partial P}{\partial x} = \frac{\partial P_I}{\partial x} \qquad (55)$$

The pressure gradient terms in the transverse mementum equations are not altered.

Solutions of the Split Difference Equations

The coupled set of linear implicit difference equations arising along rows of grid points during each step of the ADI solution procedure, together with the prescribed boundary conditions, can be written in a form having the following matrix structure.

$$\begin{vmatrix} A_0 & B_0 & C_0 & & & & \\ A_1 & B_1 & C_1 & & & & \\ & A_2 & B_2 & C_2 & & & \\ & & \cdot & \cdot & \cdot & & \\ & & \cdot & \cdot & \cdot & & \\ & & & A_{N-2} & B_{N-2} & C_{N-2} & \\ & & & & A_{N-1} & B_{N-1} & C_{N-1} \\ & & & & A_N & B_N & C_N \end{vmatrix} \begin{vmatrix} \phi_0 \\ \phi_1 \\ \phi_2 \\ \cdot \\ \cdot \\ \phi_{N-2} \\ \phi_{N-1} \\ \phi_N \end{vmatrix} = \begin{vmatrix} d_0 \\ d_1 \\ d_2 \\ \cdot \\ \cdot \\ d_{N-2} \\ d_{N-1} \\ d_N \end{vmatrix} \qquad (56)$$

For each grid point index i, ϕ_i is a column vector containing the dependent variables ρ, u, v, w. A_i, B_i, and C_i are square (4 x 4) matrices containing the implicit difference coefficients. d_i is a column vector containing only computationally known quantities. There are N + 1 grid points along the row under consideration. Difference approximations for the four governing equations are associated with symbols having subscripts 1 through N-1, the subscripts 0 and N are associated with the boundary conditions, which may involve up to three grid points. Equation (56) represents 4 (N + 1) linear equation in 4 (N + 1) dependent variables. Excluding the elements C_0 and A_N, the matrix structure of Eq. (56) is block tridiagonal, and direct solution by standard block elimination techniques (cf., Isaacson & Keller, Ref. 22) is both straightforward and efficient. The precise scheme used here consisted of Gaussian elimination for a simple tridiagonal system (sometimes called the Thomas algorithm) but with elements of the tridiagonal matrix treated as square submatrices rather than as simple coefficients. The required inverses of diagonal submatrices were obtained by a Gauss-Jordan reduction. The additional operations necessary to include the nonblock-tridiagonal elements C_0 and A_N are easily incorporated provided the original block tridiagonal coding is carefully organized.

APPENDIX B

Calculated Velocities at X/C = 0.354

U - VEL

Y/C= \ Z/C=	-0.1042	-0.0667	-0.0408	-0.0234	-0.0121	-0.0047
0.1047	1.0319	1.0327	1.0326	1.0314	1.0340	1.0426
0.0833	1.0131	1.0155	1.0160	1.0121	1.0091	1.0257
0.0656	0.9610	0.9654	0.9668	0.9603	0.9560	0.9940
0.0510	0.8451	0.8509	0.8533	0.8480	0.8588	0.9327
0.0390	0.6844	0.6913	0.6952	0.6949	0.7263	0.8266
0.0293	0.5150	0.5223	0.5272	0.5325	0.5768	0.6849
0.0214	0.3632	0.3697	0.3747	0.3832	0.4291	0.5310
0.0151	0.2382	0.2431	0.2473	0.2562	0.2960	0.3844
0.0100	0.1384	0.1415	0.1445	0.1519	0.1822	0.2540
0.0059	0.0593	0.0605	0.0621	0.0674	0.0879	0.1427
0.0026	0.0000	0.0000	0.0000	0.0000	0.0000	0.0000
0.0000	0.0000	0.0000	0.0000	0.0000	0.0000	0.0000
-0.0026	0.0000	0.0000	0.0000	0.0000	0.0000	0.0000
-0.0059	0.0736	0.0736	0.0740	0.0764	0.0889	0.1295
-0.0100	0.1656	0.1657	0.1663	0.1682	0.1804	0.2220
-0.0151	0.2737	0.2742	0.2750	0.2764	0.2874	0.3274
-0.0214	0.3981	0.3991	0.4003	0.4014	0.4102	0.4462
-0.0293	0.5357	0.5375	0.5394	0.5401	0.5465	0.5773
-0.0390	0.6773	0.6802	0.6828	0.6836	0.6873	0.7118
-0.0510	0.8042	0.8081	0.8116	0.8128	0.8146	0.8316
-0.0656	0.8913	0.8961	0.9002	0.9024	0.9046	0.9156
-0.0833	0.9280	0.9331	0.9375	0.9410	0.9462	0.9554
-0.1047	0.9426	0.9476	0.9520	0.9563	0.9639	0.9731

U - VEL (CONT'D)

Y/C= \ Z/C=	0.0000	0.0047	0.0120	0.0234	0.0408
0.1047	1.0362	1.0228	1.0203	1.0282	1.0292
0.0833	1.0288	1.0206	1.0227	1.0320	1.0341
0.0656	1.0161	1.0208	1.0255	1.0372	1.0420
0.0510	0.9818	1.0117	1.0213	1.0398	1.0507
0.0390	0.9035	0.9698	0.9947	1.0296	1.0533
0.0293	0.7834	0.8872	0.9377	0.9998	1.0446
0.0214	0.6416	0.7766	0.8561	0.9518	1.0241
0.0151	0.4990	0.6591	0.7654	0.8942	0.9954
0.0100	0.3670	0.5501	0.6797	0.8369	0.9644
0.0059	0.2496	0.4551	0.6056	0.7862	0.9356
0.0026	0.0000	0.3363	0.5447	0.7503	0.9131
0.0000	0.0000	0.3210	0.5305	0.7381	0.9033
-0.0026	0.0000	0.3186	0.5263	0.7321	0.8972
-0.0059	0.2190	0.4002	0.5559	0.7421	0.9003
-0.0100	0.3066	0.4594	0.5991	0.7675	0.9094
-0.0151	0.4038	0.5314	0.6532	0.7988	0.9195
-0.0214	0.5132	0.6195	0.7209	0.8385	0.9332
-0.0293	0.6341	0.7206	0.7992	0.8851	0.9505
-0.0390	0.7563	0.8204	0.8734	0.9268	0.9644
-0.0510	0.8615	0.9000	0.9281	0.9542	0.9713
-0.0656	0.9311	0.9461	0.9555	0.9654	0.9721
-0.0833	0.9611	0.9606	0.9606	0.9656	0.9701
-0.1047	0.9735	0.9657	0.9602	0.9642	0.9686

V - VEL

Y/C \ Z/C =	-0.1042	-0.0667	-0.0408	-0.0234	-0.0121	-0.0047
0.1047	0.01780	0.01341	0.01164	0.02088	0.04760	0.06144
0.0833	0.01357	0.00988	0.00859	0.01766	0.04413	0.06093
0.0656	0.00828	0.00535	0.00451	0.01303	0.03814	0.05716
0.0510	0.00338	0.00118	0.00073	0.00838	0.03065	0.04983
0.0390	-0.00017	-0.00176	-0.00191	0.00463	0.02304	0.04033
0.0293	-0.00200	-0.00313	-0.00312	0.00211	0.01621	0.03022
0.0214	-0.00241	-0.00318	-0.00309	0.00070	0.01053	0.02045
0.0151	-0.00198	-0.00245	-0.00235	0.00001	0.00580	0.01124
0.0100	-0.00115	-0.00138	-0.00133	-0.00034	0.00176	0.00279
0.0059	-0.00015	-0.00019	-0.00024	-0.00040	-0.00112	-0.00350
0.0026	0.00000	0.00000	0.00000	0.00000	0.00000	0.00000
0.0000	0.00000	0.00000	0.00000	0.00000	0.00000	0.00000
-0.0026	0.00000	0.00000	0.00000	0.00000	0.00000	0.00000
-0.0059	-0.00024	-0.00022	-0.00018	0.00006	0.00125	0.00510
-0.0100	0.00010	0.00020	0.00015	-0.00040	-0.00152	-0.00070
-0.0151	-0.00004	0.00019	0.00014	-0.00106	-0.00472	-0.00773
-0.0214	-0.00082	-0.00042	-0.00042	-0.00208	-0.00784	-0.01435
-0.0293	-0.00239	-0.00181	-0.00174	-0.00376	-0.01119	-0.02044
-0.0390	-0.00488	-0.00413	-0.00403	-0.00639	-0.01516	-0.02631
-0.0510	-0.00841	-0.00753	-0.00742	-0.01013	-0.01990	-0.03189
-0.0656	-0.01275	-0.01180	-0.01172	-0.01478	-0.02510	-0.03655
-0.0833	-0.01704	-0.01610	-0.01611	-0.01947	-0.02978	-0.03918
-0.1047	-0.02000	-0.01918	-0.01935	-0.02296	-0.03263	-0.03883

V - VEL (CONTINUED)

Y/C = \ Z/C =	0.0000	0.0047	0.0121	0.0234	0.0408
0.1047	0.03993	-0.01614	0.01755	0.04487	0.05134
0.0833	0.03995	-0.02577	0.01439	0.04417	0.05171
0.0656	0.03864	-0.03358	0.01047	0.04273	0.05183
0.0510	0.03495	-0.03880	0.00544	0.03999	0.05120
0.0390	0.02852	-0.04141	0.00016	0.03617	0.04969
0.0293	0.02049	-0.04126	-0.00424	0.03206	0.04771
0.0214	0.01206	-0.03857	-0.00673	0.02873	0.04594
0.0151	0.00389	-0.03395	-0.00669	0.02704	0.04504
0.0100	-0.00362	-0.02806	-0.00402	0.02734	0.04528
0.0059	-0.00898	-0.02081	0.00129	0.02966	0.04664
0.0026	0.00000	-0.00244	0.01307	0.03429	0.04821
0.0000	0.00000	0.00776	0.02039	0.03772	0.04964
-0.0026	0.00000	0.01771	0.02773	0.04123	0.05113
-0.0059	0.01403	0.03363	0.03836	0.04613	0.05328
-0.0100	0.00881	0.03887	0.04590	0.05146	0.05627
-0.0151	0.00211	0.04292	0.05205	0.05595	0.05894
-0.0214	-0.00414	0.04704	0.05762	0.06011	0.06152
-0.0293	-0.00950	0.05148	0.06282	0.06401	0.06403
-0.0390	-0.01410	0.05537	0.06706	0.06720	0.06614
-0.0510	-0.01771	0.05773	0.06993	0.06955	0.06780
-0.0656	-0.01966	0.05798	0.07122	0.07106	0.06908
-0.0833	-0.01925	0.05610	0.07091	0.07174	0.06999
-0.1047	-0.01641	0.05265	0.06922	0.07166	0.07052

W - VEL

Y/C = \ Z/C =	-0.1042	-0.0667	-0.0408	-0.0234	-0.0121	-0.0047
0.1047	-0.0826	-0.0927	-0.1000	-0.1046	-0.1072	-0.1086
0.0833	-0.0871	-0.0974	-0.1048	-0.1093	-0.1115	-0.1130
0.0656	-0.0815	-0.0901	-0.0962	-0.0999	-0.1015	-0.1037
0.0510	-0.0633	-0.0685	-0.0722	-0.0745	-0.0759	-0.0803
0.0390	-0.0406	-0.0421	-0.0435	-0.0444	-0.0461	-0.0526
0.0293	-0.0180	-0.0163	-0.0155	-0.0151	-0.0172	-0.0246
0.0214	0.0030	0.0075	0.0104	0.0120	0.0100	0.0024
0.0151	0.0233	0.0305	0.0356	0.0383	0.0367	0.0294
0.0100	0.0469	0.0574	0.0646	0.0687	0.0678	0.0605
0.0059	0.0803	0.0953	0.1056	0.1113	0.1112	0.1034
0.0026	0.0000	0.0000	0.0000	0.0000	0.0000	0.0000
0.0000	0.0000	0.0000	0.0000	0.0000	0.0000	0.0000
-0.0026	0.0000	0.0000	0.0000	0.0000	0.0000	0.0000
-0.0059	0.0963	0.1119	0.1220	0.1278	0.1288	0.1224
-0.0100	0.0748	0.0864	0.0942	0.0988	0.1001	0.0959
-0.0151	0.0671	0.0762	0.0824	0.0861	0.0873	0.0846
-0.0214	0.0657	0.0730	0.0779	0.0808	0.0818	0.0800
-0.0293	0.0639	0.0695	0.0730	0.0751	0.0759	0.0745
-0.0390	0.0590	0.0623	0.0644	0.0655	0.0658	0.0646
-0.0510	0.0507	0.0517	0.0521	0.0521	0.0520	0.0510
-0.0656	0.0399	0.0387	0.0375	0.0366	0.0360	0.0351
-0.0833	0.0284	0.0254	0.0230	0.0213	0.0201	0.0192
-0.1047	0.0184	0.0141	0.0107	0.0084	0.0069	0.0058

W - VEL (CONT'D)

Y/C = \ Z/C =	0.0000	0.0047	0.0121	0.0234	0.0408
0.1047	-0.1093	-0.1102	-0.1093	-0.1088	-0.1086
0.0833	-0.1144	-0.1157	-0.1158	-0.1163	-0.1174
0.0656	-0.1068	-0.1096	-0.1111	-0.1136	-0.1170
0.0510	-0.0857	-0.0909	-0.0937	-0.0932	-0.1047
0.0390	-0.0597	-0.0670	-0.0698	-0.0755	-0.0835
0.0293	-0.0327	-0.0417	-0.0430	-0.0483	-0.0566
0.0214	-0.0063	-0.0171	-0.0159	-0.0195	-0.0266
0.0151	0.0195	0.0057	0.0107	0.0098	0.0051
0.0100	0.0484	0.0283	0.0389	0.0423	0.0409
0.0059	0.0866	0.0543	0.0740	0.0838	0.0860
0.0026	0.0000	-0.0001	0.0531	0.0800	0.0923
0.0000	0.0000	0.0002	0.0519	0.0792	0.0930
-0.0026	0.0000	0.0005	0.0527	0.0809	0.0959
-0.0059	0.1063	0.0750	0.0962	0.1109	0.1190
-0.0100	0.0857	0.0676	0.0813	0.0920	0.0995
-0.0151	0.0780	0.0676	0.0774	0.0860	0.0927
-0.0214	0.0756	0.0692	0.0766	0.0835	0.0890
-0.0293	0.0713	0.0670	0.0725	0.0774	0.0808
-0.0390	0.0622	0.0592	0.0628	0.0657	0.0668
-0.0510	0.0492	0.0471	0.0491	0.0503	0.0499
-0.0656	0.0339	0.0326	0.0336	0.0338	0.0329
-0.0833	0.0185	0.0176	0.0183	0.0181	0.0174
-0.1047	0.0053	0.0044	0.0052	0.0050	0.0044

REFERENCES

1. Sternfeld, H., R. H. Spencer, and J. O. Schairer: An Investigation of Noise Generation on a Hovering Rotor. Report D210-10229-1, U.S. Army Research Office, Durham, North Carolina. January 1971.

2. Landgrebe, A. J.: An Analytical and Experimental Investigation of Helicopter Rotor Hover Performance and Wake Geometry Characteristics. USAAMRDL Technical Report 71-24, Eustis Directorate, U.S. Army Air Mobility Research and Development Laboratory, Fort Eustis, Va. June 1971.

3. Durand, W. F., Ed.: Aerodynamic Theory, II. Dover Publications, Inc. 1963.

4. Hall, G. F.: Unsteady Vortex Lattice Techniques Applied to Wake Formation and Performance of the Statically Thrusting Propeller. NASA CR-132686. 1975.

5. Adamczyk, J. J.: Passage of an Isolated Airfoil Through A Three-Dimensional Disturbance. Ph.D. Thesis, Dept. of Mechanical Engineering. University of Connecticut. May 1971.

6. Adamczyk, J. J.: Analytical Investigation of Compressibility and Three-Dimensionality on the Unsteady Response of an Airfoil in a Fluctuating Flow Field. AIAA Paper No. 73-683, Presented at AIAA 6th Fluid and Plasma Dynamics Conference. July 16-18, 1973.

7. Giesing, J. P., T. P. Kalman and W. P. Rodden: Subsonic Steady and Oscillatory Aerodynamics for Multiple Interfering Wings and Bodies. AIAA Journal of Aircraft, Vol. 9, No. 10., pp. 693-702. October 1972.

8. Chu, S., and S. E. Windall: Prediction of Unsteady Airloads for Oblique Blade-Gust Interactions in Compressible Flow. AIAA Journal, Vol. 12, No. 9. September 1974.

9. Abbott, I. H., and A. E. von Doenhoff: Theory of Wing Sections. Dover Publications, Inc., 1959.

10. Lighthill, M. J.: A New Approach to Thin Airfoil Theory. The Aeronautical Quarterly, III, November 1971.

11. Laschka, B.: Zur Theorie der Harmonisch Schwingenden Tragenden Fläche bei Unterschallan Stromung. Zeitscrift für Flugwissenschaffen, II, No. 7, July 1963.

12. Briley, W. R. and H. McDonald: An Implicit Numerical Method for the Multidimensional Compressible Navier-Stokes Equations. United Aircraft Research Laboratories Report, M911363-63-6. 1973.

13. Patankar, S. V. and D. B. Spalding: A Calculation Procedure for Heat, Mass and Momentum Transfer in Three-Dimensional Parabolic Flows. Int. J. Heat and Mass Transfer, 15, p. 1787. 1972.

14. Caretto, L. S., R. M. Curr and D. B. Spalding: Computational Methods in Applied Mechanics and Engineering. 1, p. 39. 1973.

15. Briley, W. R.: Numerical Method for Predicting Three-Dimensional Steady Viscous Flow in Ducts. Journal of Computational Physics. 14, p. 8. 1974.

16. Patankar, S. V., V. S. Pratap, and D. B. Spalding: Prediction of Laminar Flow and Heat Transfer in Helically Coiled Pipes. Journal of Fluid Mechanics, 62, p. 539. 1974.

17. McDonald, H. and W. R. Briley: Three-Dimensional Supersonic Flow of a Viscous or Inviscid Gas. Journal of Computational Physics, 19, p. 150. 1975.

18. Briley, W. R. and H. McDonald: Calculations of Three-Dimensional Turbulent Subsonic Flows in Curved Passages. United Technologies Research Center Report, R75-911596-8, 1975.

19. Pai, S. I.: Viscous Flow Theory, Part I - Laminar Flow. D. Van Nostrand Co., Inc., Princeton, New Jersey. 1956.

20. Hinze, J. O.: Turbulence. McGraw-Hill Book Co., Inc., New York. 1959.

21. Yanenko, N. N.: The Method of Fractional Steps, Translation Edited by M. Holt, Springer-Verlag, New York. 1971.

22. Isaacson, E., and H. B. Keller: Analysis of Numerical Methods. John Wiley & Sons, Inc., New York. 1966.

23. Roberts, G. O.: Computational Meshes for Boundary Layer Problems. Proceedings of the Second International Conference on Numerical Methods in Fluid Dynamics. Springer-Verlag, New York, p. 171. 1971.

24. Douglas, J. and J. E. Gunn: A General Formulation of Alternating Direction Methods. Numarische Math., Vol. 6, 1964.

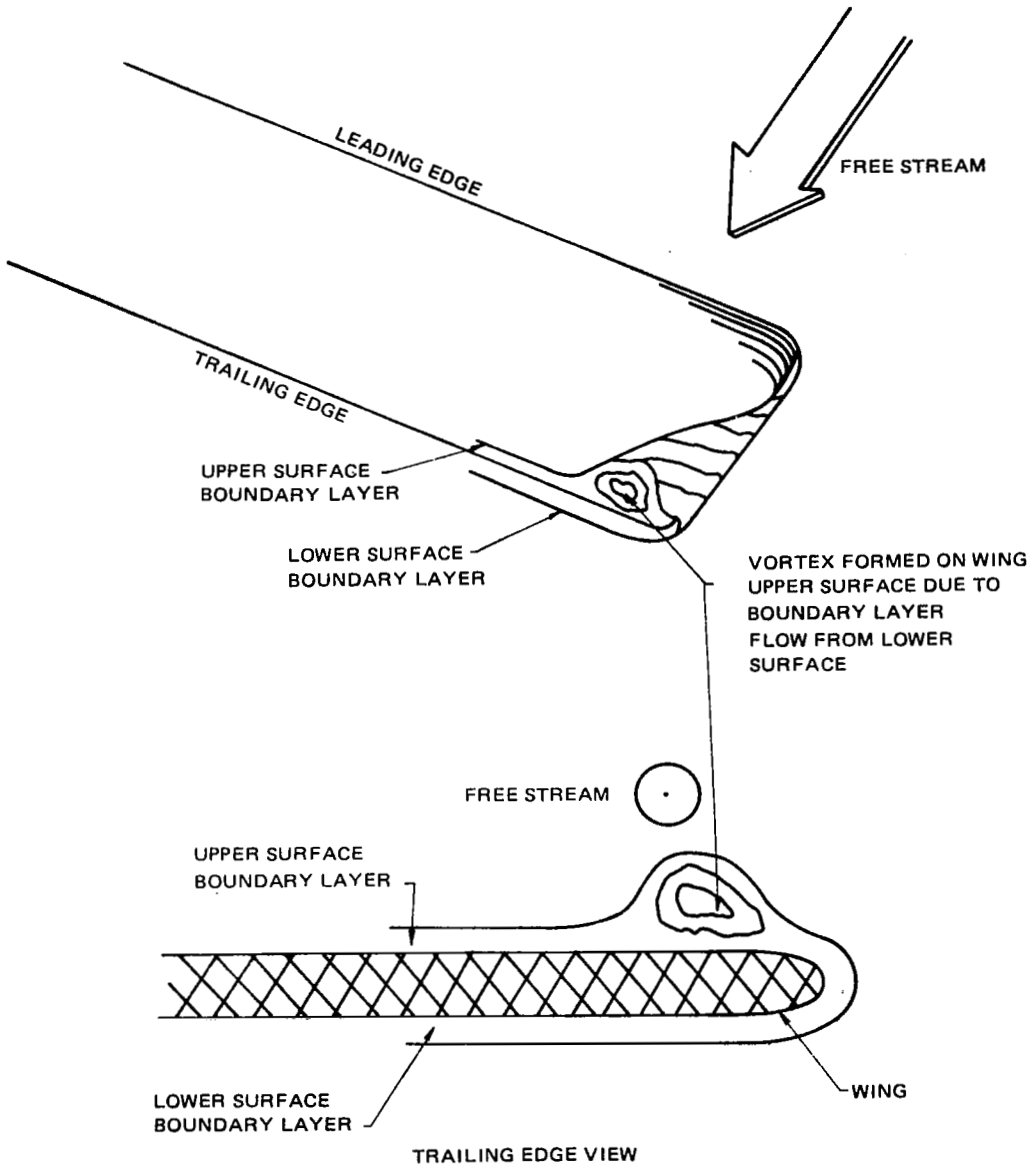

Figure 1. – Schematic of vortex formation at tip of wing with finite thickness.

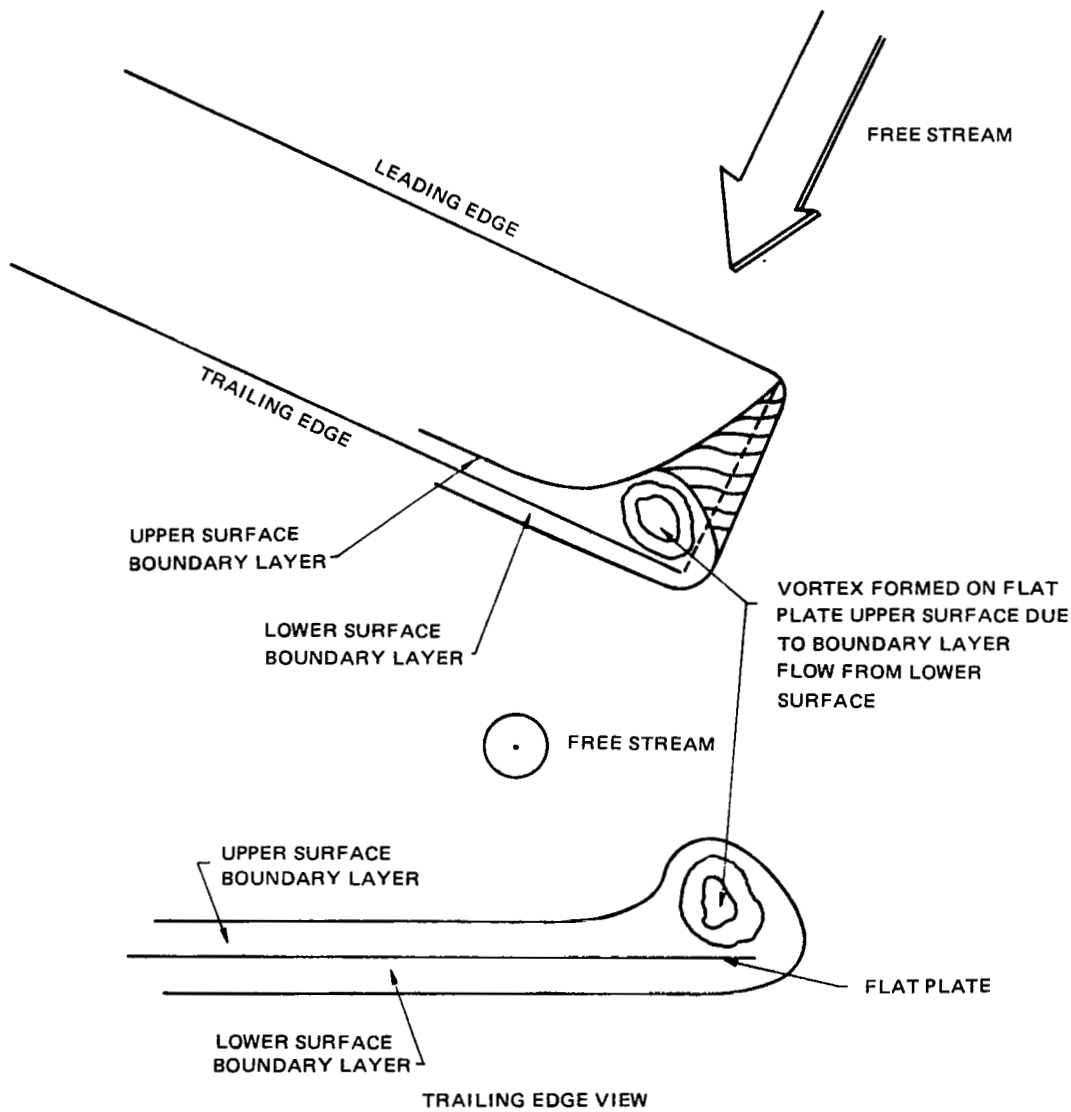

Figure 2. — Schematic of vortex formation at tip of thin flat plate

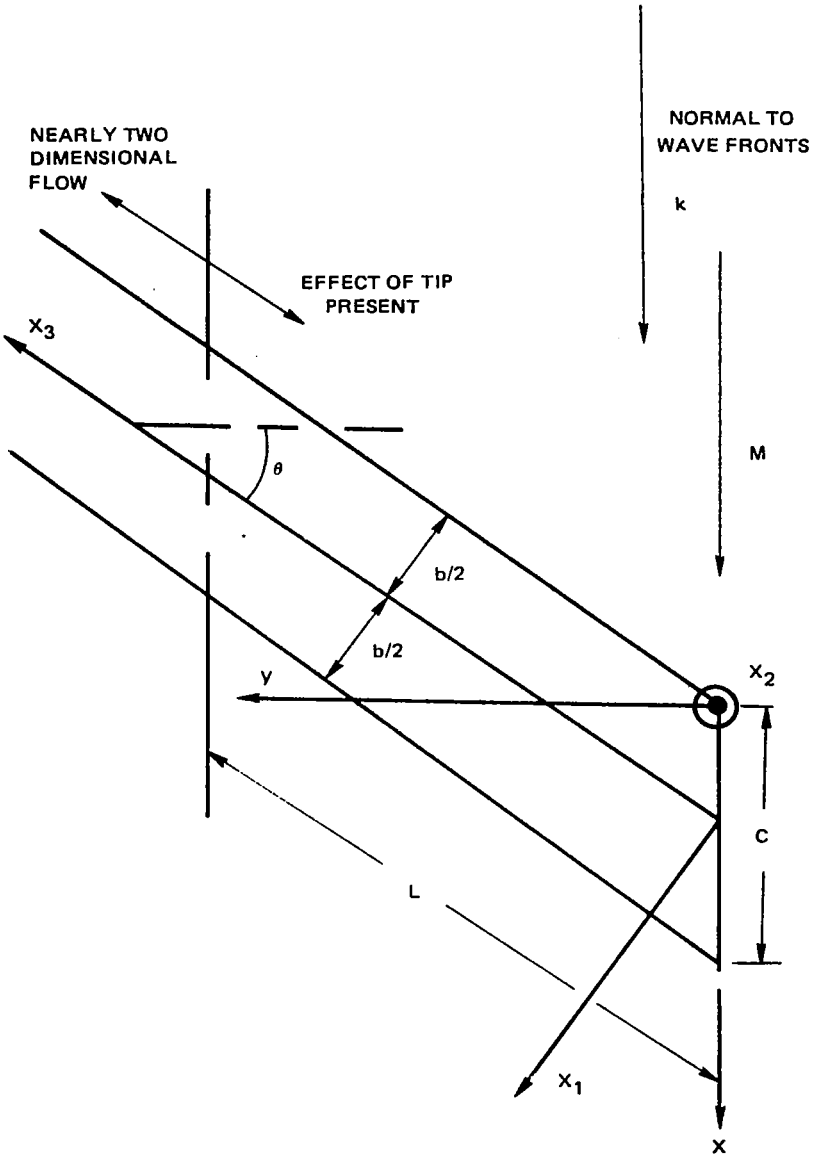

Figure 3. — Geometry of encounter of semi-infinite wing with a sinusoidal gust

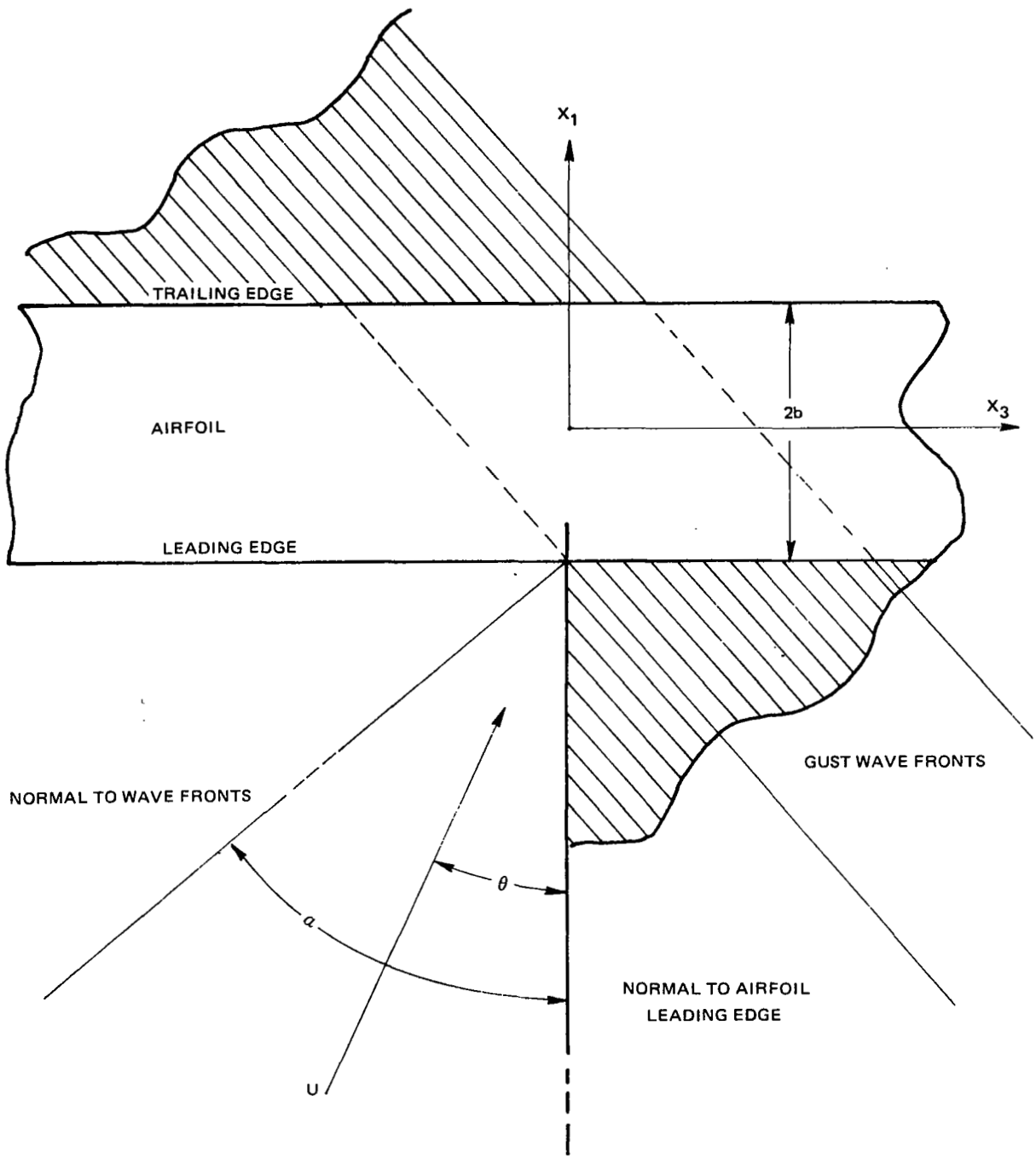

Figure 4. — Geometry of encounter of infinite wing with gust wave fronts

a) RELATIVE MACH NUMBER M*

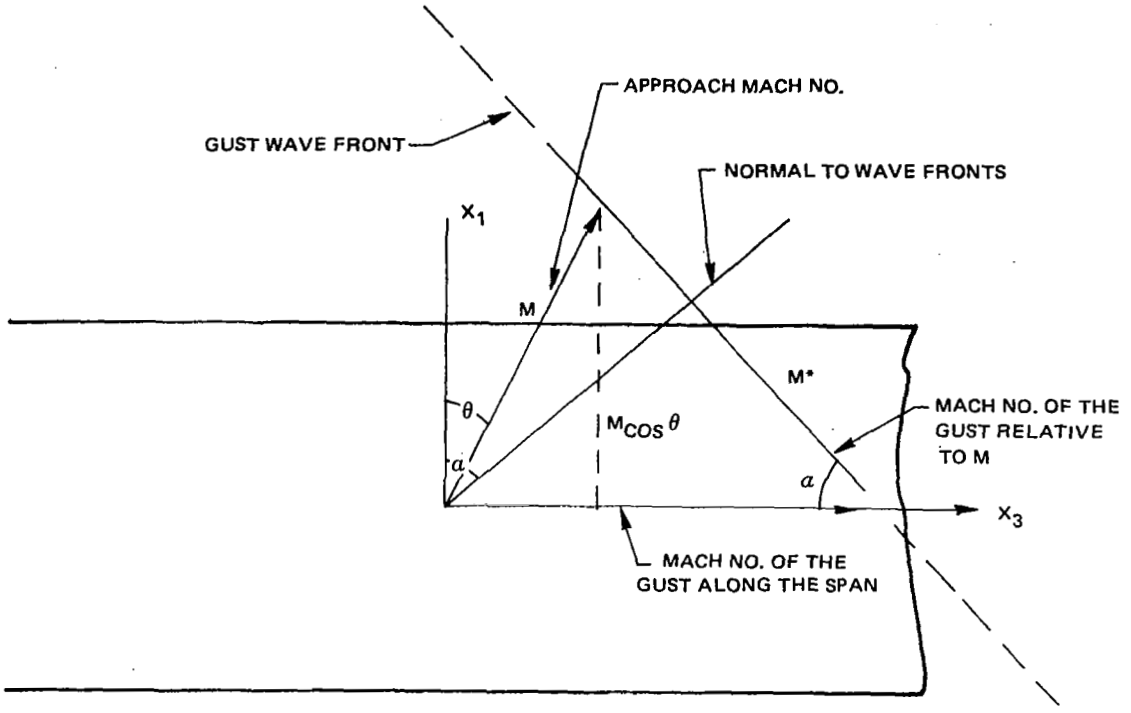

b) ANGLE ϵ

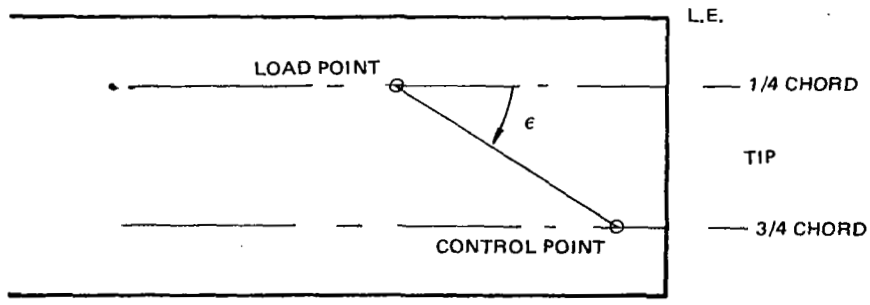

Figure 5. — Geometric definitions

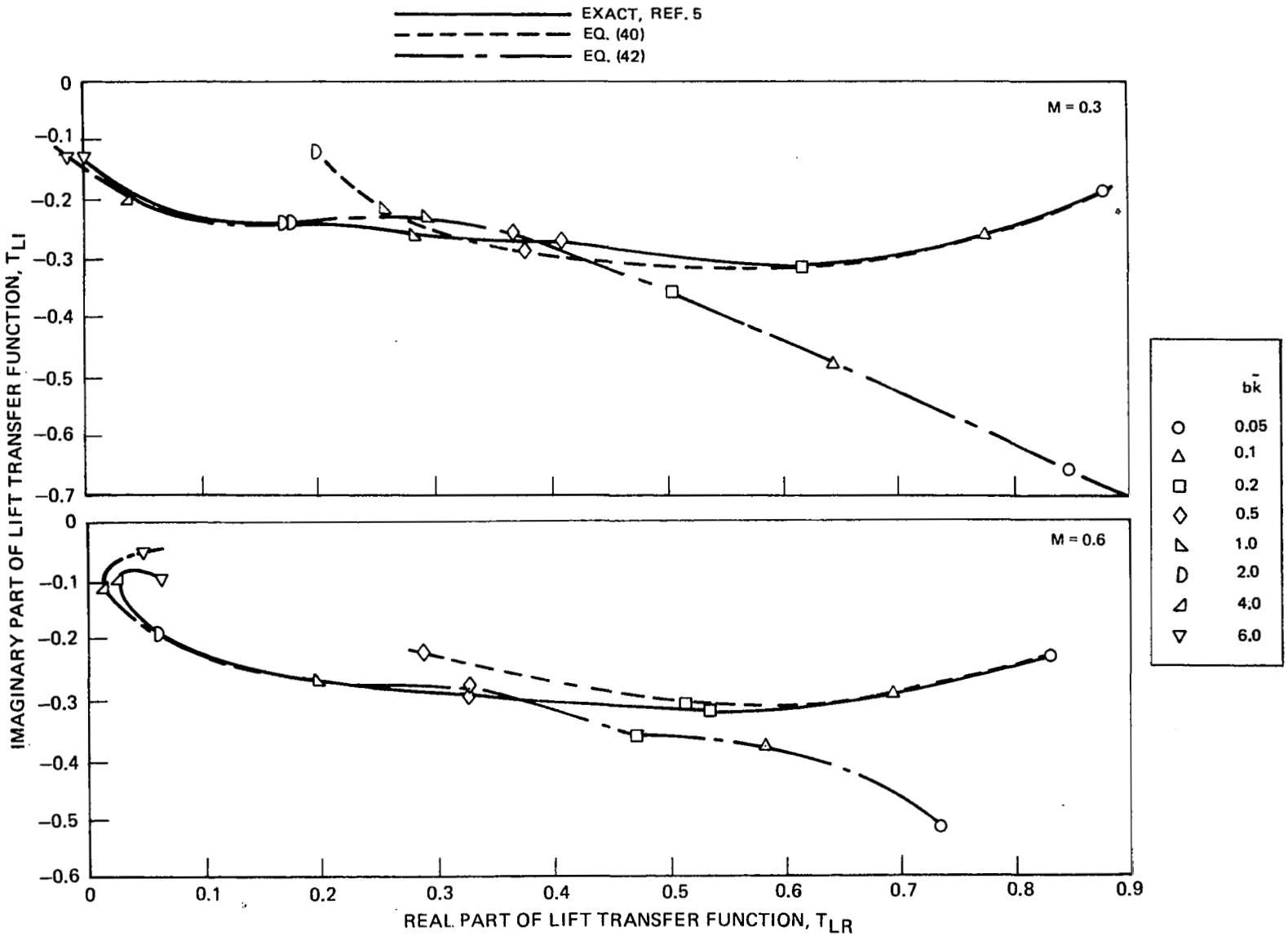

Figure 6. Comparison of lift transfer functions

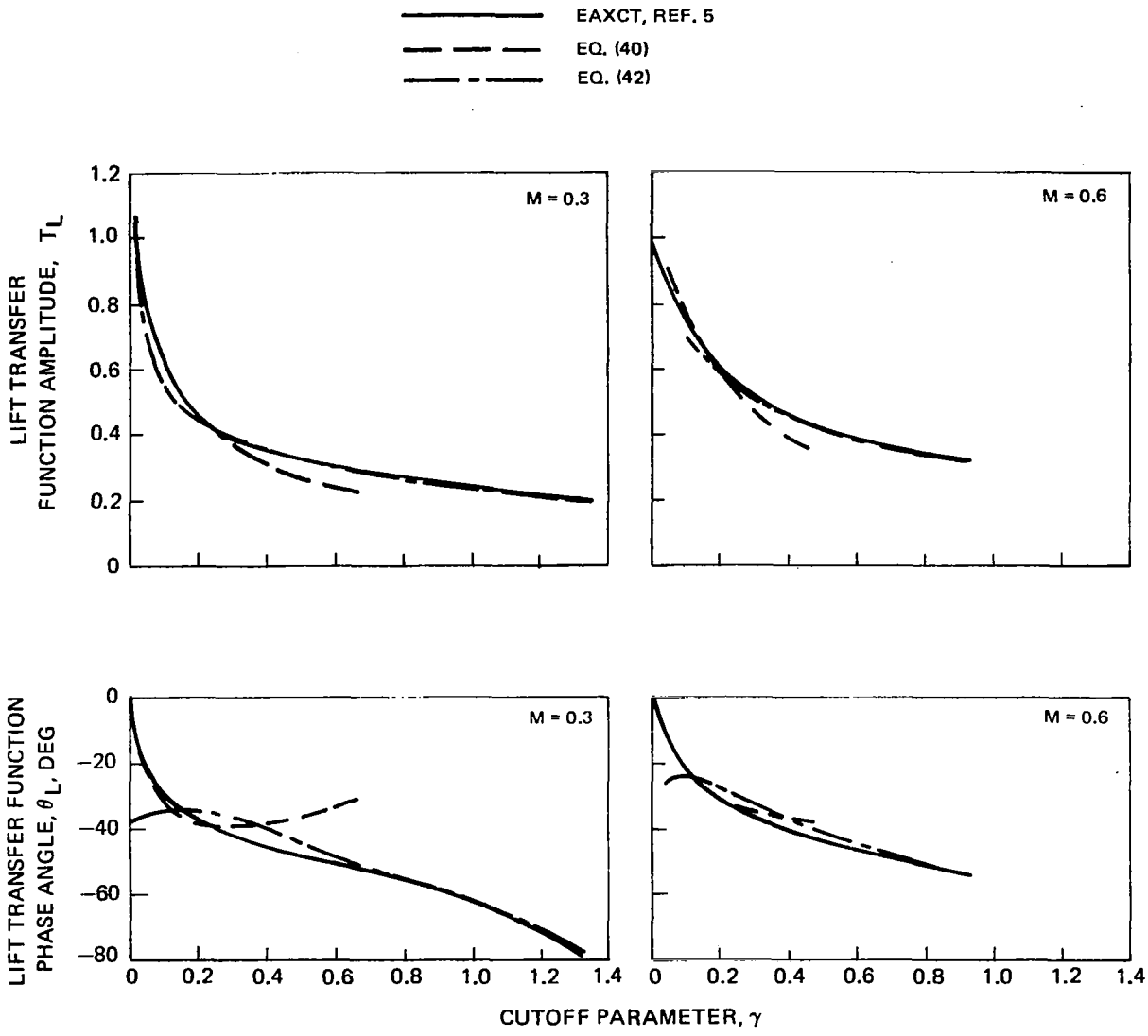

Figure 7. — Amplitude and phase of unsteady lift transfer function for an infinite wing versus cutoff parameter

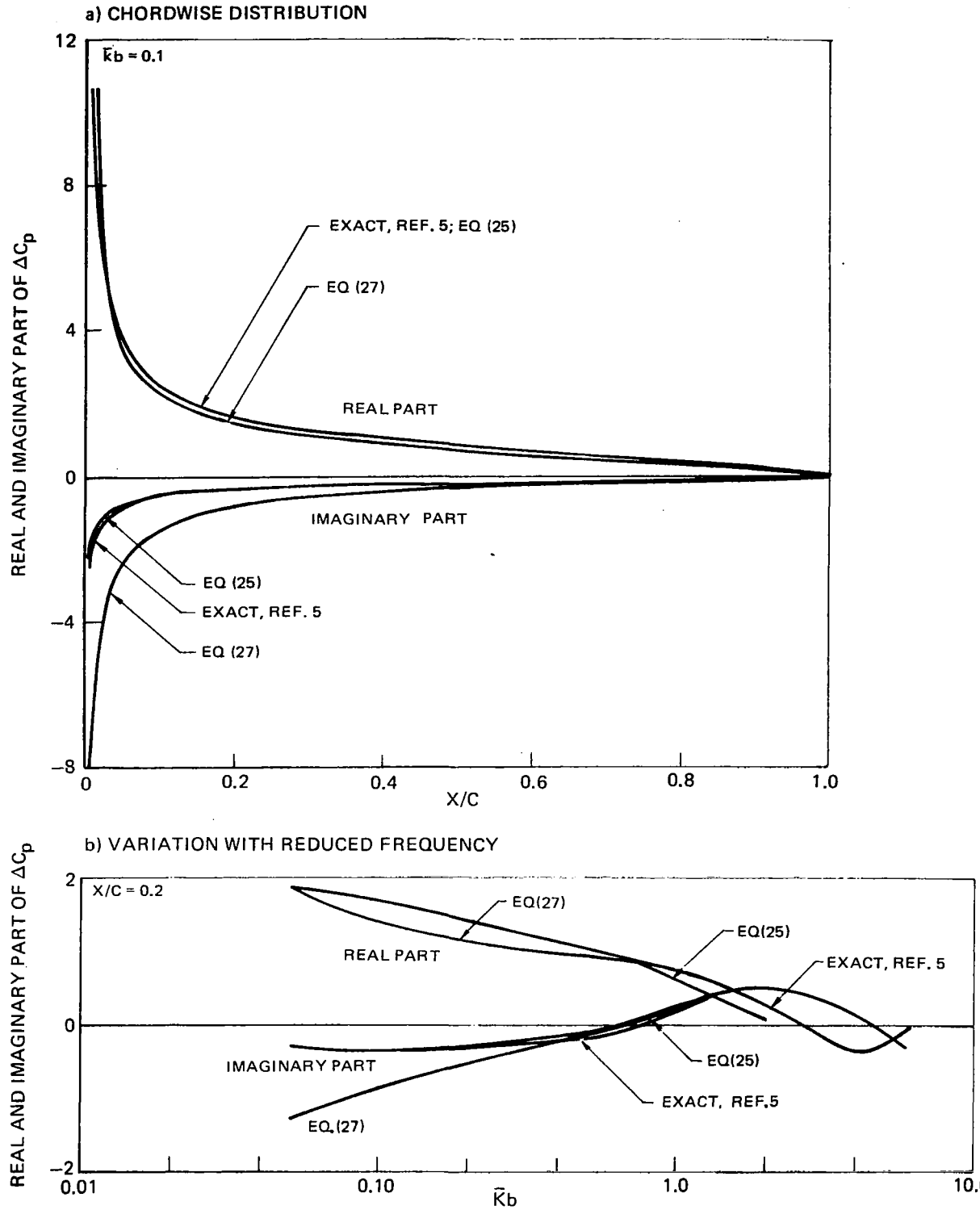

Figure 8. — Real and imaginary part of pressure difference coefficient for M = 0.3

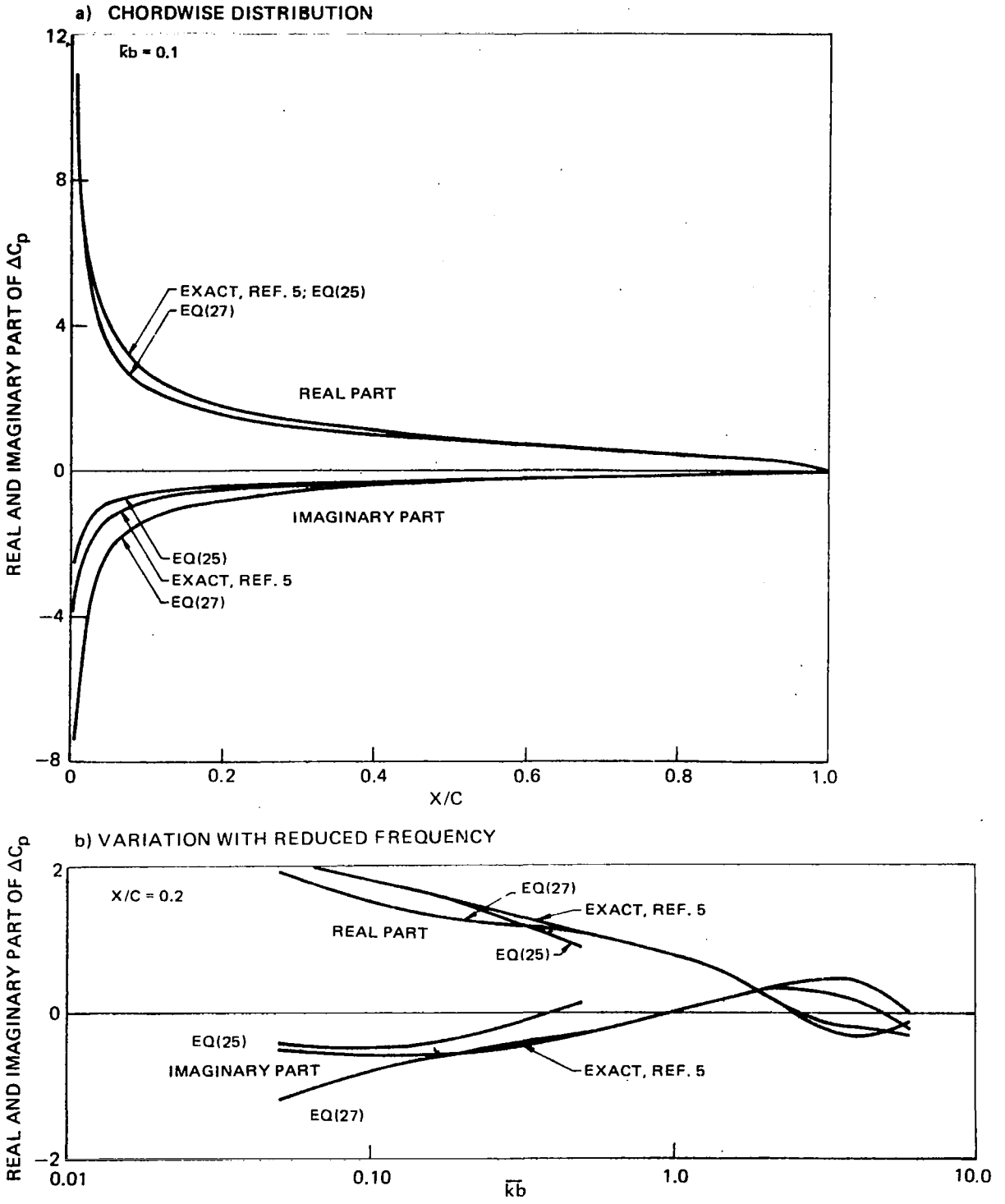

Figure 9. — Real and imaginary part of pressure difference coefficient for M = 0.6

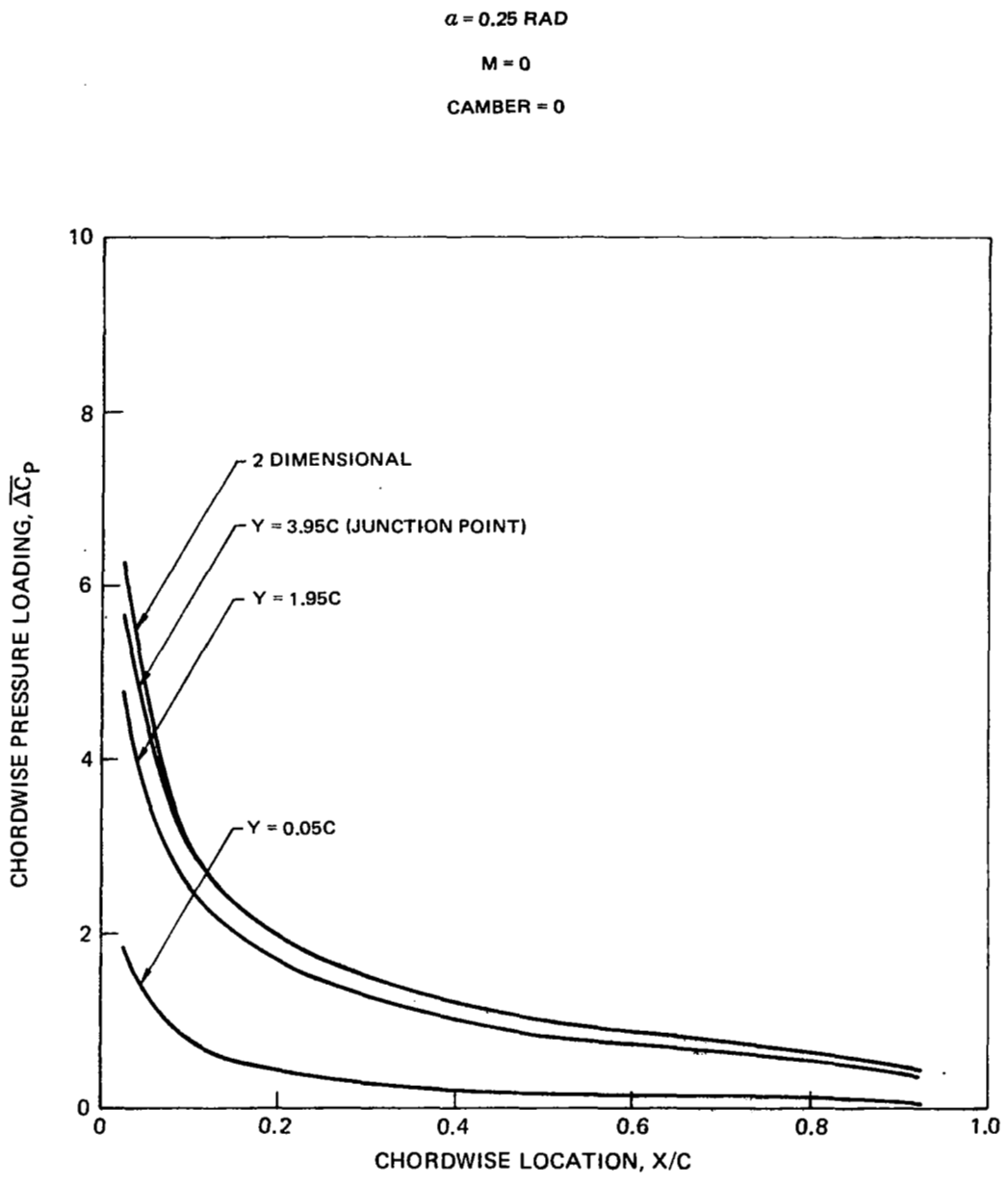

Figure 10. Effect of spanwise position on steady chordwise pressure distribution for an unswept semi-infinite wing

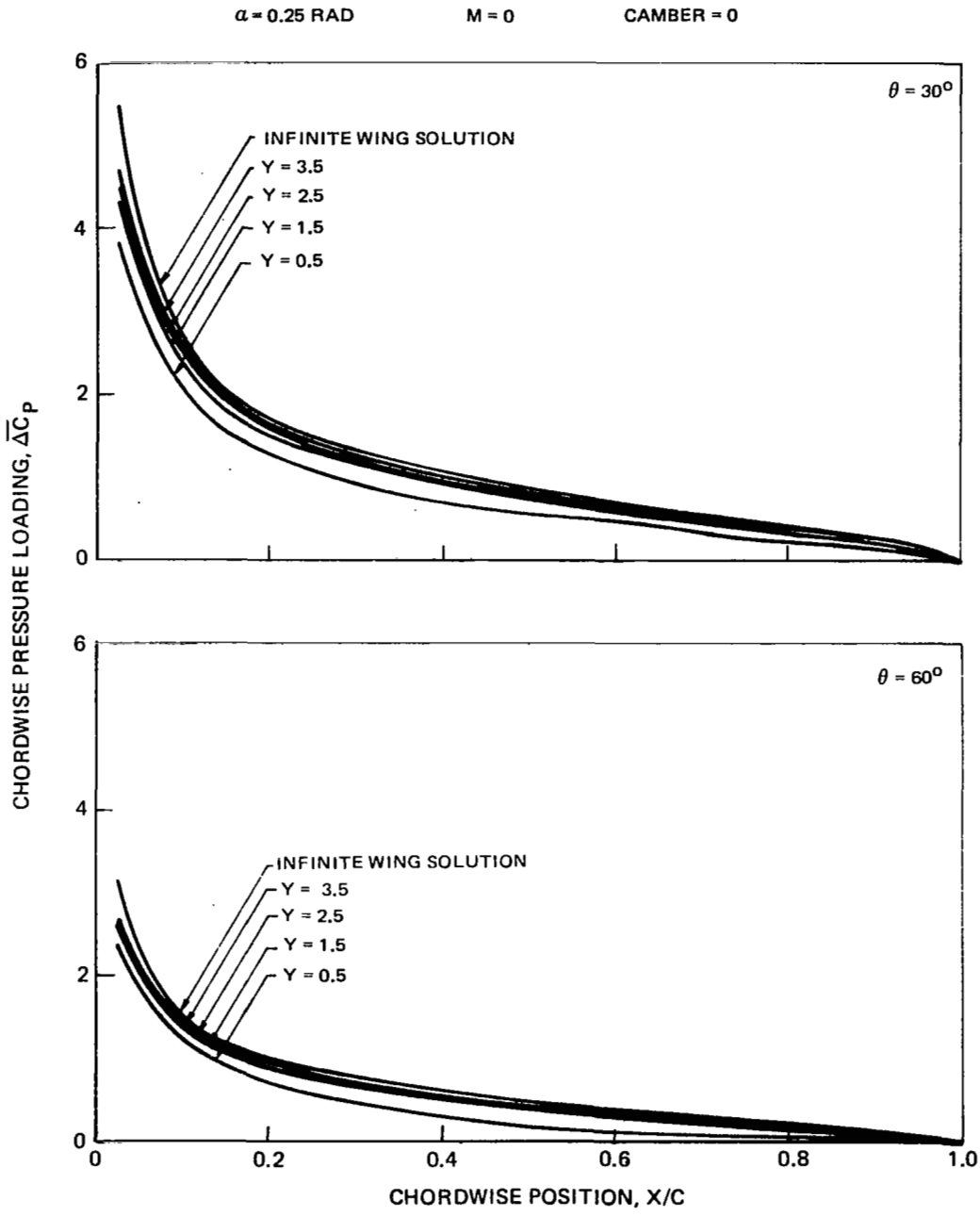

Figure 11. — Effect of spanwise position on steady chordwise pressure distribution for a swept semi-infinite wing

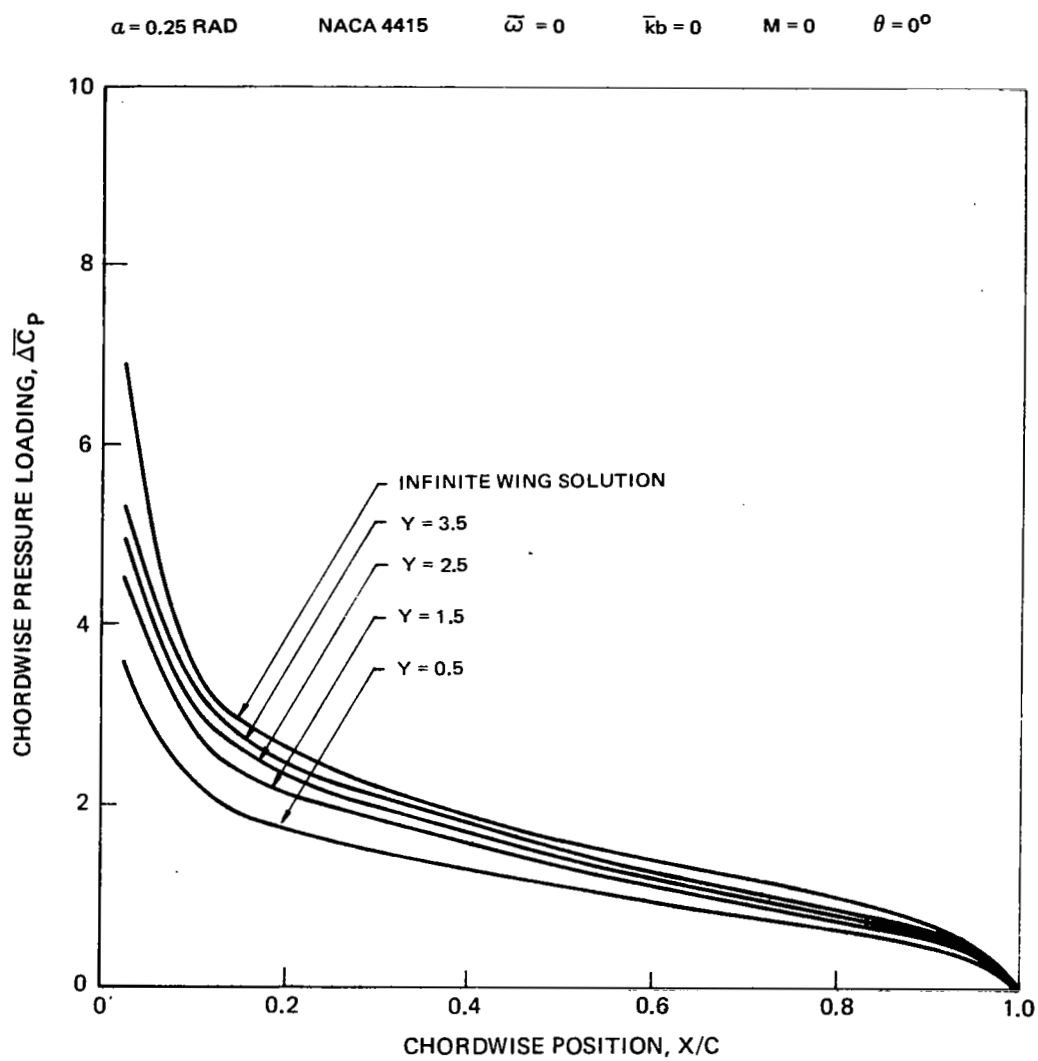

Figure 12. — Steady response of cambered, unswept semi-infinite wing at angle of attack

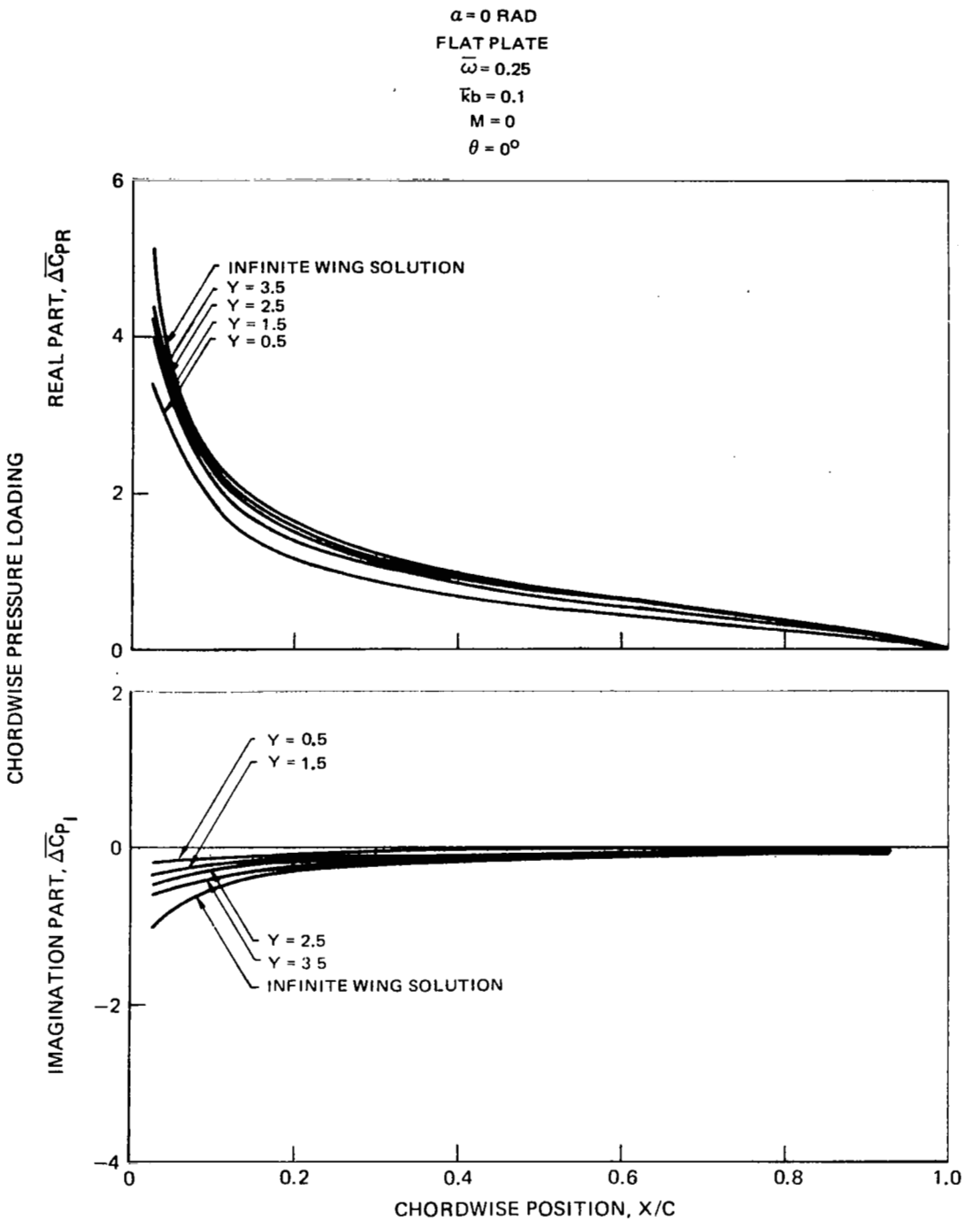

Figure 13. — Unsteady response of flat plate semi-infinite wing at zero angle of attack

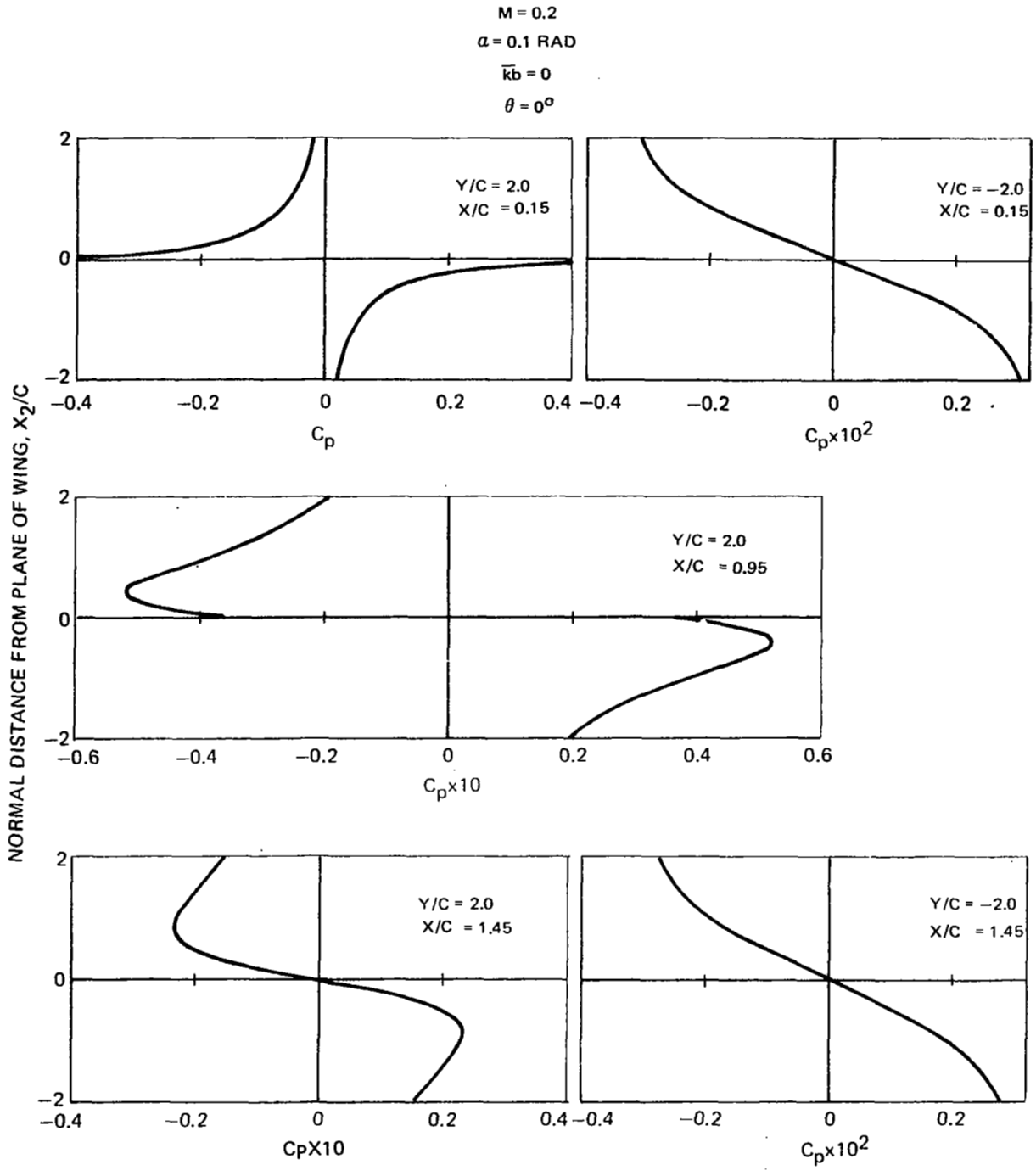

Figure 14. — Pressure distribution in vicinity of tip of semi-infinite wing

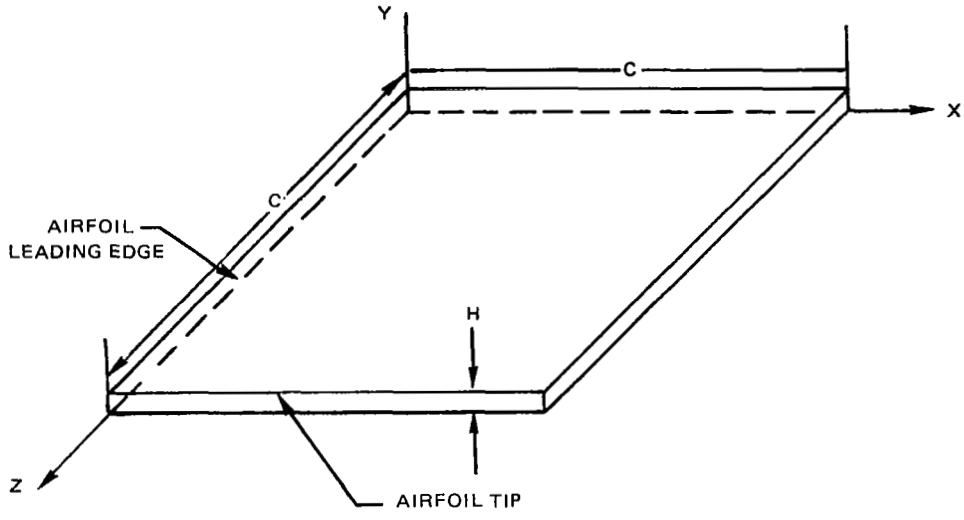

Figure 15. — Viscous flow coordinate system.

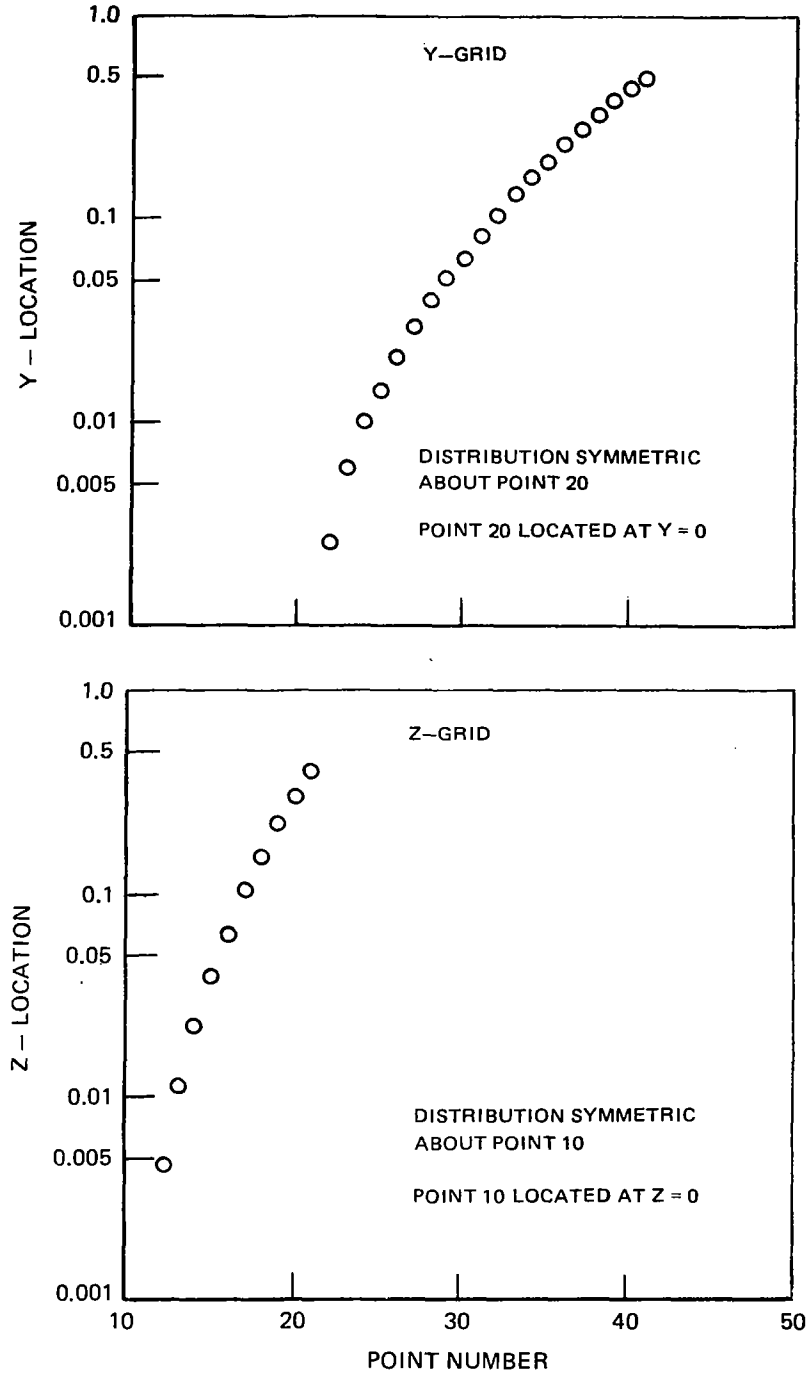

Figure 16. — Grid point locations.

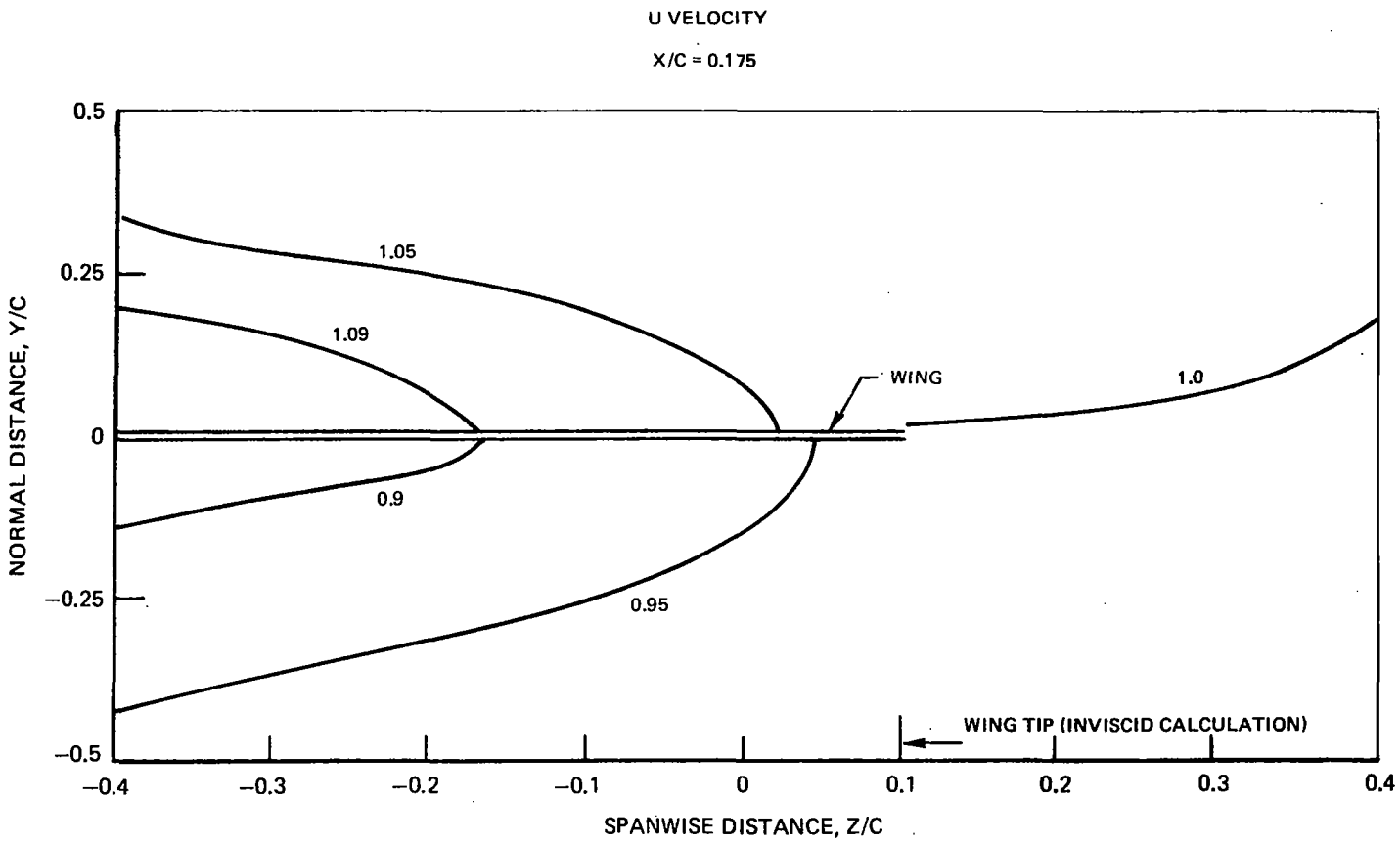

Figure 17. Inviscid flow calculation

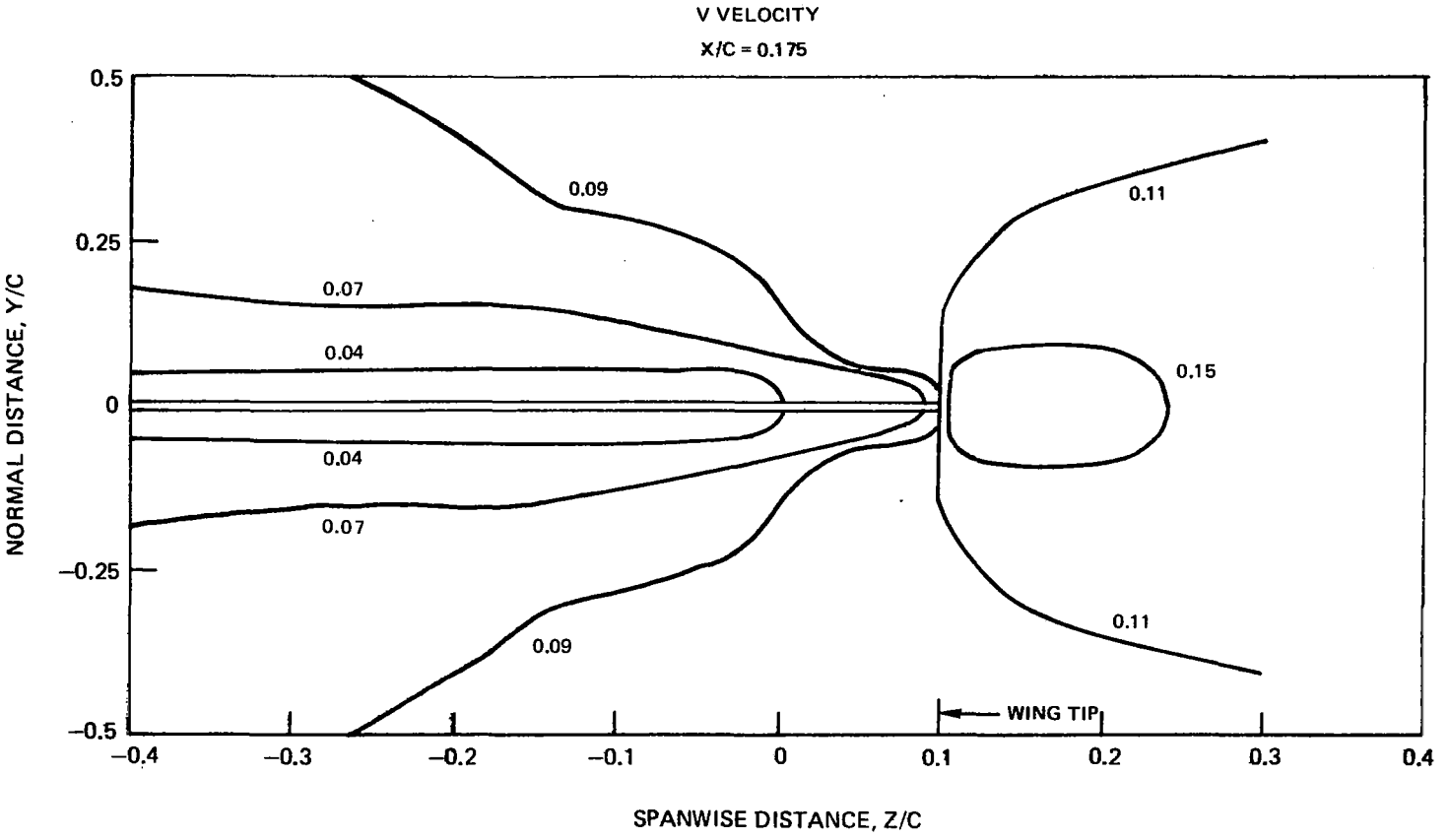

Figure 18. — Inviscid flow calculation.

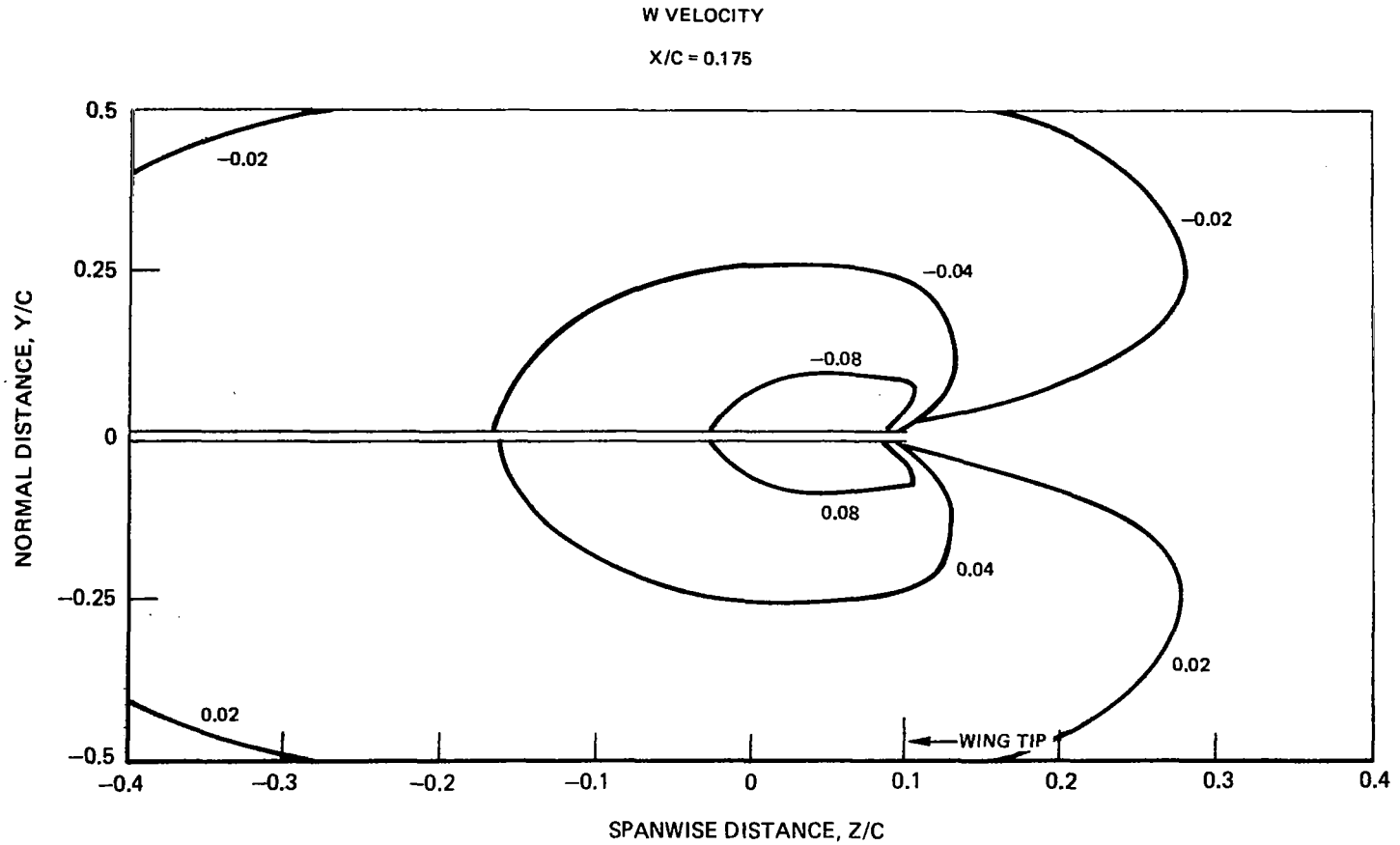

Figure 19. — Inviscid flow calculation.

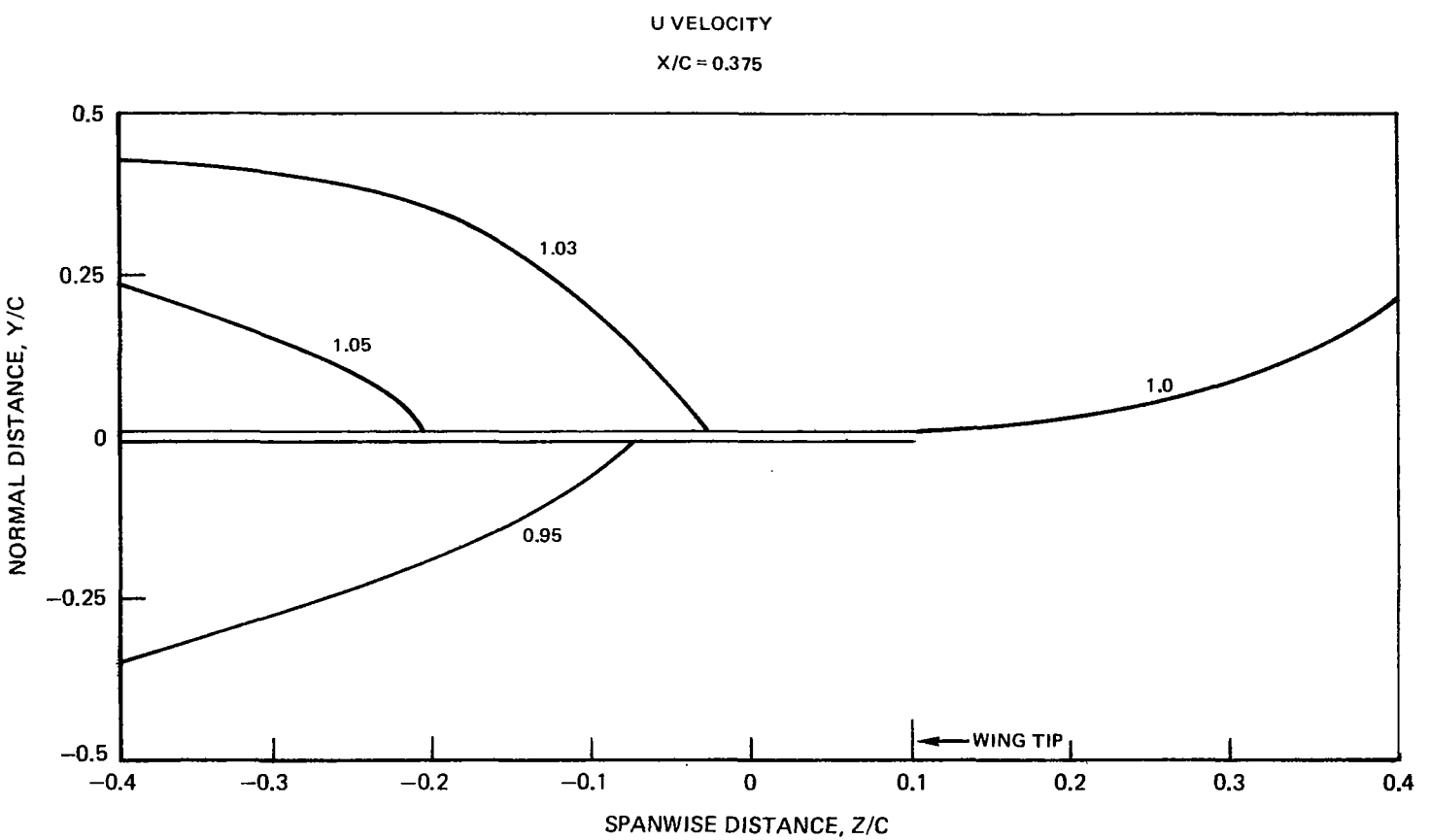

Figure 20. Inviscid flow calculation.

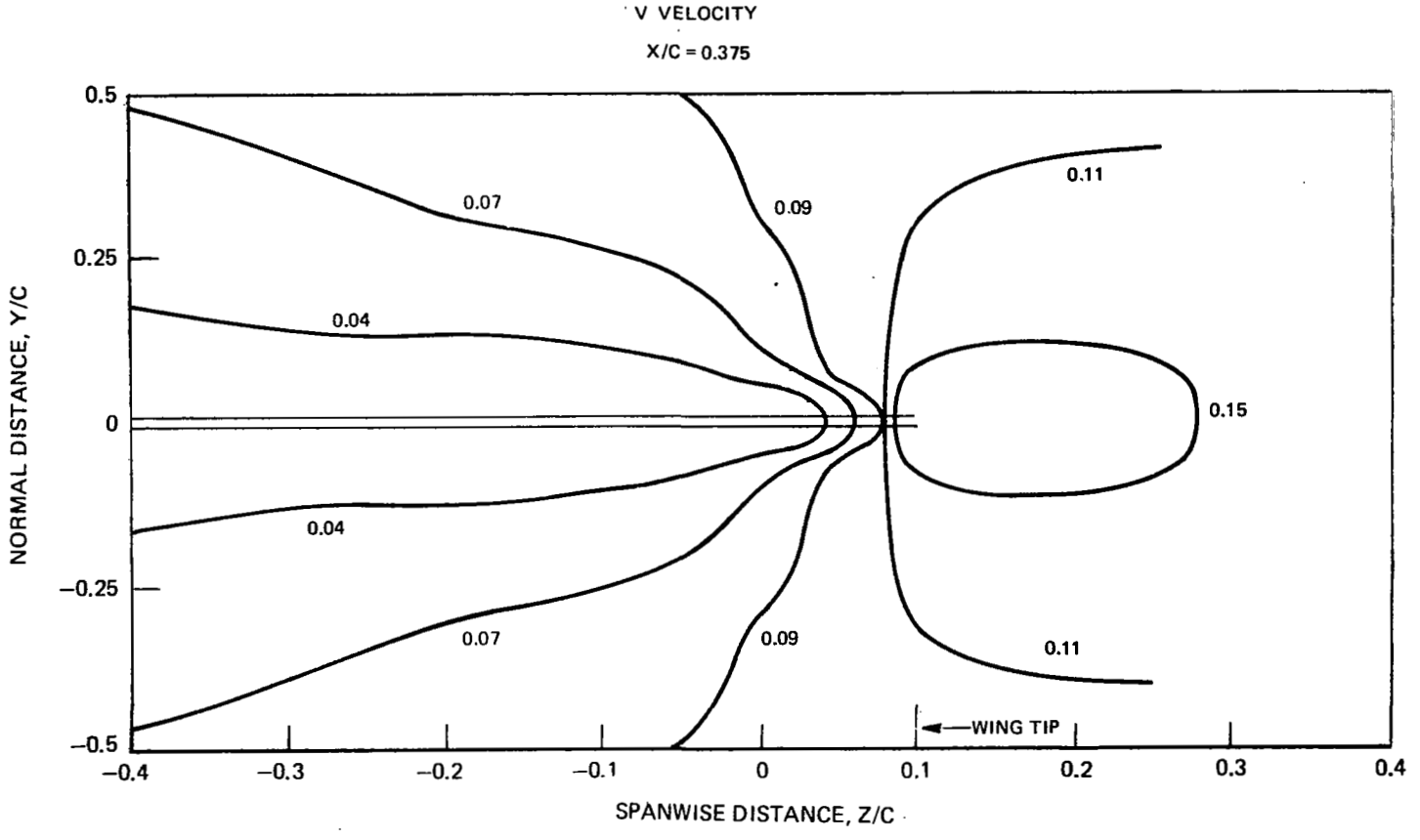

Figure 21. — Inviscid flow calculation.

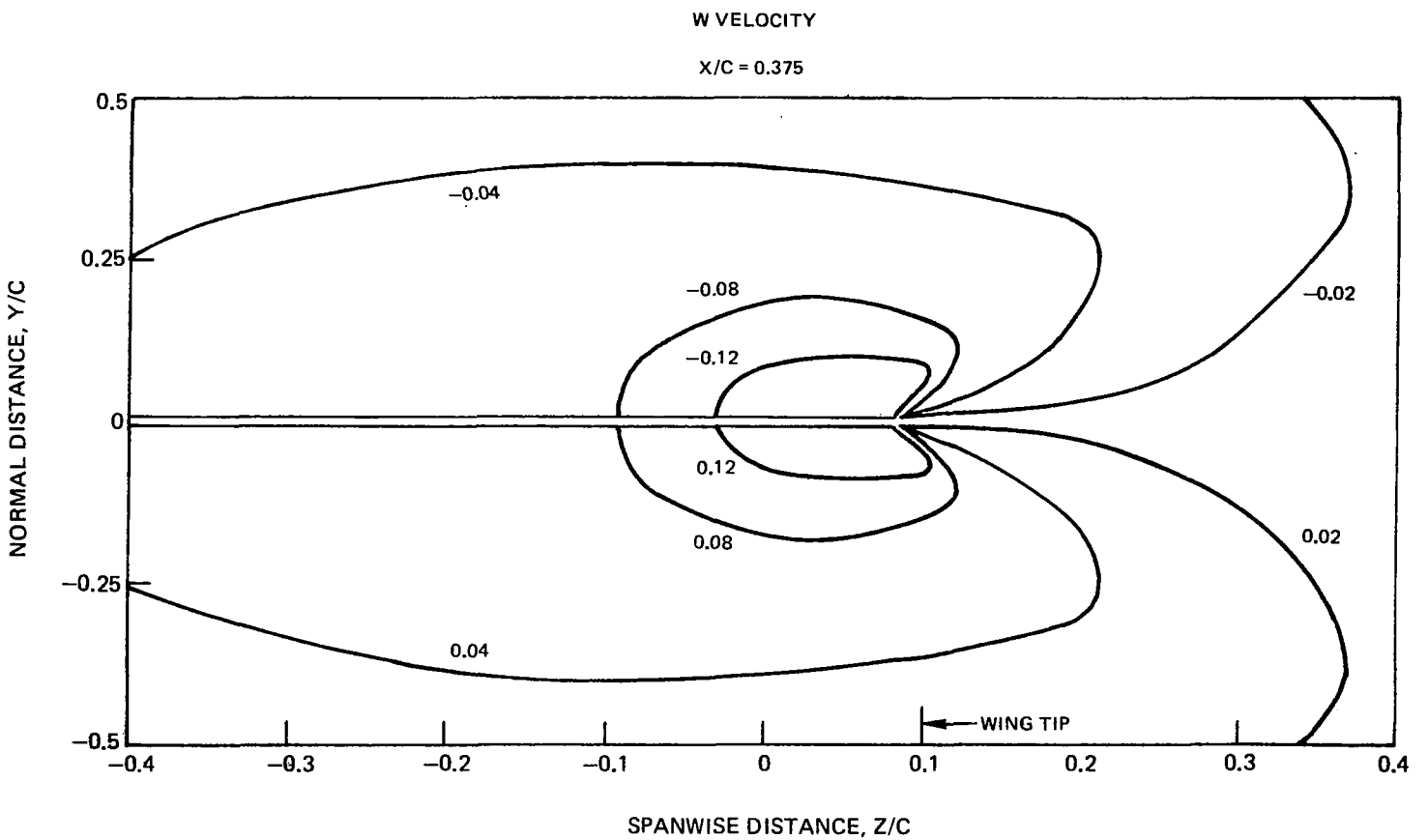

Figure 22. — Inviscid flow calculation.

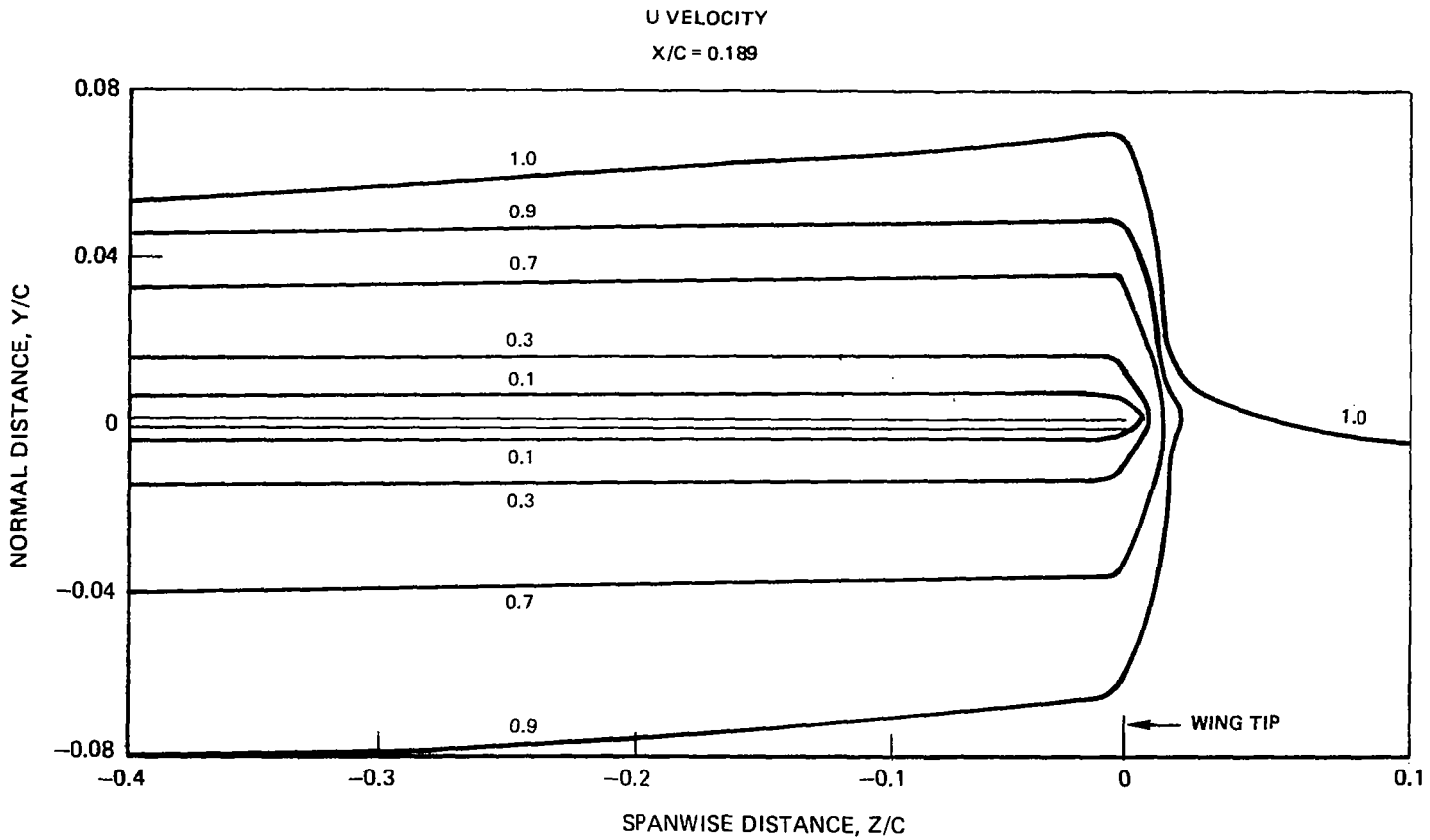

Figure 23. — Viscous flow calculation.

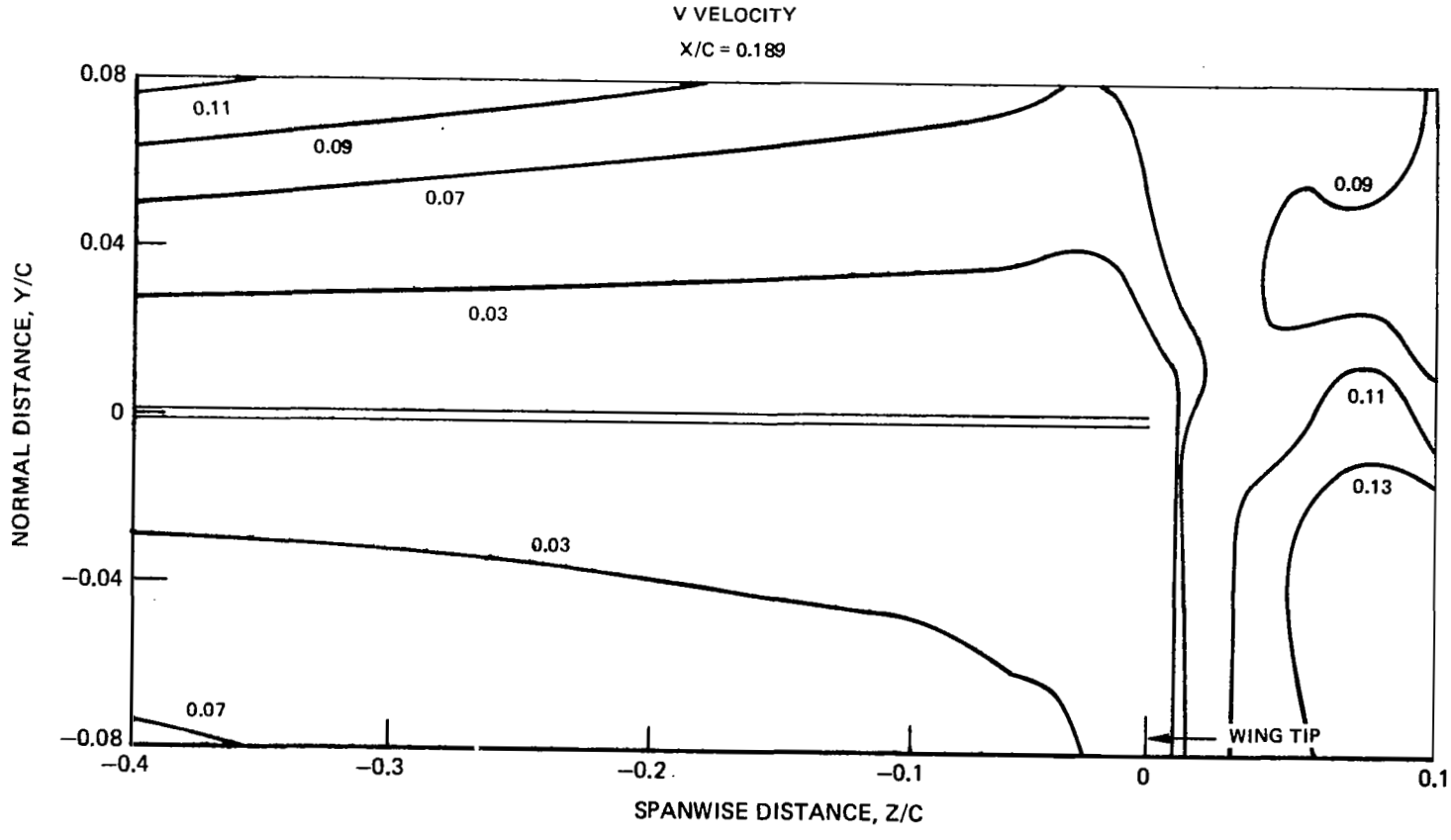

Figure 24. – Viscous flow calculation.

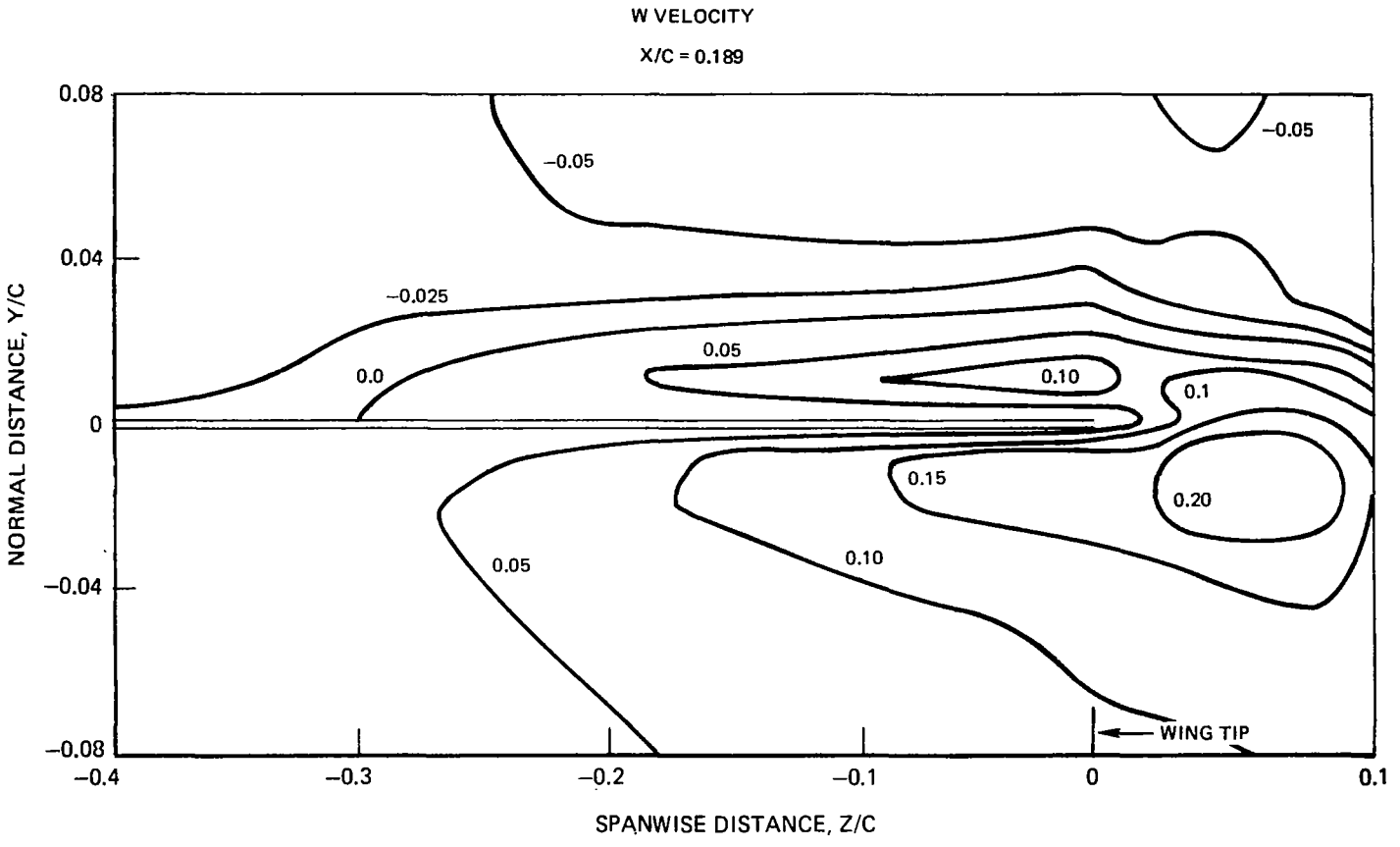

Figure 25. – Viscous flow calculation.

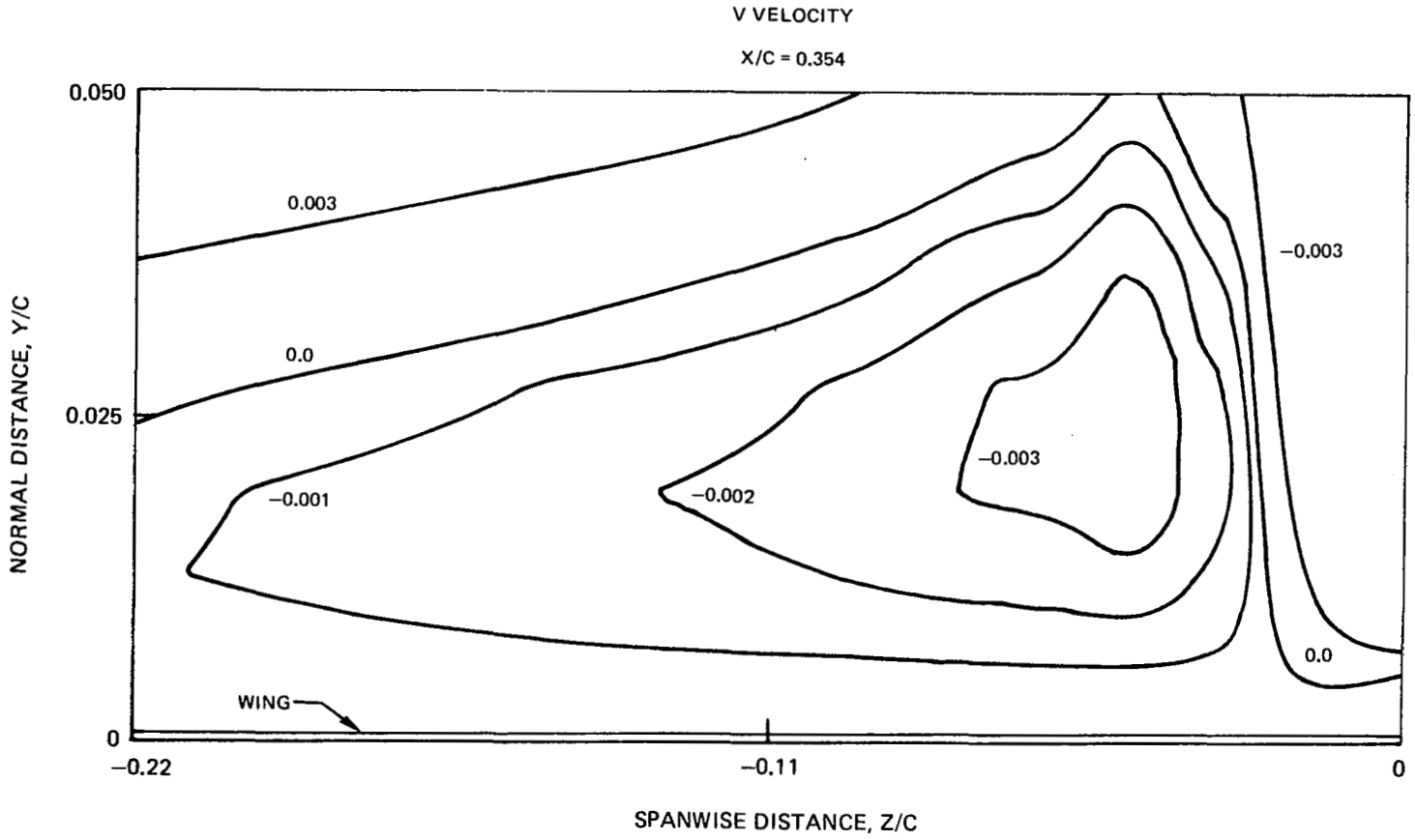

Figure 26. — Viscous flow calculation.

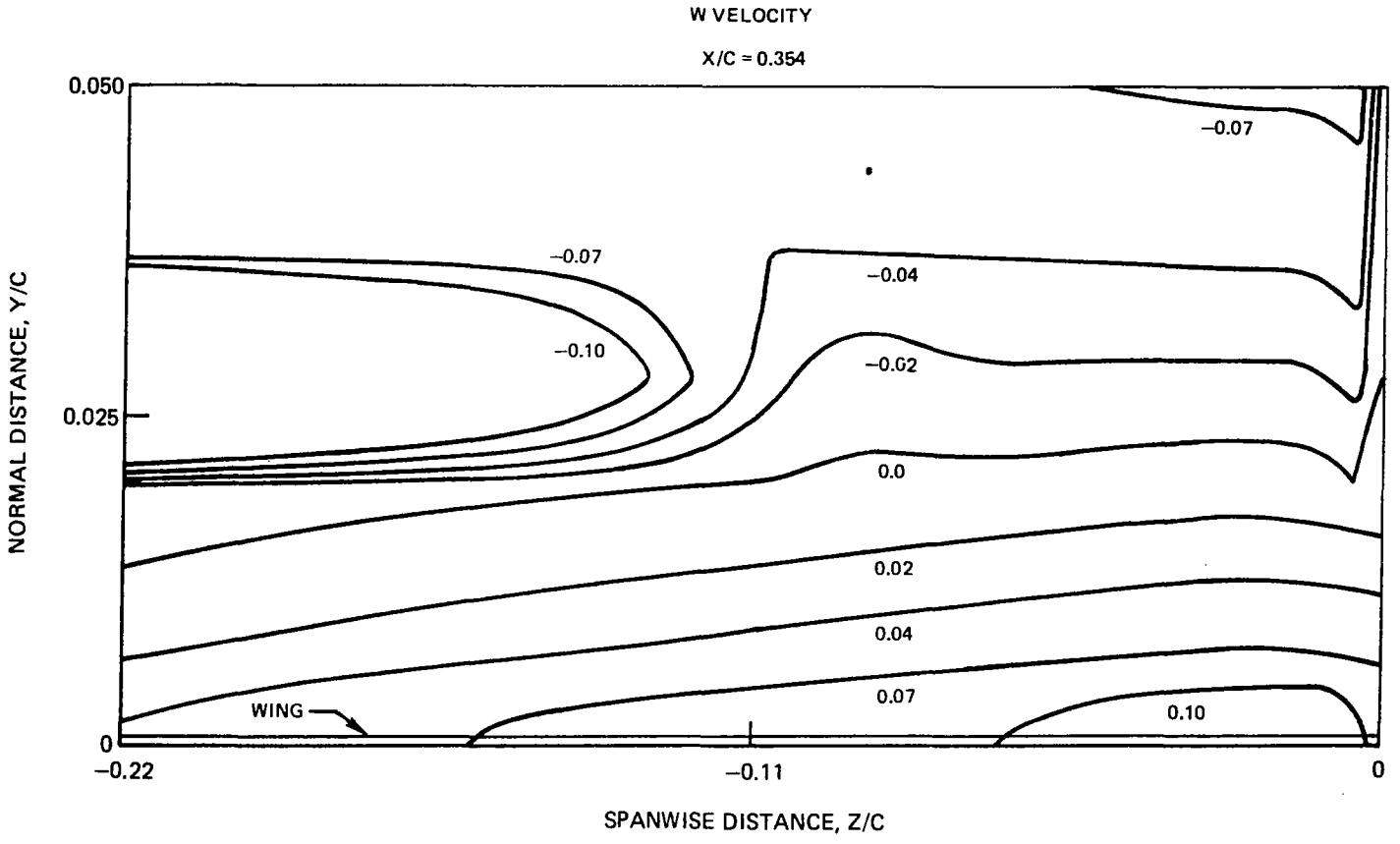

Figure 27. — Viscous flow calculation.

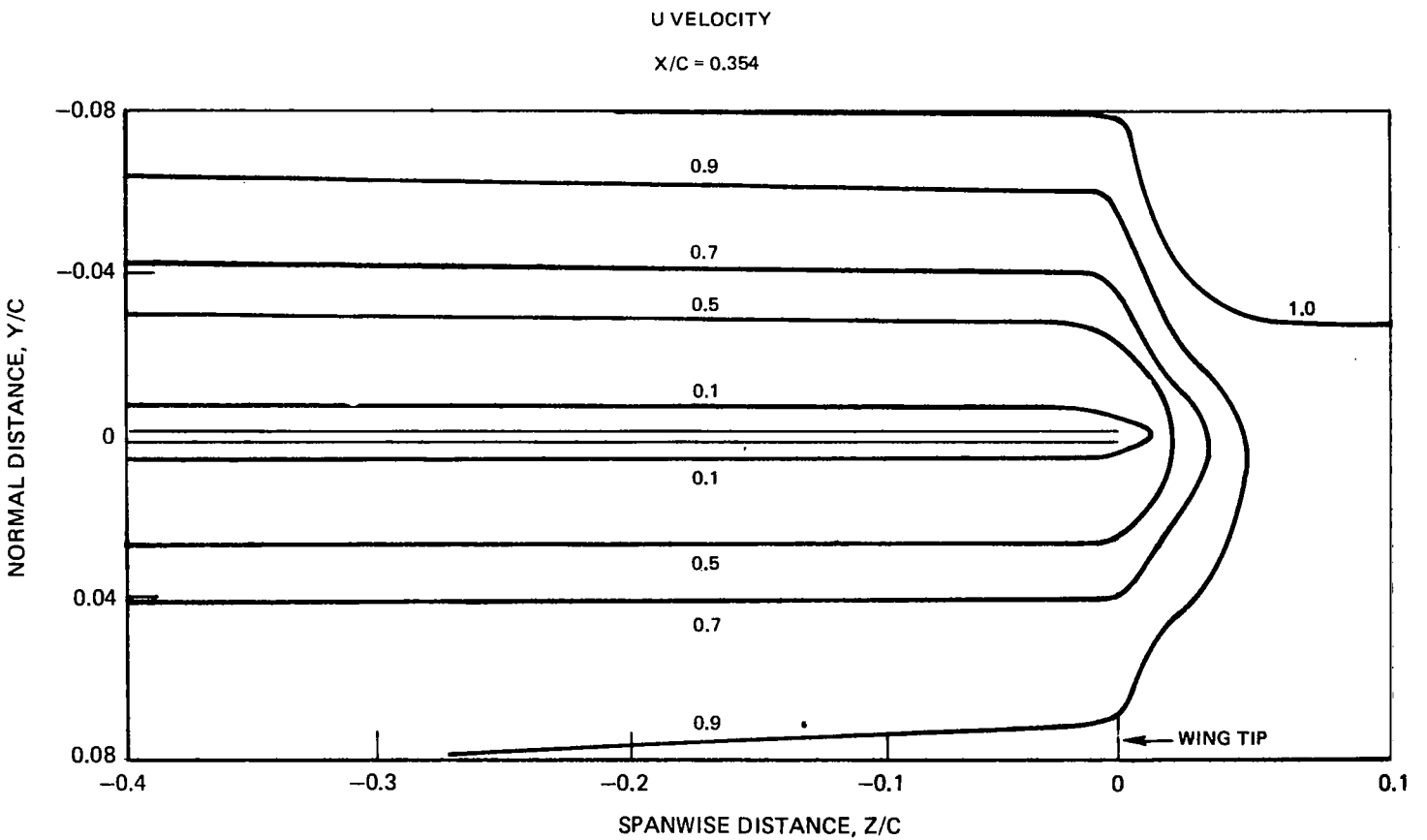

Figure 28. — Viscous flow calculation.

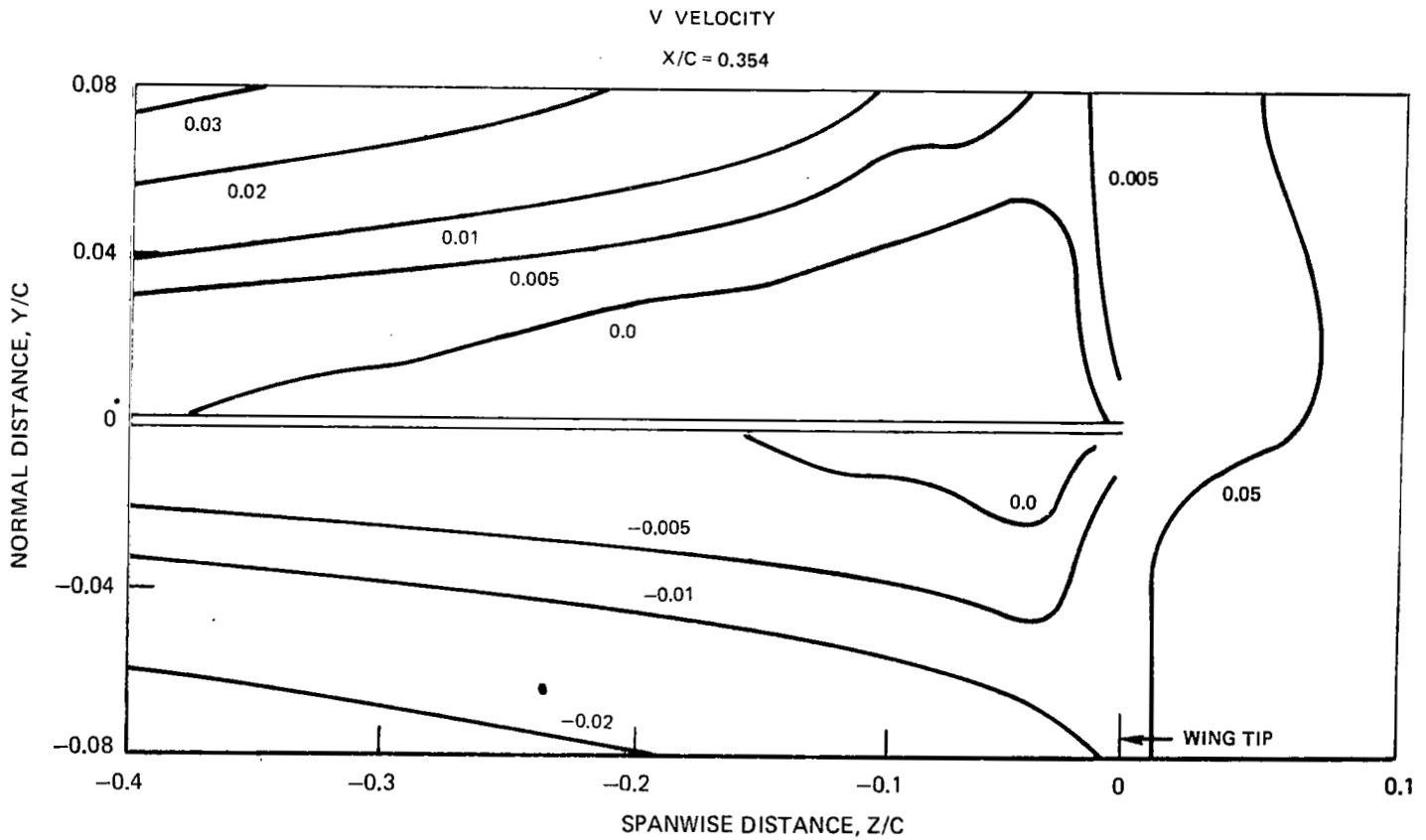

Figure 29. – Viscous flow calculation.

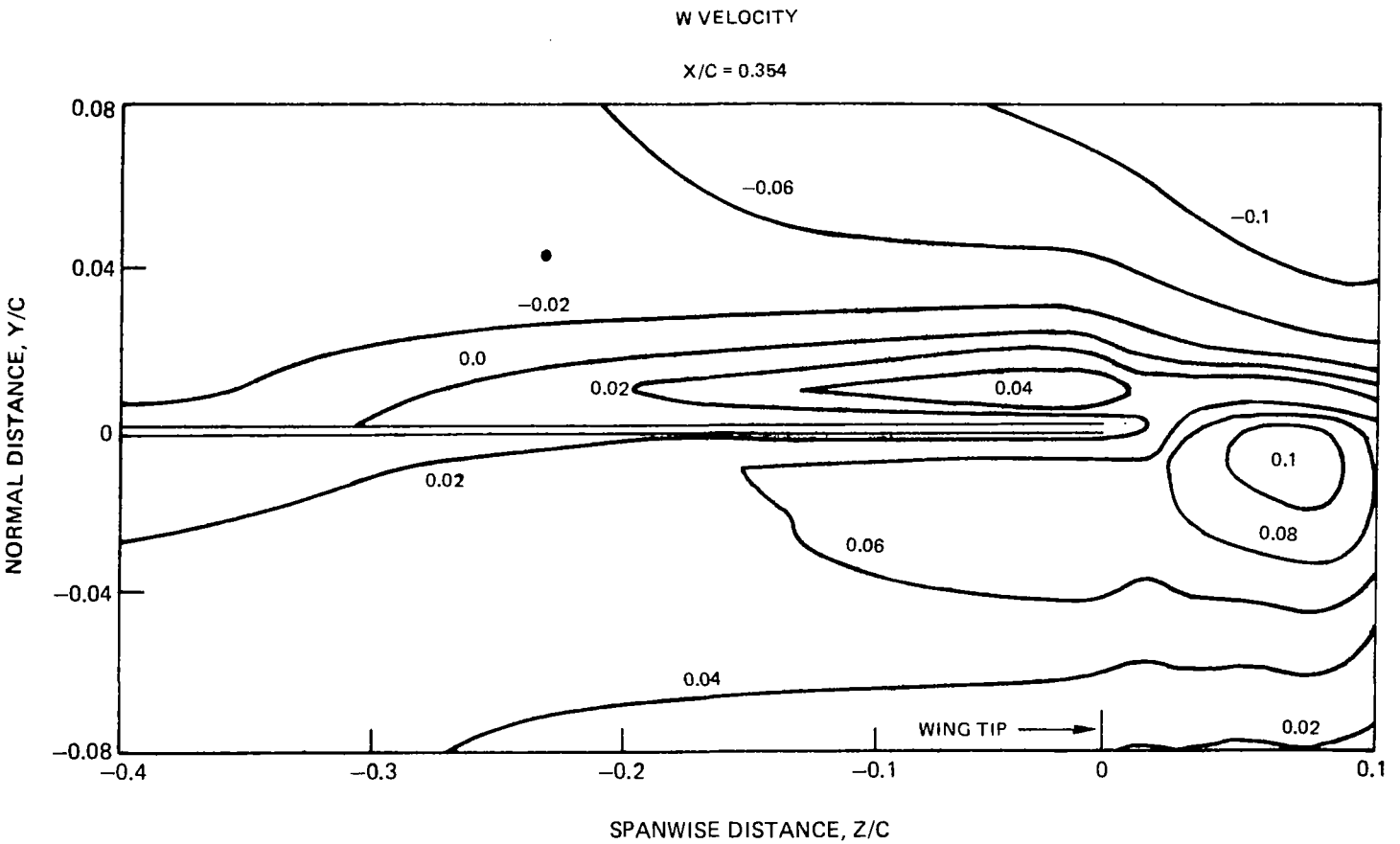

Figure 30. — Viscous flow calculation.